



## A state-of-the-art review on flow boiling at high reduced pressures

D.B. Marchetto<sup>a</sup>, D.C. Moreira<sup>a</sup>, R. Revellin<sup>b</sup>, G. Ribatski<sup>a</sup>



<sup>a</sup> Heat Transfer Research Group, São Carlos School of Engineering - University of São Paulo, São Carlos/SP, Brazil

<sup>b</sup> Univ de Lyon, INSA Lyon, CNRS, CETHIL, UMR5008, 69621 Villeurbanne, France

### ARTICLE INFO

#### Article history:

Received 21 February 2022

Revised 4 April 2022

Accepted 17 April 2022

Available online 6 May 2022

#### Keywords:

High-pressure

Near-critical pressure

Flow boiling

Two-phase flow

Prediction methods

### ABSTRACT

As the state of a fluid approaches the critical point, significant changes of its thermophysical properties are noticed, which can greatly alter the observed transport behavior. In particular, notable variation in the liquid-to-vapor phase-change characteristics occur, with densities of both phases converging to the same value, the reduction of surface tension, and sudden increase of the specific heat capacity, for example. Such variations can lead to the non-satisfactory predictions of operational parameters in heat exchangers, since most of the available predicting methods were developed for synthetic refrigerants at low saturation pressures and temperatures, typical of refrigeration applications. However, it should be noted that applications that involve flow boiling at high reduced pressures are continuously growing, but experimental data at such conditions are scarce, which leads to a lack of predicting models that incorporate such data in their development. Hence, this review focus on flow boiling studies that comprise experiments at reduced pressures between 0.5 and 1 and identify gaps in the literature that are worthy of investigation. Although large discrepancies between data obtained at similar conditions by different groups were found, the rise of reduced pressure generally increases the heat transfer coefficient and decreases both pressure drop and the critical heat flux. A detailed discussion on the mechanisms responsible for the diverse trends that were observed was carried out. Finally, three extensive databases containing experimental results of pressure drop, heat transfer coefficient, and critical heat flux were raised and compared with prediction methods from the literature. Statistical analyses reveal that in general the available methods fail to predict more than 60% of the pressure drop and heat transfer coefficient databases within an error margin of 30%, while for critical heat flux some methods were able to predict more than 70% of the database within the same error margin.

© 2022 Elsevier Ltd. All rights reserved.

### 1. Introduction

In the past years, flow boiling has been extensively investigated, resulting in development of numerous methods to predict pressure drop ( $\Delta p$ ), heat transfer coefficient (HTC), and critical heat flux (CHF). In general, these methods are suitable to the range of operational conditions (flow rate, inlet subcooling, saturation temperature, fluid properties) based on which they were developed. Such methods are essential in the design of heat exchangers, and the higher their accuracy, the more trustworthy are the calculations of required pumping power, heat transfer area, and heat flux operation limit, resulting in smaller components with extended range of operational conditions. It should be noted that most of the cur-

rently available prediction methods for  $\Delta p$  and HTC in flow boiling were based on experimental results obtained for synthetic refrigerants at low saturation pressures and temperatures, typical of refrigeration and air-conditioning applications [1–4]. For the prediction of the CHF, however, many methods were developed for high pressures and temperatures, but generally using water as working fluid, suitable to the commonly found operational conditions of water-cooled nuclear reactors [5–8]. Although these are still some of the main motivations for flow boiling investigation, there is a growing interest involving several high-pressure applications, including near-critical conditions.

It is well-known that liquid and vapor can only be distinguished as separate phases at temperature and pressure conditions below the critical point, and that the properties of a substance vary considerably in the vicinity of this condition. Thus, it is useful to quantify how close to this singular behavior a substance is through the concept of reduced pressure ( $p_r$ ), which is the ratio of working pressure ( $p_{sat}$ , for flow boiling) to the critical pressure ( $p_{crit}$ ) of a given substance. As an example, Fig. 1 shows the variation of some thermophysical properties of the fluid R245fa with the in-

**Abbreviation:** CERN, European Organization for Nuclear Research; CFC, Chlorofluorocarbon; CHF, Critical heat flux; DNB, Departure from nucleate boiling; DO, Dryout; GWP, Global warming potential; HCFC, Hydrochlorofluorocarbon; HFC, Hydrofluorocarbon; HTC, Heat transfer coefficient; LHC, Large Hadron Collider; LWR, Light water reactor; MAPE, Mean absolute percentage error; ODP, Ozone depleting potential; ORC, Organic Rankine cycle; SCWR, Supercritical water reactor.

## Nomenclature

$Bo$	Boiling number [-]
$D_H$	Hydraulic diameter m
$f$	Fanning friction factor [-]
$G$	Mass velocity kg/m <sup>2</sup> s
$h$	Heat transfer coefficient kW/m <sup>2</sup> K
$i_{lv}$	Enthalpy of vaporization kJ/kg
$\Delta i_{in}$	Enthalpy of subcooling kJ/kg
$L$	Channel length m
$L_H$	Heated length m
$N$	Amount of extracted data [-]
$p$	Pressure kPa
$p_r$	Reduced pressure [-]
$p_{sat}$	Saturation pressure kPa
$\Delta p$	Pressure drop kPa
$q''$	Heat flux kW/m <sup>2</sup>
$Re$	Reynolds number [-]
$T$	Temperature °C
$\Delta T_{sub}$	Degree of subcooling °C
$x$	Vapor quality [-]
$z$	Flow Direction m

### Greek letters

$\lambda_{30\%}$	Fraction of data predicted within error bands of 30% [-]
$\mu$	Viscosity Pa.s
$\rho$	Density kg/m <sup>3</sup>
$\sigma$	Surface tension N/m

### Subscripts

$2\varphi$	two-phase
$CHF$	critical heat flux
$crit$	critical
$exp$	experimental
$f$	frictional
$fluid$	real fluid
$in$	inlet
$l$	liquid
$max$	maximum
$table$	look-up table
$v$	vapor
$water$	water equivalente flow

crease of  $p_r$ , where it is possible to observe the increase in vapor density and decrease in liquid density, converging to the same value at  $p_r = 1$ . In addition, the enthalpy of vaporization and the surface tension gradually reduce, while the liquid specific heat slightly increases as  $p_r$  rises. As  $p_{sat}$  approaches the critical pressure in conditions usually called as near-critical [9,10], strong non-linear behavior is observed for various properties, with a sharp increase of the liquid specific heat and steep decrease in the enthalpy of vaporization. The beginning of the near-critical region varies for each fluid: for R134a, near-critical pressures correspond to  $p_r > 0.76$  [9], while for CO<sub>2</sub> it could be considered as  $p_r > 0.85$  [10]. In the present work, for simplicity, near-critical pressures will be assumed as  $p_r \geq 0.8$ .

The changes in these thermophysical properties considerably affect the two-phase flow characteristics and heat transfer mechanisms. Although there is still no consensus regarding the macro-to-microscale transition, several criteria [12–14] indicate smaller threshold diameters at higher  $p_r$ , which is mainly associated with the surface tension reduction. The criteria proposed by Tibiriçá and Ribatski [14] consider the liquid film uniformity during annular flow patterns and the absence of stratified flow in microchannels.

For both criteria, the reduction of the surface tension forces implies in the decrement of the threshold diameter. The flow patterns and their transitions are significantly affected by the  $p_r$  increase [15–18]. The progressive flow stratification with increasing  $p_r$  was reported [16,18], even for small diameter tubes (1 and 2 mm) [16], which is in accordance with one of the criteria proposed by Tibiriçá and Ribatski [14]. The shrinkage in the departure diameter of vapor bubbles at higher pressures was also reported [16].

The decline of capillarity effects at high  $p_r$ , as well as the flow velocity and slip-ratio decrease, contribute to a diminution in pressure drop. Lower enthalpy of vaporization and surface tension intensify the nucleation of vapor bubbles, resulting in a stronger contribution of nucleate boiling effects on the heat transfer. During pool boiling, the total heat flux at the wall is given by the contribution of intensive evaporation at the contact line and convection to liquid between the nucleation sites [19]. The first one dominates the heat transfer at high  $p_r$ , due to the increase of the density of nucleation sites [19]. However, the intensified nucleation activity allied to the reduction in the enthalpy of vaporization can induce an early CHF, which leads to a premature heat transfer deterioration. These different behaviors verified at high pressures may lead to a non-satisfactory accuracy of the prediction methods proposed for low reduced pressures [20,21].

In spite of the lack of predictive methods proposed for such conditions, engineering applications that involve operational conditions for flow boiling of diverse fluids at high reduced pressures continue to grow, increasing the need for accurate prediction of parameters related to heat transfer and fluid flow, particularly motivated by the demands for increased overall efficiency of energy systems and reduced environmental impacts of power generation and refrigeration equipment. Organic Rankine cycles (ORCs) have been a current subject of interest in the literature, due to the possibility of working with low-grade heat sources and waste heat, with a significant number of experimental and simulation studies published in the last years [22,23]. Despite the similar configuration to conventional water Rankine cycles, ORCs use organic working fluids, which have critical temperatures considerably lower than water. This characteristic allows the use of low-grade heat sources including geothermal, biomass, solar power and industrial waste heat [24,25]. These sources operate at 100–250°C, which corresponds to evaporating temperatures of 50–150°C and leads to intermediate-to-high reduced pressures ( $p_r$ ) of evaporation for most of the organic fluids [25].

In refrigeration, carbon dioxide has received a lot of interest as a substitute for synthetic refrigerants [26], due to its non-toxicity, non-flammability, null ozone depleting potential (ODP) and negligible global warming potential (GWP) [27]. The low critical temperature of CO<sub>2</sub> ( $T_{crit}=31.1^\circ\text{C}$ ) leads to its operation at intermediate-to-high reduced pressures, even in refrigeration systems. In addition, the CO<sub>2</sub> trans-critical cycle is frequently pointed out as a high-efficiency and low-cost alternative for refrigeration and heat pump applications [10]. The use of flow boiling of CO<sub>2</sub> in electronics cooling was also assessed [28], and is noteworthy that near-critical pressures can be reached during this application. In a recent effort to reduce their carbon footprint, the European Organization for Nuclear Research (CERN) has replaced Hydrofluorocarbons (HFCs) by CO<sub>2</sub> in the cooling system of the sensors from their Large Hadron Collider (LHC) particle accelerator, which motivated a series of experiments carried out by Hellenschmidt and Petagna [26,29].

Other applications that involve flow boiling in high pressures include: light water reactors (LWR) [30]; water circulating fluidized beds [31,32], with their fuel flexibility, high combustion efficiency and efficient pollution control; and supercritical pressurized water-cooled reactors (SCWR) [9,33], which are pointed out as the next generation technology in terms of economic efficiency. Although this last example is designed to work at supercritical conditions

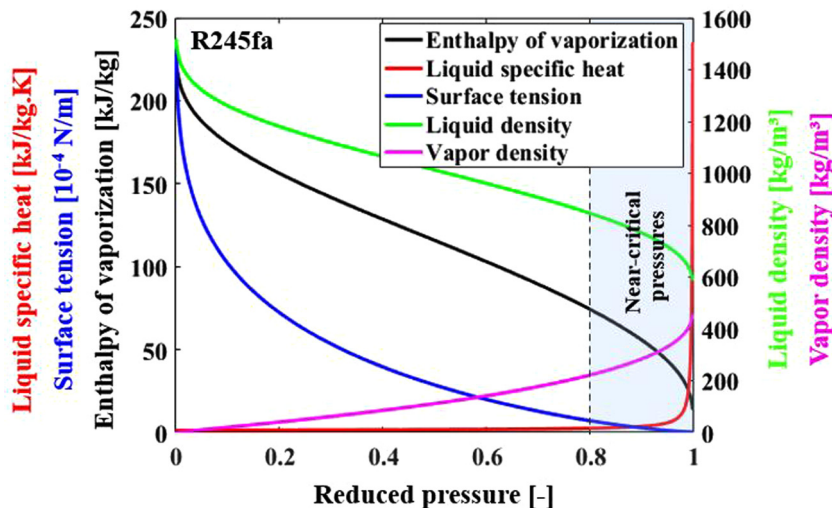


Fig. 1. Effect of reduced pressure on R245fa thermophysical properties. Properties obtained by CoolProp library [11].

in full operation, the operating conditions comprise high subcritical pressures during startup and shutdown, and in the eventuality of a fluid leak, the pressure can also decrease to high subcritical conditions [9]. Even though flow boiling at high reduced pressures occur in various applications, the available experimental data for high  $p_r$  in the literature is scarce, which can be attributed to the difficulty in conducting experiments at high-temperatures and high-pressure conditions. As a consequence, the available predictive methods for flow boiling heat transfer and fluid flow seldom consider data for high  $p_r$  during their developments, which contribute to a non-satisfactory accuracy of these methods when applied to high  $p_r$  [20,21].

Some literature reviews on flow boiling discuss the role of diverse mechanisms and assess the accuracy of prediction methods through the comparison with extensive databases [34–39], but these works are not directed to high reduced pressure or its effects. In this context, the current investigation presents a broad review of experimental works that included data for  $\Delta p$ , HTC and CHF at reduced pressures higher than 0.5. The main trends of these parameters observed in the literature are described and the mechanisms are discussed, while some contradicting data are identified and possible reasons for such conflicts are indicated. Based on these experimental studies, three extensive databases were raised, containing a total of 7475 experimental points, with 54% of them corresponding to  $p_r \geq 0.5$ . The Engauge Digitizer (v. 12.1) software [40] was used to extract graphical data from these studies. The databases were compared with predictive methods from the literature, and it was noted that few of them were able to predict more than 60% of the  $\Delta p$  and HTC data within error margins of 30%, while for CHF some models predicted more than 70% of the database within the same margin. Fluid properties were taken from the Coolprop library [11], with exception of those from the refrigerants R1234yf, R1234ze(E), R448A and R452A, which were obtained from the Engineering Equation Solver [41]. Finally, this review also highlights topics on which further research is needed.

## 2. Pressure drop

Pressure drop is an important parameter considering components for thermal systems. The pressure gradient is composed by three parcels: gravitational, accelerational and frictional. Due to the complexity of the frictional component during two-phase flow inside channels, several experimental studies were carried out in the past years in order to evaluate it. As a consequence, a significant

number of the predictive methods are empirical. The following sections present a critical discussion about the literature concerning pressure drop at high reduced pressures, as well as a comparison between experimental data extracted from the available studies and 21 prediction methods.

### 2.1. Analysis of experimental studies under high pressures

**Table 1** presents a summary of studies involving the adiabatic frictional pressure drop at  $p_r \geq 0.5$ , indicating the corresponding experimental conditions that were evaluated. A two-phase frictional pressure drop database including 1486 experimental results from 14 published papers was compiled in the present study. The database consists of 1351 adiabatic data extracted from 13 studies indicated in **Table 1**, and 135 experimental results for diabatic R134a flows reported by Vijayarangan et al. [42]. Most of the data points were obtained for single-channels, while 254 points correspond to multi-channels. The majority of the collected data are for circular channels, but 267 data points for rectangular test sections are also included in the database. In addition, 1168 data points correspond to horizontal flows, and 318 consist of vertical upward flows.

As verified in **Table 1**, nine different fluids were included in the database. It should be remarked that, although the present analysis is focused on  $p_r \geq 0.5$ , the analyzed studies also reported data points at  $p_r < 0.5$ . These 781 experimental results were also included in the database, in order to compare the accuracy of the prediction methods at low and high reduced pressures. **Fig. 2** presents the data distribution according to reduced pressure, hydraulic diameter, mass velocity and vapor quality. Data for synthetic refrigerants (R134a, R22, R245fa, R404A, R410A and R448A) are grouped in **Fig. 2(a)** due to the similarity of their thermophysical properties. The shortage of experimental results at near-critical pressures is evident in **Fig. 2(a)**.

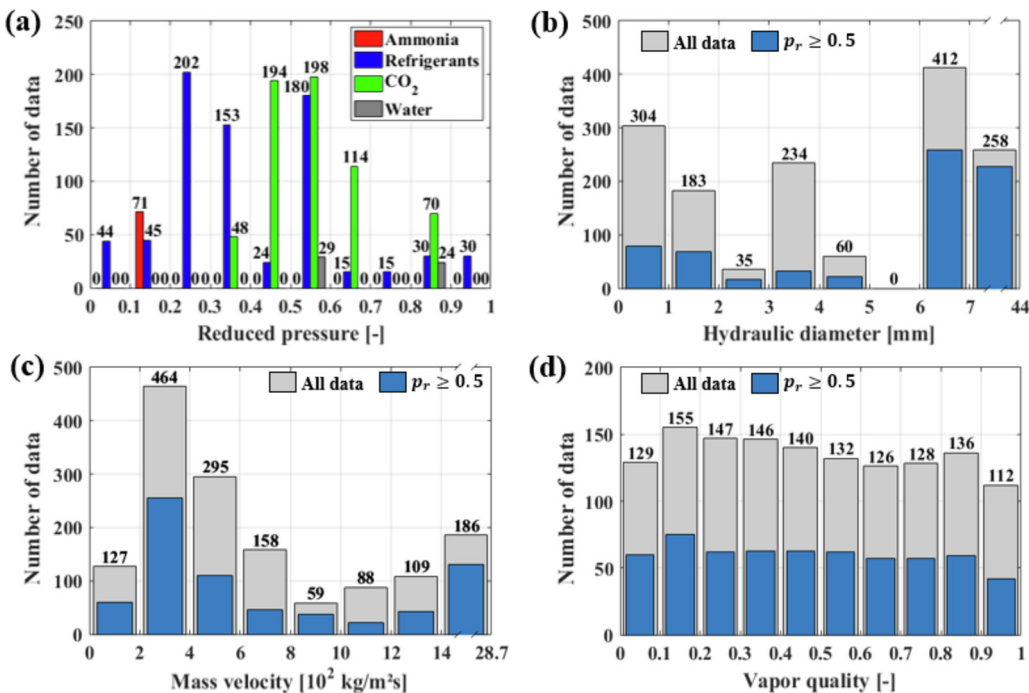
As shown in **Fig. 2(b)**, the hydraulic diameter varied between 0.53 and 44 mm. Almost 35% of the database consists of experimental results for  $D_H < 3$  mm, considered by Kandlikar [54] as the threshold diameter for macro-to-microscale transition. However, depending on the criterion, only 32% [12], 22% [13] and 0% [14] of the data points actually fall in the microchannels classification. It is important to mention that most of the data at  $p_r \geq 0.5$  correspond to  $D_H \geq 6$  mm (**Fig. 2b**). The mass velocity of the collected data varied from 50 to 2866 kg/m<sup>2</sup>s, with almost 75% of the experimental results falling in the range of  $G < 1000$  kg/m<sup>2</sup>s,

**Table 1**

Experimental studies concerning adiabatic two-phase frictional pressure drop at high reduced pressures.

Authors	Shape/orientation/n° of channels	Material	D <sub>H</sub> /L [mm]	Fluids ( $p_r$ [-])	G [kg/m <sup>2</sup> s]	x [-]	N
<i>Studies at 0.5 ≤ p<sub>r</sub> &lt; 0.8</i>							
Charnay et al. [21]	C/H/1	SS	3/350	R245fa (0.13-0.53)	100-1000	0-1	177
Mastrullo et al. [27]	C/H/1	SS	6/-	CO <sub>2</sub> (0.38-0.54)	201-349	0.08-0.98	28
Zhang and Webb [43]	C/H/1-8	Copper/Aluminum	2.13-3.25/560-914	R134a (0.25-0.47), R22 (0.21-0.39), R404A (0.36-0.51)	400-1000	0.20-0.89	68
Adams et al. [44]	R/H/6-14	Aluminum	1.02-1.54/991	CO <sub>2</sub> (0.69), ammonia (0.12), R245fa (0.07-0.08)	50-440	0.03-0.99	183
Jeong et al. [45]	R/H/3	Aluminum	2/5000	CO <sub>2</sub> (0.47-0.61)	700	0.01-0.85	24
Vassallo and Keller [46]	R/VU/1	-	4.8/118-187	R134a (0.22-0.59)	510-2040	0.03-0.72	60
Ducoulombier et al. [47]	C/H/1	SS 316L	0.53/191	CO <sub>2</sub> (0.36-0.54)	200-1400	0-1	268
Kim and Jeong [48]	C, CF/H/6-8	Aluminum	0.64-0.80/1100	CO <sub>2</sub> (0.54-0.61)	400-600	0-1	36
Grauso et al. [49]	C/H/1	SS 304	6/1000	CO <sub>2</sub> (0.57-0.64), R410A (0.19-0.52)	152-513	0-1	274
Lillo et al. [50]	C/H/1	SS 316L	6/237.5	R448 (0.27-0.46), R404A (0.33-0.55)	152-601	0.04-0.98	110
<i>Studies at p<sub>r</sub> ≥ 0.8</i>							
Wang et al. [51]	C, CR/H, VU/1	SA-213T12	17.63-19.80/2000	Water (0.57-0.97)	400-1050	0-1	29
Liu et al. [52]	C/VU/1	-	11.6/4371	Water (0.82)	378-1892	0.03-0.81	24
Hammer et al. [53]	C/VU, VD/1	-	44/13700	CO <sub>2</sub> (0.88)	155-2866	0.02-0.90	70

C: Circular smooth; R: Rectangular; CR: Circular rifled; CF: Circular finned; H: Horizontal; VU: Vertical upward; VD: Vertical downward; D<sub>H</sub>: Hydraulic diameter; L: Length; SS: Stainless steel. N: Quantity of data points extracted.

**Fig. 2.** Pressure drop data points distribution against (a) reduced pressure, (b) hydraulic diameter, (c) mass velocity, and (d) vapor quality.

as verified in Fig. 2(c). Only adiabatic data points are presented in Fig. 2(d), as the vapor quality varies along channels under heat transfer conditions.

As well as for low pressures, all the studies in Table 1 verified that initially the two-phase frictional pressure gradient,  $(dp/dz)_{f,20}$ , increases with rising  $x$ , which is associated with the two-phase viscosity reduction and raising of two-phase specific volume, resulting in the increase of flow velocity and interfacial shear [47]. This behavior is maintained until the pressure gradient reaches its maximum, from which it starts to decrease with subsequent increments of  $x$ . According to Charnay et al. [21], the vapor quality corresponding to the peak in  $(dp/dz)_{f,20}$  ( $x_{max}$ ) occurs in three situations: (i) Coinciding with the liquid film dryout inception; (ii) coinciding with the transition to mist flow pat-

tern; (iii) preceding the inception of the liquid film dryout. The absence of liquid phase in contact with the surface justifies situations (i) and (ii), since the lower viscosity of the vapor compared to the liquid phase results in the reduction of the flow-surface shear [21]. In contrast, situation (iii) occurs under conditions in which the liquid film still exists along the entire perimeter of the tube, which has been verified in the literature for  $p_r < 0.5$  [55-57]. Recently, Moreira et al. [55] experimentally evaluated the liquid film thickness and the interfacial wave frequencies during two-phase adiabatic vertical flows of R245fa at  $p_r = 0.04$ , and verified that the  $(dp/dz)_{f,20}$  peak is linked to the disappearance of disturbance waves. Fig. 3 summarizes the frictional pressure gradient behaviors identified in the studies from Table 1, indicating vapor quality ( $x$ ), mass velocity ( $G$ ) and reduced pressure effects.

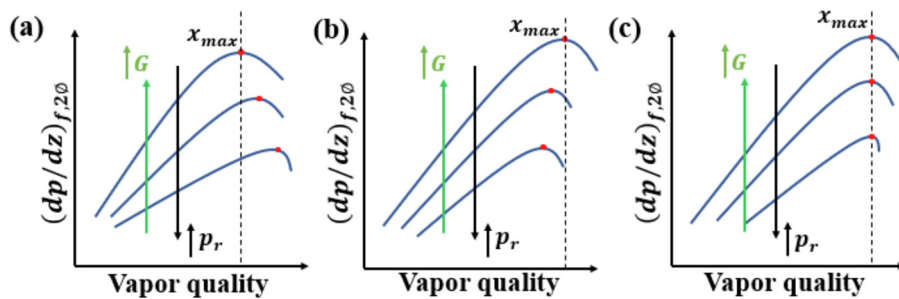


**Fig. 3.** Typical trends of two-phase frictional pressure gradient with vapor quality verified in adiabatic studies from the literature, indicating the effects of mass velocity and reduced pressure moving the peak to (a) increasing, (b) decreasing, and (c) steady vapor quality values.

As seen in Fig. 3, all studies reported rises in pressure gradient with increasing  $G$ , an effect that is associated with the higher flow velocities and, consequently, the increment of shear. However, the mass velocity increase resulted in different effects on  $x_{max}$ , as also depicted in Fig. 3. Some authors verified the anticipation of the pressure gradient peak with increasing  $G$  (Fig. 3a) [21,44,49,50], a behavior that is frequently observed at low reduced pressures and described by Tibiriçá and Ribatski [58] in their literature review. Da Silva [57] speculates that the  $x_{max}$  reduction is associated with the higher entrainment rate at high mass velocities, anticipating the damping of disturbance waves at the interface. The second effect identified in the literature was the increase of  $x_{max}$  with increasing  $G$  (Fig. 3b), which was only reported by Ducoulombier et al. [47], specially at mass velocities lower than  $1000 \text{ kg/m}^2\text{s}$ , and no reason for this behavior was discussed by the authors. Other studies indicated no relevant effect of mass velocity on the vapor quality corresponding to the pressure peak, as illustrated in Fig. 3c [48,51].

Another effect that was reported in all investigations and is shown in Fig. 3 is the reduction of  $(dp/dz)_{f,20}$  with increasing  $p_r$ . This effect is associated with the increase of the vapor phase density, which reduces the two-phase velocity [47]. Furthermore, the approximation of  $\rho_l$  and  $\rho_v$  with increasing  $p_r$  reduces the interfacial shear, as the difference between the velocities of liquid and vapor phases is reduced [50]. An interesting effect was verified by Grauso et al. [49] when comparing the frictional pressure gradient for  $\text{CO}_2$  and R410A in horizontal flows. These authors reported that at the same saturation temperature, R410A presented higher  $(dp/dz)_{f,20}$  than  $\text{CO}_2$ , which is associated to the lower  $p_r$  of the first fluid. However, when evaluated at the same reduced pressure, these fluids presented almost identical pressure gradients due to the proximity between their thermophysical properties.

Most works reported a shift of the  $(dp/dz)_{f,20}$  peak to higher  $x$  with increases in the reduced pressure, as seen in Fig. 3(a) [21,49–51]. This behavior is regularly reported in the literature concerning pressure drop during flow boiling at low  $p_r$  [58], and might be associated with the vapor phase velocity and slip ratio reductions, decreasing the entrainment rate and delaying the disappearance of disturbance waves. Few studies reported the reduction of  $x_{max}$  with increasing  $p_r$  represented in Fig. 3(b) [47] and non-relevant effects of  $p_r$  on  $x_{max}$ , as illustrated in Fig. 3(c) [47,48]. In fact, Ducoulombier et al. [47] reported non-monotonic effects of the reduced pressure on  $x_{max}$ , with its increase as  $p_r$  augmented from 0.36 to 0.41 and its reduction for further augmentation of reduced pressure up to 0.54 at  $G=200 \text{ kg/m}^2\text{s}$ . These authors also observed a progressive dampening of reduced pressure effects on  $x_{max}$  at higher mass velocities, which is probably associated with the opposite effects of  $p_r$  and  $G$  on the entrainment. In these cases, it is possible that the  $(dp/dz)_{f,20}$  decrement after its peak is associated with the liquid film dryout, as several flow boiling studies verified its anticipation with increasing  $p_r$  [24,32,59,60].

Although Table 1 is mainly focused on studies concerning smooth channels, high-pressure experimental investigations on finned [48] and rifled tubes [51,61] are also found in the literature, and it is well recognized that the presence of internal ribs or fins increases the frictional pressure drop. It is also important to mention that, in addition to the adiabatic studies in Table 1, several experimental works concerning diabatic pressure drop at  $p_r \geq 0.5$  were found in the literature [29,42,62–65]. In these studies, only total pressure drop data were presented, and most of them did not inform the thermodynamic state of the working fluid at the inlet of the channel, making it impossible to estimate the frictional component. Different from adiabatic flows, it is expected that the heat flux effect on the cross-sectional temperature profile affects  $(dp/dz)_{f,20}$ , especially at near-critical pressures, since the thermophysical properties present non-linear variations with temperature under these conditions. Nonetheless, this behavior has not been discussed in the literature yet.

## 2.2. Comparison of prediction methods with experimental results

Since the database contains some diabatic results, a data reduction procedure was performed to extract the frictional component of the total pressure drop and compare it with the prediction methods. Among the high  $p_r$  diabatic studies found in the literature, only Vijayarangan et al. [42] informed the thermodynamic state of the test fluid at the inlet of the channel and had their results included in the present database. A theoretical one-dimensional model was developed to estimate the accelerational, gravitational, single-phase, and two-phase frictional components of pressure drop at a given experimental condition. The model was implemented in Matlab® v.R2021b, using the CoolProp library [11] to estimate fluid properties. It was assumed steady-state, uniform and one-dimensional heat flux at the inner surface of the tube, and the channel was divided into 200 discrete elements, for which energy balance and pressure drop calculations were performed. During the evaluation of the accelerational and gravitational components of pressure drop at the elements, the homogeneous model was adopted to estimate the void fraction. Although the Steiner [66] version of the Rouhani-Axelson [67] drift flux model has been considered in a previous analysis, the observed differences in the two-phase frictional component of the pressure drop using this approach or the homogeneous model to calculate the void fraction were lower than 2%. For the single-phase region, the Fanning friction factor was estimated according to the Hagen-Poiseuille theory ( $f = 16/Re$ ) and Blasius [68] correlation ( $f = 0.079Re^{-0.25}$ ), respectively for laminar and turbulent regimes. In the two-phase region, the frictional pressure gradient was calculated according to each of the 21 prediction methods considered in this work. Average properties between the inlet and outlet of the discrete element were considered during the calculation of the frictional pressure drop.

**Table 2**

Statistical analysis results of the comparison between the pressure drop database and prediction methods, indicating the experimental conditions for which they were developed.

Authors	$0 < p_r < 1$		$p_r \geq 0.5$		Test conditions or application ranges
	MAPE	$\lambda_{30\%}$	MAPE	$\lambda_{30\%}$	
<i>Homogeneous methods</i>					
Ducoulombier et al. [47]*	57.2	69.5	28.1	69.0	Adiabatic; C/S/H; CO <sub>2</sub> ; $D_H$ : 0.53 mm; $p_r$ : 0.36–0.54; G: 200–1400 kg/m <sup>2</sup> s; 608 data points
McAdams et al. [69]	32.9	45.6	30.8	61.1	Benzene-oil
Cicchitti et al. [70]	28.3	66.7	27.4	69.8	-
Dukler et al. [71]	32.5	46.6	28.9	64.2	$D_H$ : 12.3–127 mm; 2620 data points
Beattie and Whalley [72]	29.2	57.2	27.6	69.4	Adiabatic; C/S/H,V; 13510 data points
Lin et al. [73]	31.3	50.7	29.6	63.7	Adiabatic; C/S/H; R12; $D_H$ : 0.66–1.17 mm; $p_r$ : 0.15–0.32; G: 1440–5090 kg/m <sup>2</sup> s; 238 data points
Awad and Muzychka [74] v.1	29.1	62.2	28.7	66.8	Adiabatic/Evaporation; C,R,S,M/H; R12, R22, R134a, R410A, R290, argon, ammonia; $D_H$ : 0.15–14 mm; $p_r$ : 0.07–0.49
Awad and Muzychka [74] v.2	30.5	52.6	29.6	63.8	
<i>Two-phase multiplier-based methods</i>					
Zhang and Webb [43]	38.9	61.2	28.6	65.5	Adiabatic; C/S,M/H; R22, R134a, R4404A; $D_H$ : 2.13–3.25 mm; $p_r$ : 0.21–0.51; G: 400–1000 kg/m <sup>2</sup> s
Ducoulombier et al. [47]	230.6	56.6	31.4	61.3	C/S/H; CO <sub>2</sub> ; $D_H$ : 0.529 mm; $p_r$ : 0.36–0.54; G: 200–1400 kg/m <sup>2</sup> s; 608 data points
Lockhart and Martinelli [75]	158.1	15.7	221.1	6.8	Adiabatic; C/S/H; Air/water, air/oil, hydrocarbons/air; $p_r$ : 110.3–358.5 kPa; $D_H$ : 1.49–25.83 mm
Chisholm [76]	61.8	43.7	64.4	34.0	Adiabatic/Evaporation; C/S/H; Air/water, Air/oil, hydrocarbons/air; $D_H$ : 1.49–25.83 mm
Friedel [77]	38.7	59.5	48.3	41.4	C,R/S,H,V; Air/water, air/oil; R12; $D_H$ : >4 mm; 25000 data points
Mishima and Hibiki [78]	110.9	32.4	174.6	19.0	C,R/S,V; Air/water; $D_H$ : 1–4 mm; $p_r$ : 101.3 kPa
Yamamoto et al. [79]	36.2	47.0	38.3	54.6	Adiabatic; C/S/H; CO <sub>2</sub> ; $D_H$ : 0.51–2 mm; $p_r$ : 0.61–0.75; G: 200–1000 kg/m <sup>2</sup> s
Kim and Mudawar [80]	29.1	68.5	36.9	57.7	Adiabatic/Evaporation; C,R,S,M/H,V; R12, R134a, R22, R245fa, R410A, FC-72, ammonia, CO <sub>2</sub> , water; $D_H$ : 0.349–5.35 mm; $p_r$ : 0.005–0.78; G: 33–2738 kg/m <sup>2</sup> s; 2378 data points
<i>Empirical methods</i>					
Müller-Steinhagen and Heck [81]	27.3	67.9	30.4	62.3	Adiabatic; C/S/H,V; Water, hydrocarbons, Air/water, water/argon, air/oil, R11, R12, R22, argon, nitrogen, neon, air/water/carboxyl methyl cellulose; $D_H$ : 4–392 mm; 9313 data points
Xu and Fang [82]	69.1	47.4	44.9	52.8	Evaporation; C,R,F,S,M/H,V; R11, R12, R134a, R22, R32/R125, R123, CO <sub>2</sub> , R407C, R410A, R404A, R507, R507A, R417A, ammonia, $D_H$ : 0.81–19.1 mm; $p_r$ : 0.36–0.54; G: 25.4–1150 kg/m <sup>2</sup> s; 2622 data points
Sempértegui-Tapia and Ribatski [83]	36.7	51.7	39.4	49.8	Adiabatic; C,R,T,S/H; R134a, R1234yf, R1234ze(E), R600a; $D_H$ : 0.634–1.1 mm; $p_r$ : 0.11–0.31; G: 100–1600 kg/m <sup>2</sup> s; 1468 data points
Tibiriçá et al. [84], v.1	32.1	63.9	38.7	53.5	Adiabatic/Evaporation; C,R,T,S,M/H; R12, R134a, R22, R404A, R410A, R236fa, air/water, CO <sub>2</sub> , R290, R245fa, R1234ze(E), R1234yf, R600a, ammonia; $p_r$ : 0.05–0.54; $D_H$ : 0.509–3.25 mm; G: 100–7700 kg/m <sup>2</sup> s; 1076 data points
Tibiriçá et al. [84], v.2	31.9	63.9	38.9	53.3	

C: Circular; R: Rectangular; F: Flattened; T: Triangular; S: Single-channel; M: Multi-channels; H: Horizontal; V: Vertical. \*192 data points were excluded from the comparison with the homogeneous method proposed by Ducoulombier et al. [47]. Statistical parameters given in %.

The methods for predicting two-phase frictional pressure drop were segregated as follows: based on the homogeneous model, based on two-phase multipliers, and based on empirical correlations. The statistical results of the comparisons between these methods and the described database are shown in Table 2, represented by the mean absolute percentage error (MAPE) and the percentage of the database that was predicted with an error margin of 30% ( $\lambda_{30\%}$ ). The statistical results presented in Table 2 are divided in two columns: considering the whole  $p_r$  range, and only for  $p_r \geq 0.5$ . Table 2 also describes the experimental conditions for which the methods were developed.

The methods based on the homogenous model adopt different correlations for the friction factor, some of which consider the surface roughness, a parameter that in general was not informed by the authors in the studies listed in Table 1. Therefore, in the present paper, these surface roughness-based friction factor correlations were replaced by the Blasius [68] correlation for turbulent regime ( $Re_{20} > 2000$ ). In the case of laminar flow, the Hagen-Poiseuille theory and Shah and London [85] correlation were adopted for circular and rectangular channels, respectively. It should be remarked that 192 data points were not compared against the homogeneous method proposed by Ducoulombier et al. [47], since the calculated pressure gradients were negative. Therefore, the statistical results presented in Table 1 for this method consider only the data points for which comparisons were possible. These authors adjusted a two-phase viscosity correlation based

on their own CO<sub>2</sub> pressure drop data ( $p_r = 0.36 – 0.54$ ), which includes the reduced pressure effect. However, for  $p_r > 0.675$ ,  $\mu_{20}$  and the pressure gradient become negative.

According to Table 2, seven of eight methods based on the homogeneous model predicted the database with MAPE lower than 33%. The only exception was the correlation proposed by Ducoulombier et al. [47], for which the MAPE was 57.2%, even though it presented the largest parcel of data predicted within error bands of  $\pm 30\%$ . The high MAPE given by this method is associated with the overprediction of data acquired at low reduced pressures, conditions for which the calculated two-phase viscosity is unusually high. Fig. 4 compares the  $\mu_{20}$  extracted from the R245fa frictional pressure drop experimental data of Adams et al. [44] and Charnay et al. [21] with various two-phase viscosity models adopted in different works listed in Table 2. The significant overestimation of the two-phase viscosity at low-pressure using the method proposed by Ducoulombier et al. [47] is evident in Fig. 4(a). Nevertheless, when  $p_r$  is increased, the two-phase viscosities calculated by this method approaches those of Cicchitti et al. [70], as seen in Fig. 4(b).

As indicated in Table 2, all the homogeneous-based methods evaluated showed higher accuracy for  $p_r \geq 0.5$  in comparison with  $p_r < 0.5$ . This result is consistent with the homogeneous model hypothesis of not accounting for the slipping ratio between liquid and vapor phases, which is lower at high  $p_r$  due to the approximation between  $\rho_l$  and  $\rho_v$  [21,47]. Fig. 5 presents the MAPE dis-

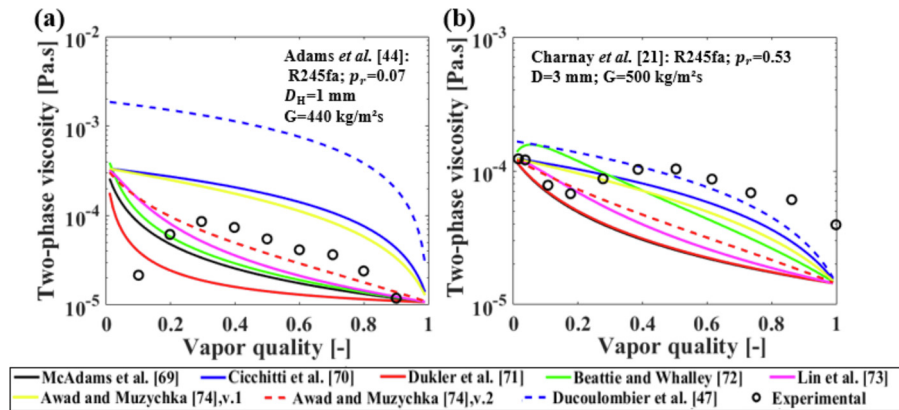


**Fig. 4.** Comparison between the two-phase viscosities calculated according to the homogeneous model considering different two-phase viscosity definitions and experimental data extracted from (a) Adams et al. [44] and (b) Charnay et al. [21].

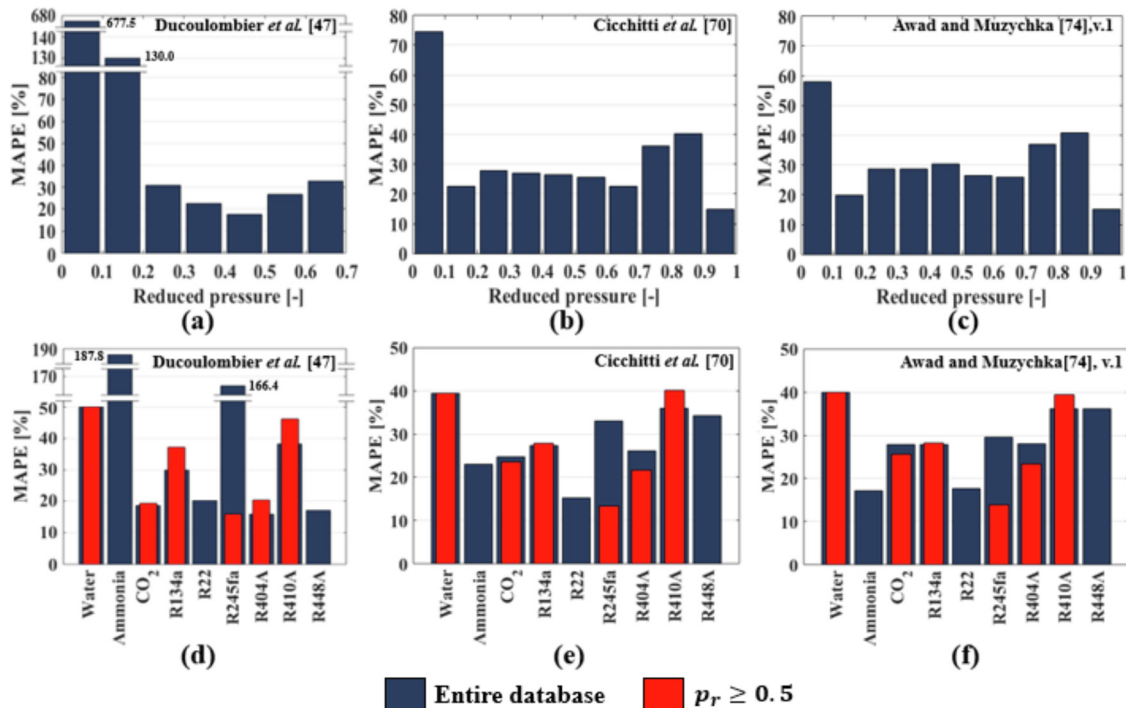


**Fig. 5.** MAPE distribution for the methods of (a,d) Ducoulombier et al. [47], (b,e) Cicchitti et al. [70] and (c,f) Awad and Muzychka [74], v.1 according to (a,b,c) reduced pressure and (d,e,f) working fluid.

tributions according to  $p_r$  and test fluids for the three methods based on the homogeneous model that were able to predict the largest parcel of data within error bands of 30% [47,70,74]. All the ammonia experimental data are within the reduced pressure range of 0.1 – 0.2, while 20% of R245fa experimental results correspond to  $0 < p_r < 0.1$ , which justifies the high inaccuracy of the method of Ducoulombier et al. [47] for these fluids. High deviations at low  $p_r$  are also verified for the other two methods [70,74], as shown in Fig. 5(b) and (c).

In general, the reduced pressure effect on the accuracy of the methods based on the homogenous model was less pronounced at  $0.2 < p_r \leq 0.7$ , as shown in Fig. 5(a-c). For  $p_r \geq 0.7$ , the 169 experimental results included in the database were extracted from only 3 studies [42,52,53]. Fifteen R134a experimental data from Vijayarangan et al. [42] fall within the  $p_r$  range of 0.7 – 0.8, while 60 data points are in the near-critical pressure region ( $0.8 \leq p_r < 1$ ). High MAPEs (32.5%–40.3%) were obtained by the homogeneous-based methods when comparing with the data of Vijayarangan et al. [42] at  $0.7 \leq p_r < 0.8$ . In contrast, the near-critical data of

this study were accurately predicted by these methods, especially at  $0.9 - 1$ . It should be highlighted that the methods based on the homogeneous model were more accurate at saturation pressures approaching the critical point ( $0.9 \leq p_r < 1$ ) than two-phase multipliers or empirical methods. Mean absolute percentage errors for these methods did not exceed 16% at this  $p_r$  range, as shown in Fig. 5(b,c).

The methods based on the homogenous model were also accurate in predicting the water data at  $p_r = 0.82$  reported by Liu et al. [52], presenting MAPEs between 22.4% and 26.0%. The high mean absolute percentage errors verified at  $p_r = 0.8 - 0.9$  in Fig. 5(b,c) are associated with the underprediction of the CO<sub>2</sub> data at  $p_r = 0.88$  extracted from the study of Hammer et al. [53], with values of MAPE between 46.7% and 55.8% for these data points. However, it should be remarked that only the method proposed by Kim and Mudawar [80] predicted at least 60% of this dataset within error bands of  $\pm 30\%$ , which is unexpected, since this method was proposed for microchannels and the channel diameter in the experiments conducted by Hammer et al. [53] was 44 mm.

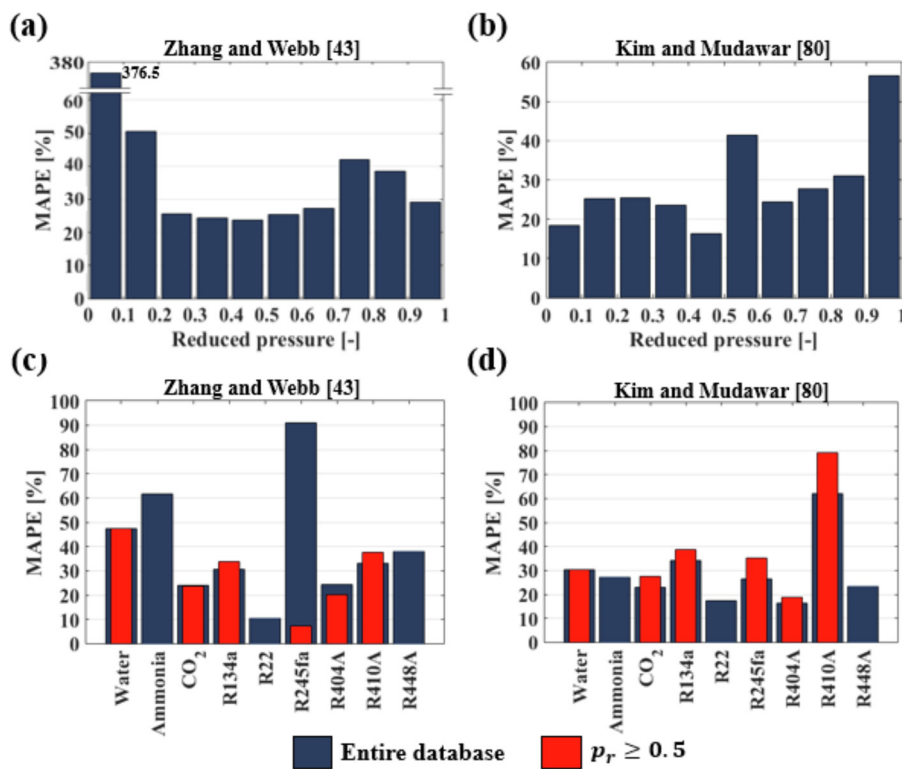


**Fig. 6.** MAPE distribution for the methods of (a,c) Zhang and Webb [43] and (b,d) Kim and Mudawar [80] according to (a,b) reduced pressure and (c,d) working fluid.

The statistical results presented in Table 2 indicate that the methods based on two-phase multipliers generally show higher deviations than the methods based on the homogenous model. The exceptions are the methods proposed by Zhang and Webb [43] and Kim and Mudawar [80], which predicted more than 60% of the database within error bands of  $\pm 30\%$ . The MAPE distributions for these methods according to  $p_r$  and test fluids are presented in Fig. 6.

A significant overprediction of the experimental data for  $p_r < 0.2$  is noted with the method of Zhang and Webb [43], as shown in Fig. 6(a), even though the reduced pressure effect was explicitly included in the calculations. As previously mentioned, most of the data points for  $p_r < 0.2$  correspond to experimental results for ammonia and R245fa, which justifies the high deviations for these fluids verified in Fig. 6(c). For  $p_r > 0.2$ , the reduced pressure effect on the Zhang and Webb [43] MAPE was similar to that previously verified in Fig. 5(b,c).

The method proposed by Kim and Mudawar [80] presented reduced MAPEs at low  $p_r$ , seen in Fig. 6(b). However, high deviations are verified in the ranges of reduced pressure of 0.5–0.6 and 0.9–1. Mean absolute percentage error increase for  $0.5 < p_r < 0.6$  is due to the overestimation of R410A data extracted from the study of Grauso et al. [49], as confirmed in Fig. 6(d). Only 8% of the database used in the development of Kim and Mudawar [80] method correspond to experimental results for R410A at  $p_r < 0.5$  flowing inside macrochannels, and no data points for near-critical conditions were considered in their database, justifying the higher MAPEs that were noticed for  $0.5 < p_r < 0.6$  and  $p_r \geq 0.9$ .

It is also important to highlight the 199.2% MAPE reduction verified in Table 2 for the two-phase multiplier method proposed by Ducoulombier et al. [47] when only data points at  $p_r \geq 0.5$  are analyzed. Although the homogeneous-based method proposed by the same authors presented lower MAPE and higher  $\lambda_{30\%}$  for  $p_r \geq 0.5$ , the two-phase multiplier approach solved the problem of negative pressure gradients at  $p_r > 0.675$ , being applicable in all  $p_r$  ranges. However, the overestimation of low reduced pressure data

was even more accentuated for the two-phase multiplier-based method, justifying the extremely high MAPE obtained by it for the entire database.

As verified in Table 2, only two strictly empirical methods, predicted more than 60% of the database within error bands of 30% [81,84], with the first one presenting the lowest MAPE of all 21 methods evaluated. Fig. 7 presents the MAPE distributions for the methods of Müller-Steinhagen and Heck [81] and Tibiriçá et al. [84], according to  $p_r$  and test fluids. Both methods presented higher deviations for  $p_r = 0 - 0.1$ , with a progressive reduction of the MAPE with increasing reduced pressure up to 0.5. At reduced pressures higher than 0.5, the method proposed by Müller-Steinhagen and Heck [81] presented slight MAPE oscillations with the variation of  $p_r$ , while the correlation of Tibiriçá et al. [84] has shown a progressive loss of accuracy with increasing the reduced pressure in the range of  $0.6 < p_r < 1$ . Considering the test fluids in Fig. 7(c,d), the highest deviations are noted for ammonia and R410A data. Curiously, the method of Müller-Steinhagen and Heck [81] presented a MAPE for CO<sub>2</sub> data only 2.4% higher than the homogeneous method of Ducoulombier et al. [47], although the first one did not consider experimental data for this fluid in its development.

In summary, only a limited parcel of the prediction methods available in the literature consider experimental results at  $p_r \geq 0.5$ , as indicated in Table 2. In general, the data points under this condition correspond to CO<sub>2</sub> and, for most of the methods, do not represent a significant parcel of the database used in their development. In addition, none of them considered near-critical pressure results. Despite this scarcity of high-pressure methods, some of them showed reasonable accuracy in predicting the database raised in the present study, with MAPEs lower than 30% and predicting more than 65% of the database within an error margin of 30%, as were the cases of the method based on the homogeneous model proposed by Cicchitti et al. [70] and the empirical method of Müller-Steinhagen and Heck [81]. Despite the lowest MAPE obtained by the second method, its accuracy for  $p_r \geq 0.5$  is lower

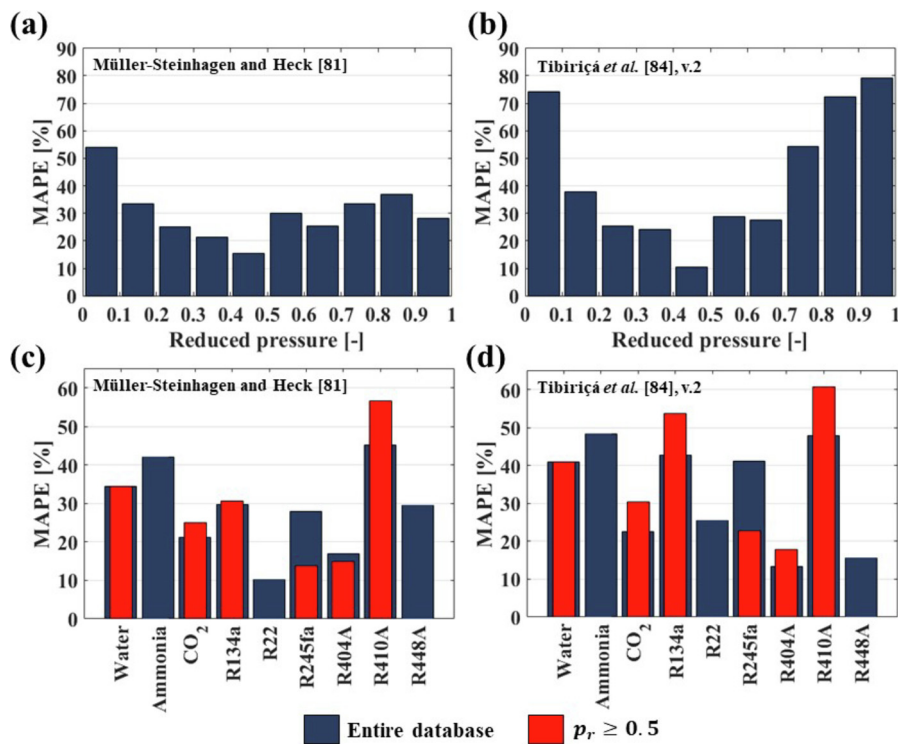


**Fig. 7.** MAPE distribution for the methods of (a,c) Müller-Steinhagen and Heck [81] and (b,d) Tibiriçá et al. [84] according to (a,b) reduced pressure and (c,d) working fluid.

than that of the homogeneous-based methods and the correlation of Zhang and Webb [43]. Based on the observed results, it is clear that the development of new methods and experimental studies at high pressures are still required.

### 3. Heat transfer coefficient

The strong effect of thermophysical properties on heat transfer makes the saturation pressure a key parameter in the heat transfer coefficient behavior. In order to clarify the effect of  $p_r$  in flow boiling heat transfer, a summary of experimental studies concerning the evaluation of heat transfer coefficient at high reduced pressures is presented in this item. Based on these studies, an extensive HTC database was collected and compared against 31 prediction methods from the literature through a statistical analysis.

#### 3.1. Analysis of experimental studies under high pressures

**Table 3** presents a summary of studies concerning the experimental evaluation of the HTC at reduced pressures higher than 0.5. The evident predominance of CO<sub>2</sub> as working fluid is associated with its low critical temperature. In addition to that, several studies presented HTC data for synthetic refrigerants, however, only three of them reported experimental results at near-critical pressures [25,33,112], all for R134a. Many studies reported HTC data for water at near-critical pressures, which is in line with the growing interest in SCWRs. Among the studies concerning synthetic refrigerants, two of them investigated low-GWP refrigerants flowing in plate heat exchangers at typical ORC evaporation temperatures [62,65]. Desideri et al. [65] suggested that R1233zd(E) is a possible substitute to R245fa in ORC evaporators due to their similar thermo-hydraulic performance, and Zhang et al. [62] reported that the HTCs evaluated for the R1234yf refrigerant were higher than those of R134a. Regarding the flow orientation, some investigations evaluated the heat transfer at intermediate slopes between horizontal and vertical [95,107,109], but none of which used synthetic

refrigerants. Considering solar thermal powered ORCs with direct evaporation [115], the heat transfer behavior in inclined channels is a relevant research topic to be further explored. Finally, in addition to the studies focused on smooth and straight channels, experimental works for near-critical water were also carried out in rifled tubes [116–118], which enhance heat transfer, and rod bundles [119,120], representing fuel assemblies used in nuclear reactors.

A total of 6376 flow boiling heat transfer coefficient experimental data points for plain tubes were extracted from forty papers presented in **Table 3**. Some studies presented wall-temperature data instead of HTC [103,105,107,109] and their results were not included in the database, since the estimation of local  $T_{sat}$  can introduce significant errors in the analysis. It is important to mention that 1623 post-CHF data points were excluded from the analysis, so the evaluated database was composed by 4753 experimental results, with 57.6% of them obtained at  $p_r \geq 0.5$ . About 96% of the database corresponds to single-channels. Regarding the geometry of the test sections, 4508, 186 and 59 data points were obtained for circular, rectangular and annular cross-sectional channels, respectively. Most of the experimental data corresponds to horizontal channels, but 266 and 85 data points for vertical and 45° inclined flow were respectively included in the database. **Fig. 8** depicts the data distribution according to reduced pressure, hydraulic diameter, mass velocity and vapor quality.

As displayed in **Fig. 8(a)**, the database comprises experimental data for water, ammonia, CO<sub>2</sub> and nine refrigerants: R125, R134a, R22, R245fa, R404A, R410A, R448A, R452A and propane. Most experimental results for  $p_r \geq 0.4$  was obtained for CO<sub>2</sub>. The shortage of near-critical pressure data is also verified, which is justified by the critical heat flux anticipation (reduction of  $x_{crit}$ ) with increasing  $p_r$ , resulting in the exclusion of several post-CHF near-critical pressure data. About 25% of the database corresponds to  $D_H < 3$  mm, as seen in **Fig. 8(b)**. However, more than 70% of this small-diameter data were obtained at  $p_r \geq 0.5$ . Therefore, it is expected that most of this database does not correspond to mi-

**Table 3**

Experimental studies concerning flow boiling heat transfer coefficient at high reduced pressures.

Authors	Shape/orientation/ n° of channels	Material	D <sub>H</sub> /L [mm]	Fluids (p <sub>r</sub> [-])	G [kg/m <sup>2</sup> s]	q'':[kW/m <sup>2</sup> ]	N*
<i>Studies at 0.5 ≤ p<sub>r</sub> &lt; 0.8</i>							
Mastrullo et al. [17]	C/H/1	SS 304	6/780	R410A (0.12-0.52), CO <sub>2</sub> (0.57)	200-350	5-20	268(239)
Charnay et al. [24]	C/H/1	SS	3/185	R245fa (0.13-0.53)	300-1000	10-50	302(275)
Hellenschmidt and Petagna [26]	C/H/1	SS	0.5-2.15/170-180	CO <sub>2</sub> (0.23-0.69)	500-1800	5-35	291
Jeong et al. [45]	R/H/3	Aluminum	2/5000	CO <sub>2</sub> (0.47-0.61)	450-750	4-12	86(82)
Lillo et al. [50]	C/H/1	SS 316	6/193.7	R448A (0.27-0.46), R404A (0.33-0.54)	150-600	10-40	232(206)
Grauso et al. [59]	C/H/1	SS	6/1200	CO <sub>2</sub> (0.57-0.64), CO <sub>2</sub> /Propane (-)	201-350	10-20.1	106(96)
Mastrullo et al. [60]	C/H/1	SS 316	6/193.7	R452A (0.31-0.65), R404A (0.33-0.42)	149-600	10-40.1	152(138)
Zhang et al. [62]	PHX/H/-	-	3.4/317	R134a (0.41-0.65), R1234yf (0.48-0.74), R1234ze(E) (0.35-0.55)	86-137	9.8-36.8	-
Oh and Son [63]	C//H/1	SS 316	4.57-7.75/4200	CO <sub>2</sub> (0.54-0.78), R22 (0.16), R134a (0.12)	200-1000	20-40	137(109)
Desideri et al. [65]	PHX/H/-	-	3.4/317	R245fa (0.35-0.64), R1233zd(E) (0.28-0.53)	62-103.5	9-37	-
Yun et al. [86]	C/H/1	SS	6/1400	R134a (0.09), CO <sub>2</sub> (0.54-0.61)	170-340	10-20	184
Yoon et al. [87]	C/H/1	SS 316	7.5/5000	CO <sub>2</sub> (0.47-0.78)	318	12.5 18.6	53(31)
Yun et al. [88]	R/H/6-10	-	1.14-1.54/-	R134a (0.09), CO <sub>2</sub> (0.54)	200-400	10-20	67(61)
Cho and Kim [89]	C,CF/H/1	-	4-7.72/5000	CO <sub>2</sub> (0.47-0.78)	212-656	6-20	179
Choi et al. [90]	C/H/1	SS	1.5-3/2000	R22 (0.14), R134a (0.10), CO <sub>2</sub> (0.61)	200-600	10-40	353(343)
Choi et al. [91]	C/H/1	SS	1.5-3/2000-3000	CO <sub>2</sub> (0.41-0.61)	200-600	10-40	30(19)
Hihara and Dang [92]	C/H/1	SS 316	2-6/-	CO <sub>2</sub> (0.54-0.69)	360-720	36	61(38)
Kim et al. [93]	C,CF/VU/1	-	4/1440	CO <sub>2</sub> (0.41-0.78)	212-530	15-45	72(56)
Oh et al. [94]	C/H/1	SS 316	7.75/5000	CO <sub>2</sub> (0.41-0.54), R22(0.12), R134a (0.09)	200-500	10-30	108
Cho et al. [95]	C,CF/+45°/1	-	4/1440	CO <sub>2</sub> (0.36-0.78)	318-530	15-60	85
Choi et al. [96]	C/H/1	SS	1.5-3/1000-2000	CO <sub>2</sub> (0.47-0.64), Ammonia (0.04-0.06), Propane (0.11-0.16)	100-600	5-70	344(309)
Del Col [97]	C/H/1	Copper	8/1000	R22 (0.27), R125 (0.39), R134a (0.19-0.29), R410A (0.49-0.50)	200-400	9-52.5	71(63)
Pamitran et al. [98]	C/H/1	SS	1.5-3/2000	CO <sub>2</sub> (0.50-0.61), Propane (0.11-0.15), Ammonia (0.04-0.05)	50-600	15-60	33(30)
Dang et al. [99]	C/H/1	SS	4-6/1500	CO <sub>2</sub> (0.69)	720	18	24(19)
Grauso et al. [100]	C/H/1	SS 304	6/780	R410A (0.19-0.52), CO <sub>2</sub> (0.57)	149-526	5-21.4	283(264)
Jiang et al. [101]	C/H/1	SS	1-2/300	CO <sub>2</sub> (0.36-0.61)	95-1335	5.7-34.2	221(137)
Billiet et al. [102]	C/H/-	SS	3/185	R245fa (0.07-0.58)	100-1000	10.9-54	155(151)
Köckert et al. [103]	C/VU/1	X5CrNi18-10	10/3100	R134a (0.27-0.69)	300-1500	50-140	-
<i>Studies at p<sub>r</sub> ≥ 0.8</i>							
Lei et al. [10]	C/H/1	SS 304	4/700	CO <sub>2</sub> (0.85-0.99)	300-400	36-137	202(25)
Pettersen [15]	C/H/25	Aluminum	0.8/500	CO <sub>2</sub> (0.47-0.87)	190-570	5-20	49(36)
Ami et al. [16]	C/H/1	SS	0.51-2/400-1850	CO <sub>2</sub> (0.68-0.91)	300	20	102(79)
Zhang et al. [25]	C/H/1	SS	10.3/2000	R134a (0.62-0.81)	300-600	20-50	238
Shen et al. [31]	C/VD,VU/1	-	17/2000	Water (0.52-0.95)	500-1000	50-418	49(33)
Shen et al. [32]	C/VU/1	Cr-Ni-Ti	19/2000	Water (0.50-0.97)	210-350	85-200	82(56)
Mawatari and Mori [33]	C/VU/1	Inconel	4.4/2000 600	R134a (0.96-0.99), R22 (0.96-0.99)	400-1000	9-48	322(26)
Gasche [104]	R/H/1	Aluminum	0.74/50.8	CO <sub>2</sub> (0.84)	58-235	1.8	49(43)
Zhu et al. [105]	C/VU/1	SS Cr-Ni-Ti	26/1000	Water (0.41-1.36)	600-1200	200-600	-
Ozawa et al. [106]	C/H/1	SS	0.51-2/400-1850	CO <sub>2</sub> (0.68-0.91)	300-900	25-40	146(110)
Gang et al. [107]	C/+20°/1	SS Cr-Ni-Ti	26/2000	Water (0.41-1.27)	600-900	300-600	-
Wang et al. [108]	A/VU/1	SS Cr-Ni	12/1400	Water (0.50-0.86)	350-1500	200-600	117(59)
Wang et al. [109]	C/VD,-45°/1	-	20/2000	Water (0.52-1.02)	450-1000	101-418	-
Zahlan et al. [110]	C/VU/1	Inconel	8-22/1940-2000 600/625	CO <sub>2</sub> (0.89-0.95)	200-2000	48-160	147(36)
Eter et al. [111]	C/VU/1	Inconel	8/1940 600	CO <sub>2</sub> (0.88-0.96)	497-2004	59.8-279.9	343(0)
Guo et al. [112]	C/H/1	Copper	10/2000	R134a (0.10-0.88), R245fa (0.11-0.31), R134a/R245fa (-)	100-318	6-24	319(260)
Keniar et al. [113]	C/H/1	Copper	1.55/300	CO <sub>2</sub> (0.70-0.81)	100-500	15-72	128(128)
Lei et al. [114]	C/H/1	SS 304	5/730	CO <sub>2</sub> (0.84-0.97)	100-190	34.3-105	186(111)

A: Annular; C: Circular smooth; CF: Circular finned; PHX: Plate heat exchanger; R: Rectangular; H: Horizontal; VU: Vertical upward; VD: Vertical downward; SS: Stainless steel; N: Quantity of data points extracted \*(the number inside parentheses indicate the number of pre-CHF data).

crochannels, given the effect of  $p_r$  on the macro to micro-scale transition, previously discussed. Fig. 8(c) reveals that about 80% of the data points correspond to  $G$  lower than 600 kg/m<sup>2</sup>s, and Fig. 8(d) shows lower data concentration at high  $x$ , which is linked to the exclusion of post-CHF experimental results, since most predictive methods are not applicable at this condition. It is important to mention that the evaluated heat fluxes varied between 1.8 and 600 kW/m<sup>2</sup>, but only 250 of the 4753 data points fall within the range of  $q'' > 60$  kW/m<sup>2</sup>. Fifty-five percent of these 250 exper-

imental points correspond to water data, which has high  $i_{lv}$  and demands higher heat fluxes to achieve the same vapor quality as other fluids at the same mass flux.

Experimental results of the studies presented in Table 3 show that HTC augmentation is usually observed with increments in heat flux and reduced pressure, regardless of the conditions. Different heat transfer coefficient trends with vapor quality variation were identified for pre-CHF conditions and classified in three main groups: no influence, decreasing, and increasing behaviors.

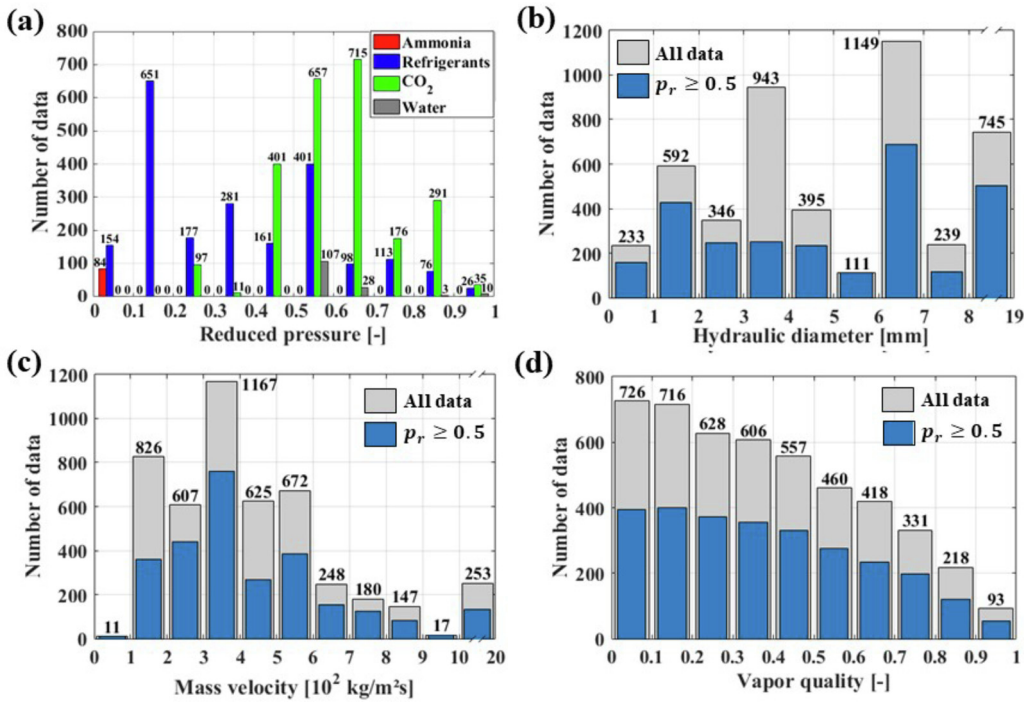


Fig. 8. Heat transfer coefficient data distribution against (a) reduced pressure, (b) hydraulic diameter, (c) mass velocity and (d) vapor quality.

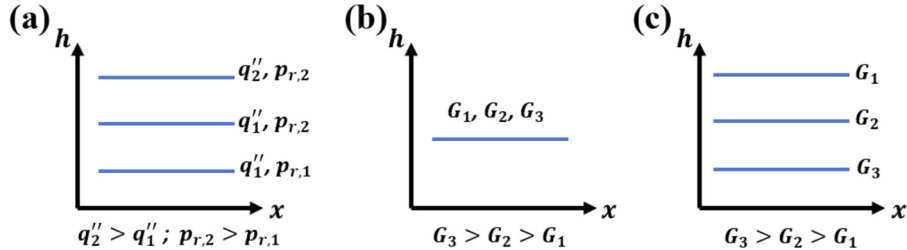


Fig. 9. Invariable HTC with vapor quality showing (a) enhancement effects of heat flux and reduced pressure, (b) negligible effects of mass velocity, and (c) deterioration with mass velocity.

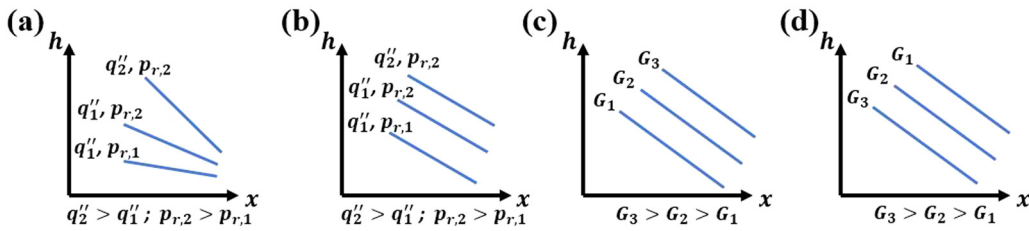
The most frequently reported behavior was the invariability of HTC with rising vapor quality that can be attributed to the domination of nucleate boiling effects, especially at near-critical pressures. Decreases in surface tension and enthalpy of vaporization at higher  $p_r$  diminish the required near-wall liquid superheating for bubble nucleation, increasing the number of active nucleation sites at the surface [19] and, consequently, enhancing nucleate boiling [97,109]. In addition, as the working pressure increases, the vapor phase velocity is reduced due to its rising density, so the convective effects become less relevant, justifying the invariability of the HTC. Fig. 9 illustrates the effects of reduced pressure, heat flux and mass velocity pointed out in the literature among studies that reported uniformity of HTC with  $x$ .

The intensification of nucleation due to the easier activation of nucleation sites results in enhancements of the heat transfer coefficient with increasing  $p_r$  and  $q''$  [15,26,31,32,59,63, 88,92,99,101,102,106,108,112–114] shown in Fig. 9(a). In contrast with this general behavior, Lei et al. [114] verified the HTC reduction with increasing  $q''$  and  $p_r$ , but have not discussed the reasons for the unexpected effects. Nevertheless, it can be speculated that at the range of experimental conditions they evaluated ( $0.84 \leq p_r \leq 0.95$ ), the temperature of the liquid near the heated surface approached  $T_{crit}$  implying in sudden variations of the thermophysical properties. Another common effect that is related to the dominance of nucleate boiling effects is the negligible influence of mass

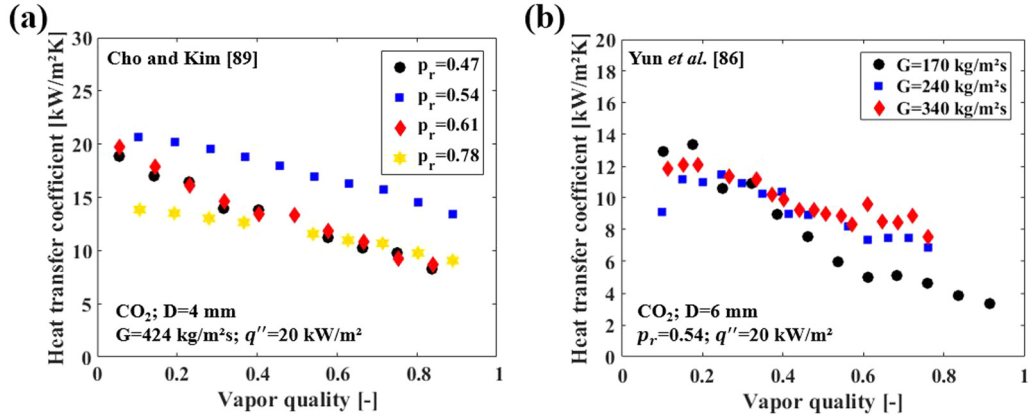
velocity depicted in Fig. 9(b) [15,32,88,92,106,108,112], but reductions with increasing  $G$  as seen in Fig. 9(c) were also documented [113,114], and could be related to the thinning of liquid film in annular flow pattern, suppressing bubbles nucleation.

Fig. 10 shows distinct decreasing patterns of HTC with vapor quality [15,24,25,86,97,102], relating the effects of mass velocity, heat flux and reduced pressure in this behavior. The decreasing behavior was commonly reported at high reduced pressures and at low mass velocities, which is in accordance with the flow boiling map proposed by Kandlikar [121], which shows a decreasing behavior associated with low  $\frac{\rho_l}{\rho_v}$  and high Boiling numbers ( $Bo = \frac{G''}{G_{lv}}$ ), directly related to high  $p_r$  and low  $G$ . The increase of the channel diameter also favored the occurrence of this behavior, which can be linked to the premature dryout of the liquid film at the upper region of the channel due to higher significance of gravitational effects, reducing the perimeter-averaged HTC [86]. A decreasing HTC behavior for a vertical channel was reported by Kim et al. [93] and, since there is no gradual drying of the tube perimeter in this case, the HTC reduction with vapor quality is probably related to the suppressed nucleation activity that occur in thinner liquid films under annular flow conditions.

As well as for the constant trend, rises in  $q''$  and  $p_r$  increased the heat transfer coefficient. Typically, the HTC increase was more pronounced at low vapor qualities [15,24,25,59,86,87,89,101], as



**Fig. 10.** Decreasing HTC with vapor quality showing enhancements with reduced pressure and heat flux that are (a) more pronounced at low vapor qualities or (b) constant for varying vapor qualities and (c) increasing or (d) decreasing effects of mass velocity.



**Fig. 11.** Non-monotonic effect of the reduced pressure and the mass velocity on the HTC reported by (a) Cho and Kim [89] and (b) Yun et al. [86].

seen in Fig. 10(a), due to stronger contribution of nucleate boiling effects. However, some experimental results presented the behavior shown in Fig. 10(b), with the maintenance of  $q''$  and  $p_r$  effects even at intermediate and high  $x$  [24,59,94]. Non-monotonic effects of  $p_r$  were also noticed in some investigations that observed decreasing HTC patterns [87,89,91], specially at low vapor qualities. As seen in the experimental data of Cho and Kim [89] presented in Fig. 11(a), when the reduced pressure rises from 0.47 to 0.54 there is an augmentation of HTC, while an opposite trend is verified for further increases of the reduced pressure up to 0.78. Although at higher  $p_r$  the reduction of  $\sigma$  and  $i_{lv}$  intensify the nucleate boiling, it is possible that the reduction of the liquid phase viscosity decreases the liquid film thickness, consequently suppressing nucleation [91]. Therefore, when the effect of  $\mu_l$  is more pronounced than that of  $\sigma$  and  $i_{lv}$ , the HTC is reduced with increasing  $p_r$ . It should be noted that all three studies that reported this behavior used  $\text{CO}_2$  as working fluid, and the HTC reduction with increasing  $p_r$  started at reduced pressures around 0.5.

Different mass velocity effects were reported in works with the decreasing HTC behavior, as depicted in Fig. 10(c) and (d). Increases in mass velocity could either result in augmentation [25,59,89] or deterioration [24,102] of the HTC, and in some cases non-monotonic effects were observed [86,94], especially at low  $x$ . Fig. 11(b) presents the experimental data of Yun et al. [86], showing the lowest values of HTC for  $x \leq 0.2$  occurring at the intermediate mass velocity. The divergence of the mass velocity effects may be associated with the occurrence or not of premature dryout at the upper region of the channel and with the vapor quality in which it would happen, e.g. if decrease in mass velocity resulted in the formation of dry patches higher  $G$  would enhance the overall HTC, but the suppression of bubble nucleation that can occur at high mass velocities would be related to the deterioration of heat transfer. Finally, some studies reported experimental results characterized by a decreasing HTC behavior at low vapor qualities followed by an invariability trend at intermediate  $x$  [17,24,50,86,100,102]. In general, this behavior occurred

at higher mass velocities than those of the strictly decreasing trend.

The last HTC trend that was identified is crescent with vapor quality, which could happen in "U-shaped curves" [122] or strictly increasing behaviors, as shown in Fig. 12. Such behavior is usually related to the domination of convective boiling effects at higher vapor quality, and even though these HTC patterns are most commonly verified at  $p_r < 0.5$ , some works also reported it at  $p_r \geq 0.5$  [17,24,90,91,96,98,100]. The pattern presented in Fig. 12(a) and (b), is characterized by a moderate HTC decrease at the beginning of the evaporation process, which is associated with the bubble nucleation frequency reduction, as a consequence of the liquid film shrinkage. With increasing  $x$ , convective boiling effects prevail over nucleate boiling, hence the vapor phase velocity enhances the HTC at moderate and high  $x$ . In some cases, the initial decreasing behavior of the HTC was negligible, showing an almost constant pattern at low  $x$  [90,91,96,97].

Usually, it is observed that  $q''$  and  $p_r$  reductions and mass velocity increases anticipate the suppression of nucleate boiling effects in the "U-shaped" heat transfer coefficient behavior [24,90,91,96,97], as indicated in Fig. 12(a) and (b), respectively. This effect is seen in Kandlikar's flow boiling map [121], in which the boiling number reduction and  $\frac{\rho_l}{\rho_v}$  increase anticipate the nucleate boiling suppression, which is expected due to the higher velocities and thinning of liquid films. Thus, the beginning of the increasing behavior occurred at lower vapor qualities, and in some cases during the entire evaporation process preceding the CHF, as depicted in Fig. 12(c) and (d). In general, increments of the reduced pressure, heat flux and mass velocity enhance the HTC in cases with patterns illustrated by Fig. 12. However, due to the significance of nucleate boiling effects,  $p_r$  and  $q''$  present a stronger influence on the HTC at low vapor qualities, while the mass velocity effect is more pronounced at high  $x$ , in which the heat transfer is dominated by convective effects. As also reported for other trends, some cases with contrasting tendencies were found, like the data reported by Shen et al. [31] at  $p_r = 0.93$  that indicated a decrease

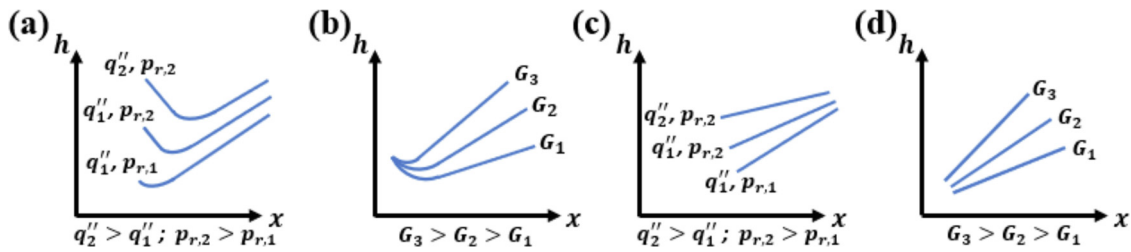


**Fig. 12.** U-shaped HTC patterns showing enhancements with (a) heat flux and reduced pressure, and (b) more pronounced increases of mass velocity at high vapor qualities, and increasing HTC with vapor quality showing more pronounced increases with (c) heat flux and reduced pressure at low vapor qualities and with (d) mass velocity at high vapor qualities.

of HTC for higher  $q''$ . As already discussed, this may be associated with sudden variations of fluid properties due to the near-critical pressure, which is supported by the fact that this unusual heat flux effect was not verified at the reduced pressure of 0.52 [31].

A number of authors have evaluated the channel diameter effect on the HTC, but only a few of them have studied it for  $p_r \geq 0.5$  [16,26,63,92,98,99,106,110]. Except for a few results from Ami et al. [16] and Hellenschmidt and Petagna [26], the reduction of tube diameter increased the heat transfer coefficient at all vapor qualities. According to Pamitran et al. [98], as the tube diameter decreases, the ratio of the contact surface area for heat transfer to the internal volume of the tube increases, intensifying nucleation density. This behavior is in agreement with the higher nucleate boiling contribution on HTC verified in several prediction methods based on the superposition of convective and nucleate boiling effects [123–125]. In addition, even though small diameter channels are related to thinner liquid films that can induce the suppression of nucleation activity, Oh and Son [63] claim that, the reduced thickness and uniform distribution of the liquid film along the perimeter of small diameter tubes, improves the heat conduction on it.

It should be highlighted that significant divergences could be identified when comparing HTC data at high  $p_r$  from different studies under similar experimental conditions, which can be seen in Fig. 13. For instance, the HTC decrement with increasing  $x$  is more pronounced in the dataset acquired by Yoon et al. [87] than by Oh et al. [94], even at slightly lower  $q''$  and higher  $G$ , as seen in Fig. 13(a). Another example is seen in Fig. 13(b), where some results from Yun et al. [86] and Grauso et al. [59] for  $x > 0.4$  have reasonable similarity, but at lower vapor qualities the HTCs measured by the first authors are up to 60% higher. Even more significant divergences are verified in Fig. 13(c), comparing the data obtained by Yun et al. [86] and Mastrullo et al. [17], with the latter reporting HTCs almost 130% higher than the first ones. It is also important to highlight the different HTC behaviors verified in these data, with a strictly decreasing behavior reported by Yun et al. [86], and a U-shaped pattern documented by Mastrullo et al. [17].

The most significant divergences were verified between the HTCs reported by Zhang et al. [25] and Guo et al. [112] data for R134a and are presented in Fig. 13(d). Differences of up to 350% between the calculated HTCs are noted, with a strictly-increasing behavior verified by Guo et al. [112] at vapor qualities preceding the CHF and a predominantly decreasing behavior reported by Zhang et al. [25], who identified dry patches at the upper region of the channel during their experiments, justifying the decreasing behavior. In contrast, Guo et al. [112] only indicate the occurrence of liquid film dryout for vapor qualities higher than 0.8, a discrepancy that can be related to surface morphology and material characteristics. It is important to remark that the experiments of Zhang et al. [25] were conducted on a stainless-steel tube directly heated by Joule effect, while Guo et al. [112] used a copper tube with a heating wire at the outside diameter of the tube, and part of the observed divergence could also be caused by distinct approaches in

data reduction procedures and calculation of heat losses. In addition, it is noteworthy that some pool-boiling HTC prediction methods include the effect of the substrate thermal effusivity ( $\sqrt{k \cdot \rho \cdot c}$ ) [126]. As the thermal effusivity of copper is about 4 times higher than that of stainless-steel, higher HTCs would be expected for the first material. However, according to the correlation of Stephan and Abdelsalam [126], a maximum increase of 44% in HTC is estimated due to copper effusivity compared to stainless steel; moreover, under flow boiling conditions, this effect should be even smaller. Differences in surface roughness could also contribute to the discrepancy between the HTCs measured by these authors. As this parameter was not informed, it is not possible to discuss its influence, however, it is speculated that it is also not enough to justify HTC differences higher than 350% between these studies. The influence of the heated surface characteristics on flow boiling heat transfer is widely investigated at low  $p_r$ , and it should be further explored at high reduced pressures.

### 3.2. Comparison of prediction methods with experimental results

The raised database was compared to twenty-seven flow boiling and four pool boiling prediction methods from the literature. Since only a few of these methods are applicable at post-CHF conditions [84,124,125,127,128], data points for  $x \geq x_{crit}$  were excluded from the analysis. The critical heat flux was quantified by a sudden drop in the derivative of the heat transfer coefficient with respect to the vapor quality ( $dh/dx$ ) corresponding to reductions of 15% or greater for  $x$  increments of 0.1 or lower. This procedure was adopted because it avoids the exclusion of data points that presented decreases in HTC compatible to the experimental uncertainties of their measurements. Four classes of flow boiling methods were defined: strictly empirical, based on superposition of convective and nucleate boiling effects, based on the energy dissipation theory and phenomenological models. The statistical analysis of the obtained results is summarized in Table 4, as well as the respective range of conditions for which each method was developed. The pool-boiling correlations that were evaluated were the ones proposed by Cooper [144], Yun et al. [145], Cheng et al. [146] and Yagov [19]. The parcel of the database predicted by them within error bands of  $\pm 30\%$  were, 47.5%, 43.7%, 51.6% and 39.9%, respectively. It was identified that the first three correlations presented higher accuracy for small diameter data, with 60.1%, 56.4%, 63.9% of the data points for  $D_H < 3$  mm predicted within error bands of  $\pm 30\%$ , respectively. This might be associated with the nucleate boiling intensification in small diameters, but these methods showed no relevant increase in accuracy with rising  $p_r$  or reducing  $x$ , conditions in which nucleate boiling effects are pronounced.

Due to the large number of evaluated methods, only those that presented lower deviations are discussed in detail. Fig. 14 presents the MAPE distributions according to test fluid for the methods that predicted the largest parcel of data within error bands of  $\pm 30\%$  [123,125,140] and that presented the lowest MAPEs considering

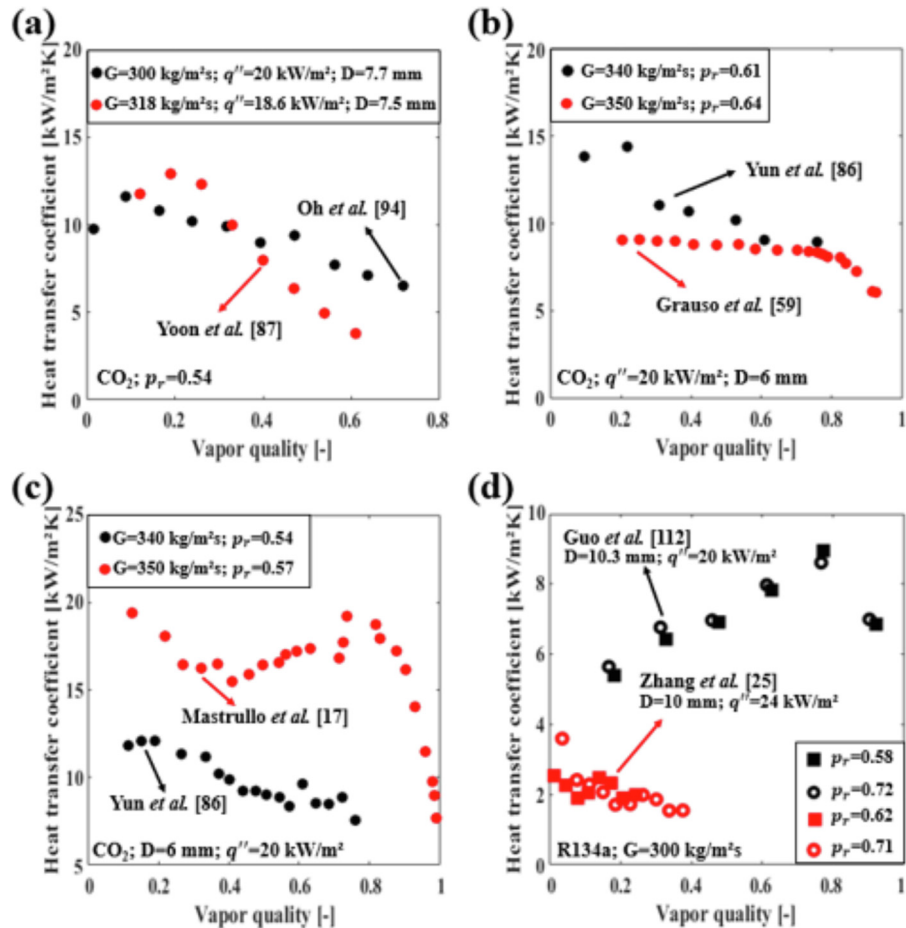


Fig. 13. Comparison between datasets of heat transfer coefficient obtained in different studies under similar experimental conditions.

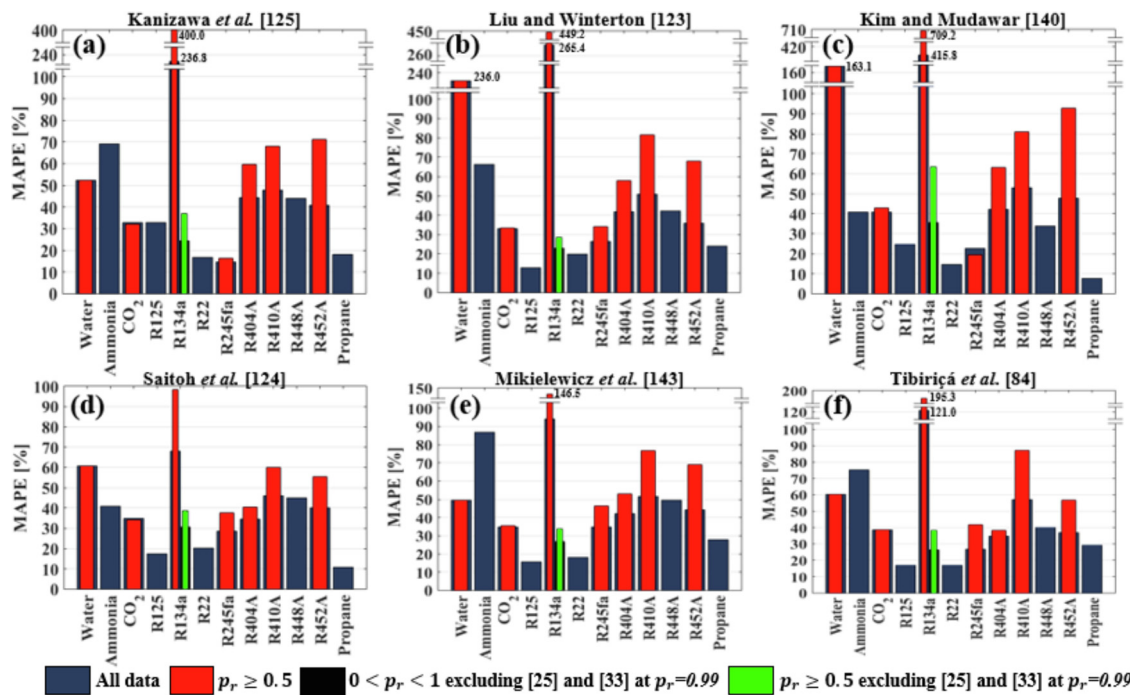


Fig. 14. MAPE distribution according to working fluid for the methods of (a) Kanizawa et al. [125], (b) Liu and Winterton [123], (c) Kim and Mudawar [140], (d) Saitoh et al. [124], Mikielewicz et al. [143] and (f) Tibiriçá et al. [84].

**Table 4**

Statistical analysis of the comparison between heat transfer coefficient database and flow boiling prediction methods, indicating the experimental conditions for which they were developed.

Authors	$0 < p_r < 0.5$		$p_r \geq 0.5$		Test conditions or application ranges
	MAPE	$\lambda_{30\%}$	MAPE	$\lambda_{30\%}$	
<b>Strictly Empirical Methods:</b>					
Kew and Cornwell [12]	71.2	50.7	101.4	44.4	C,R/S/H; R141b; $D_H$ : 1.39-3.69 mm; 697 data points
Shen et al. [32]	306.4	33.1	501.0	33.7	C/S/V; Water; $D_H$ : 19 mm; $p_r$ : 0.5-0.97; G: 170-800 kg/m <sup>2</sup> s; $q''$ : 85-505 kW/m <sup>2</sup>
Tibiriçá et al. [84]	48.8	50.9	62.7	41.8	C,R/S,M/H,V; $D_H$ : 0.38-3 mm; Water; R134a, R236fa, R245fa, R410A, R22, R290, R1234ze(E), R600a, R1234yf, CO <sub>2</sub> ; $p_r$ : 0.005-0.61; G: 23.4-1290 kg/m <sup>2</sup> s; $q''$ : 4.8-391 kW/m <sup>2</sup> ; 3902 data points
Keniar et al. [113]	58.0	41.2	71.7	46.2	C/S/H; CO <sub>2</sub> ; $D_H$ : 1.55 mm; $p_r$ : 0.7-0.81; G: 100-500 kg/m <sup>2</sup> s; $q''$ : 15-72 kW/m <sup>2</sup> ; 128 data points
Lazarek and Black [129]	66.0	48.0	91.6	43.6	C/S/V; R113; $D_H$ : 3.1 mm; $p_r$ : 0.04-0.12; G: 125-750 kg/m <sup>2</sup> s; $q''$ : 14-380 kW/m <sup>2</sup> ; 728 data points
Tran et al. [130]	278.6	36.0	442.0	33.6	C,R/S/H; R12, R113; $D_H$ : 2.4-2.92 mm; $p_r$ : 0.045-0.20; G: 44-832 kg/m <sup>2</sup> s; $q''$ : 3.6-129 kW/m <sup>2</sup> ; 296 data points
Sun and Mishima [131]	78.8	46.7	107.6	40.0	C,R/S,M/H,V; R11, R12, R123, R134a, R141b, R22, R404A, R407C, R410A, CO <sub>2</sub> , water; $D_H$ : 0.21-6.5 mm; $p_r$ : 0.005-0.61; G: 44-1500 kg/m <sup>2</sup> s; $q''$ : 5-109 kW/m <sup>2</sup> ; 2505 data points
<b>Methods based on the superposition of effects:</b>					
Choi et al. [91]	116.3	50.8	170.2	41.6	C/S/H; CO <sub>2</sub> ; $D_H$ : 1.5-3 mm; $p_r$ : 0.36-0.61; G: 200-600 kg/m <sup>2</sup> s; $q''$ : 20-40 kW/m <sup>2</sup> ; 471 data points
Del Col [97]	60.4	52.2	79.8	46.6	C/S/H; R134a, R22, R125, R410A; $D_H$ : 8 mm; $p_r$ : 0.19-0.53; G: 200-600 kg/m <sup>2</sup> s; $q''$ : 9-53 kW/m <sup>2</sup> ; 108 data points
Billiet et al. [102]	103.8	53.8	155.7	43.2	C/S/H; R245fa; $D_H$ : 3 mm; $p_r$ : 0.07-0.58; G: 100-1000 kg/m <sup>2</sup> s; $q''$ : 10-50 kW/m <sup>2</sup> ; 1214 data points
Liu and Winterton [123]	69.2	59.0	99.9	51.9	C/S,H,V; Water, R12, R22, R11, R113, R114, ethylene glycol, n-butanol, ethanol; $D_H$ : 2.95-32 mm; $p_r$ : 0.002-0.895; G: 12.4-8179.3 kg/m <sup>2</sup> s; $q''$ : 348.9-2620 kW/m <sup>2</sup> ; 4202 data points
Saitoh et al. [124]	39.2	46.6	45.8	40.1	C/S/H; R134a; $D_H$ : 0.5-10.9 mm; 2224 data points
Kanizawa et al. [125]	58.0	61.0	81.2	53.2	C/S/H; R134a, R245fa, R600a; $D_H$ : 0.38-2.6 mm; $p_r$ : 0.04-0.27; G: 49-2200 kg/m <sup>2</sup> s; $q''$ : 5-185 kW/m <sup>2</sup> ; 2047 data points
Shah [132]	50.8	40.7	65.1	29.7	C,A/S/H,V,I; Water, R12, R22, R113, cyclohexane; $D_H$ : 6-25.4 mm; $p_r$ : 0.004-0.15; G: 72-1383 kg/m <sup>2</sup> s; $q''$ : 1.26-787.5 kW/m <sup>2</sup> ; 780 data points
Gungor and Winterton [133]	54.1	46.9	71.8	37.1	R11, R12, R22, R113, R114, water; 3693 data points
Jung et al. [134]	100.2	52.5	151.7	44.7	C/S/H; R12, R152a, R22, R114, R500; $D_H$ : 9 mm; $p_r$ : 0.08; G: 250-720 kg/m <sup>2</sup> s; $q''$ : 10-45 kW/m <sup>2</sup> ; 1588 data points
Kandlikar and Balasubramanian [135]	57.0	39.4	75.3	30.8	C/S/H; R113, R141b, R123; G: 50-570 kg/m <sup>2</sup> s; $q''$ : 8.8-90.7 kW/m <sup>2</sup> *
Ozawa et al. [137]	122.0	42.0	182.3	37.2	C/S/H; CO <sub>2</sub> ; $D_H$ : 2 mm; $p_r$ : 0.68-0.91; G: 200-500 kg/m <sup>2</sup> s; $q''$ : 5-35 kW/m <sup>2</sup>
Ducoulombier et al. [138]	120.0	44.1	173.8	39.1	C/S/H; CO <sub>2</sub> ; $D_H$ : 0.529 mm; $p_r$ : 0.36-0.47; G: 200-1200 kg/m <sup>2</sup> s; $q''$ : 10-30 kW/m <sup>2</sup> ; 2710 data points
Yagov et al. [139]	75.7	50.5	110.5	37.0	C,R,F,S,M/H,V; CO <sub>2</sub> , water, helium, nitrogen, R22, R410A; $D_H$ : 0.6-18 mm; $p_r$ : 0.12-0.87; G: 44-5139 kg/m <sup>2</sup> s
Kim and Mudawar [140]	88.2	54.1	134.4	44.1	C,R/S,M/H,V; FC72, R11, R113, R123, R1234yf, R1234ze, R134a, R152a, R22, R236fa, R245fa, R32, R404A, R407C, R410A, R417A, CO <sub>2</sub> , water; $D_H$ : 0.19-6.5 mm; $p_r$ : 0.005-0.69; G: 19-1608 kg/m <sup>2</sup> s; 10805 data points
Shah [141]	50.4	41.5	64.5	30.7	C,R,T,S,M/H,V; 30 fluids including water, CO <sub>2</sub> , halocarbon refrigerants, hydrocarbons and cryogens; $D_H$ : 0.38-27.1 mm; $p_r$ : 0.005-0.79; G: 15-2437 kg/m <sup>2</sup> s; 4852 data points
<b>Energy dissipation methods:</b>					
Mikielewicz [142]	92.3	53.6	137.5	44.3	C/S,M/H,V; R11, R12, R123, R21, R22; $D_H$ : 6.4-23 mm; $p_r$ : 0.01-0.22; G: 80-4500 kg/m <sup>2</sup> s; $q''$ : 2.4-95 kW/m <sup>2</sup>
Mikielewicz et al. [143]	44.8	50.2	53.9	46.3	C,R,S,M/H,V; R11, R113, R12, R123, R141b, R134a, R22; $D_H$ : 1.1-25 mm; $p_r$ : 0.01-0.2; G: 30-1800 kg/m <sup>2</sup> s; $q''$ : 0.6-200 kW/m <sup>2</sup> ; 2760 data points
<b>Phenomenological models:</b>					
Zhang et al. [25]	62.0	14.7	67.3	12.3	C/S/H; R134a; $D_H$ : 10.3 mm; $p_r$ : 0.62-0.81; G: 300-600 kg/m <sup>2</sup> s; $q''$ : 20-50 kW/m <sup>2</sup> ; 270 data points
Wojtan et al. [127]	75.3	51.0	103.7	48.0	C/S/H; R22, R410A; $D_H$ : 8-13.84 mm; $p_r$ : 0.11-0.19; G: 70-700 kg/m <sup>2</sup> s; $q''$ : 2-57.5 kW/m <sup>2</sup> ; 1250 data points
Cheng et al. [128]	80.1	43.6	104.3	44.8	C,R,T,S,M/H; CO <sub>2</sub> ; $D_H$ : 0.6-10 mm; $p_r$ : 0.21-0.87; G: 50-1500 kg/m <sup>2</sup> s; $q''$ : 1.8-46 kW/m <sup>2</sup> ; 1124 data points

\*Experimental conditions of the new data used by the authors to update the original method of Kandlikar [136], which was proposed for 10 different fluids. C: Circular; R: Rectangular; F: Flattened; T: Triangular; S: Single-channel; M: Multi-channels; H: Horizontal; V: Vertical; I: Inclined. Statistical parameters in %.

the entire database [84,124,143], and it is seen that the largest deviations correspond to R134a data. In fact, only three methods [25,124,143] presented MAPEs lower than 100% for this fluid, and such deviations can be explained by the overestimation of the experimental data obtained by Mawatari and Mori [33] at  $p_r = 0.99$  and Zhang et al. [25] at  $0.62 \leq p_r \leq 0.81$ .

Considering the 26 experimental data extracted from the study of Mawatari and Mori [33], the methods proposed by Lazarek and Black [129], Kew and Cornwell [12] and Shah [141] were the most accurate in predicting the 15 experimental points at  $p_r = 0.97$

and  $G = 400$  kg/m<sup>2</sup>s, which can be verified in Fig. 15(a). However, no method predicted a single data point from the 11 results at  $p_r=0.99$  and  $G=700$  kg/m<sup>2</sup>s that were extracted with an absolute deviation lower than 192%. Fig. 15(b) presents the original graphical data from Mawatari and Mori [33] at  $G = 700$  kg/m<sup>2</sup>s. At the reduced pressures of 0.97 and 0.98, the CHF is clearly reached at subcooled vapor qualities ( $x < 0$ ), so the experimental results at these  $p_r$  were excluded from the database. However, the sudden HTC decrease is not verified at  $p_r = 0.99$ , indicating that CHF was not reached, so the data acquired at this condition were included

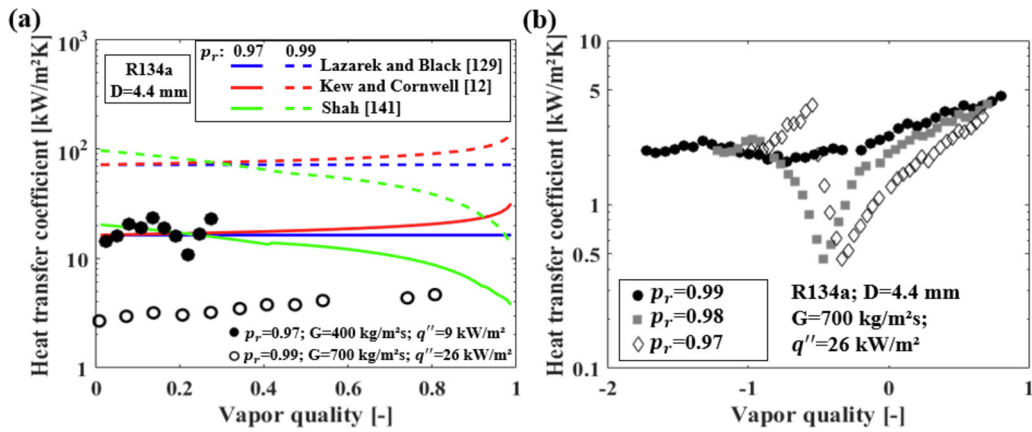


**Fig. 15.** (a) Comparison of the HTC experimental data from Mawatari and Mori [33] against prediction methods and (b) original data  $G=700 \text{ kg/m}^2\text{s}$ .

in the database. It is suggested that sharp increases in the thermal conductivity and specific heat of the vapor phase at the vicinity of the critical point result in enhanced heat transfer through the vapor film, avoiding the CHF [9].

The proximity of the liquid and vapor thermophysical properties can induce lower-than-expected HTCs at  $p_r \approx 0.99$ , since the fluid is close to the supercritical state. Nevertheless, even though some prediction methods account for an HTC reduction with increasing  $G$  when nucleate boiling effects prevail [113,124,125,137], none of them were able to predict the controversial effect of  $p_r$  or  $q''$  verified in Fig. 15(a), resulting in excessive deviations for this particular dataset. It should be highlighted, however, that this effect was also observed by Lei et al. [114] at near-critical pressures. Although the R134a experimental data extracted from Zhang et al. [25] were obtained at reduced pressures lower than 0.81, high deviations were verified for their data as well. This inaccuracy is probably associated with the reported premature partial dryout at the upper region of the channel verified at  $x < 0$ . Notwithstanding, only the prediction model proposed in this investigation was able to accurately predict their own data (MAPE=11.1%,  $\lambda_{30\%}=93.3\%$ ), while phenomenological models proposed by Wojtan et al. [127] and Cheng et al. [128], which consider different flow patterns with partial dryout, failed to predict this dataset. If the data points of Zhang et al. [25] and Mawatari and Mori [33] at  $p_r = 0.99$  were excluded from the analysis, the R134a MAPEs would be significantly reduced, as indicated in Fig. 14. Thus, it is inferred that there is no inaccuracy of the evaluated methods for this fluid, but rather for these particular experimental conditions.

High deviations are also verified in Fig. 14 for other synthetic refrigerants R448A, R404A, R410A, R448A and R452A mixtures. For the last three fluids, all the correlations shown in Fig. 14 presented MAPE increments when considering only  $p_r \geq 0.5$  data. In contrast, propane, R125 and R22 data were generally obtained at  $0.11 \leq p_r \leq 0.39$  and were accurately predicted by the methods. The accuracy of the method proposed by Kanizawa et al. [125] in predicting R245fa data ( $p_r = 0.07 - 0.58$ ) verified in Fig. 14a should be remarked, since this dataset was not considered in its development. As a comparison, only the method proposed by Billiet et al. [102] was more accurate than the one by Kanizawa et al. [125], with MAPE=12.1% and  $\lambda_{30\%}=95.5\%$ , but 75.8% of the current data points for this fluid were used in the development of the method proposed by Billiet et al. [102]. This refrigerant is frequently selected as a high-performance fluid in Organic Rankine Cycles [147–149]. The methods proposed by Lazarek and Black [129], Kanizawa et al. [125] (Fig. 14(a)), Wojtan et al. [127] and Liu and Winterton [123] (Fig. 14(b)), were the most accurate in predicting CO<sub>2</sub> data, with MAPEs of 32.0%, 32.6%, 33.0% and 33.2%, respectively. Inter-

estingly, none of these methods has used CO<sub>2</sub> data in their development, but their deviations were lower than that of methods proposed exclusively for this fluid [91,113,128,137,138].

The minimum MAPE observed in predictions of water data ( $0.5 \leq p_r \leq 0.97$ ) was 49.5% for Mikielewicz's method [143]. In particular, prediction methods proposed by Liu and Winterton [123] and Kim and Mudawar [140] were highly inaccurate in predicting data for this fluid, as depicted in Fig. 14(b) and (c), respectively. Despite the inaccuracy verified in Fig. 4 for water data, the methods of Kim and Mudawar [140], Kanizawa et al. [125] and Shah [141], predicted respectively 83.1%, 78.0% and 91.5% of the data points extracted from one [108] of the three water datasets within error bands of  $\pm 30\%$ . However, huge discrepancies are verified for the other two datasets [31,32]. Considering only the data of Shen et al. [31,32], the methods highlighted in Fig. 14 presented MAPEs between 63.0% and 280.1%. The presence of near-critical data ( $0.95 \leq p_r \leq 0.97$ ) justifies this inaccuracy. The largest parcel of water near-critical data predicted within error bands of  $\pm 30\%$  was obtained by the method of Zhang et al. [25], and corresponds to only 40%. Fig. 16 compares the experimental data extracted from the studies of Wang et al. [108] and Shen et al. [31] with the respective HTCs predicted by Kim and Mudawar [140], Kanizawa et al. [125] and Shah [141]. The inaccuracy of these methods for Shen et al. [31] data at  $p_r = 0.95$  is evident in Fig. 16(b).

Table 5 presents the effect of the reduced pressure on the mean absolute errors obtained by the most accurate methods evaluated considering both MAPE and  $\lambda_{30\%}$  with and without the data points from Zhang et al. [25] and Mawatari and Mori [33] at  $p_r = 0.99$ . The reduced pressure effect on the MAPEs was non-monotonic, but the highest deviations are observed in the range of  $0.6 \leq p_r \leq 1$ , especially when the overestimated data points extracted from these two studies are considered. The prediction method proposed by Saitoh et al. [124] presented lower MAPE variations with increasing  $p_r$ , which accounts to the lowest mean absolute percentage error obtained by this method considering the entire database. It should also be mentioned that none of the methods presented MAPE lower than 125% for the reduced pressure range between 0.9 and 1, in which non-linear thermophysical properties variations are verified.

Significant MAPE reductions are verified for all prediction methods presented in Table 5 if the experimental data from Zhang et al. [25] and Mawatari and Mori [33] at  $p_r = 0.99$  are excluded. It is noteworthy that in this situation the overall mean absolute percentage error corresponding to the method of Kanizawa et al. [125] becomes lower than that of Saitoh et al. [124], and the method proposed by Kanizawa et al. [125] would present MAPE lower than 37% in all reduced pressure ranges, excluding

**Table 5**

Effect of the reduced pressure on the mean absolute percentage errors for the most accurate methods evaluated.

	$p_r$ [-]	Liu and Winterton [123]	Saitoh et al. [124]	Kim and Mudawar [140]	Kanizawa et al. [125]	Tibirića et al. [84]	Mikielewicz et al. [143]	Number of data points
Mean absolute percentage error (MAPE) [%]	0-0.1	32.8	30.8	35.5	34.4	37.1	49.3	238
	0.1-0.2	20.6	18.7	16.5	16.3	20.3	22.8	651
	0.2-0.3	33.2	37.1	25.4	34.6	37.6	33.5	274
	0.3-0.4	24.0	31.1	19.5	23.2	28.3	31.3	292
	0.4-0.5	32.3	39.3	35.3	33.1	35.5	36.7	562
	0.5-0.6	48.0	40.9	42.8	36.2	44.5	42.3	1165
	0.6-0.7*	71.0(42.7)	36.0 (32.4)	88.9 (52.2)	61.1 (34.3)	43.4 (31.3)	43.4 (34.3)	841 (764)
	0.7-0.8*	173.7 (24.3)	50.6 (33.2)	221.2 (32.5)	149.4 (20.1)	94.3 (41.5)	68.6 (27.4)	289 (199)
	0.8-0.9*	174.2 (34.5)	61.0 (44.2)	207.5 (35.5)	139.9 (32.6)	103.8 (59.1)	83.4 (50.8)	370 (299)
	0.9-1*	606.6 (333.4)	141.7 (53.7)	1442.4 (436.6)	474.1 (130.4)	246.6 (117.9)	156.6 (79.8)	71 (60)

\* Results in parentheses correspond to the MAPEs without considering the data extracted from Zhang et al. [25] and Mawatari and Mori [33] at  $p_r = 0.99$ .

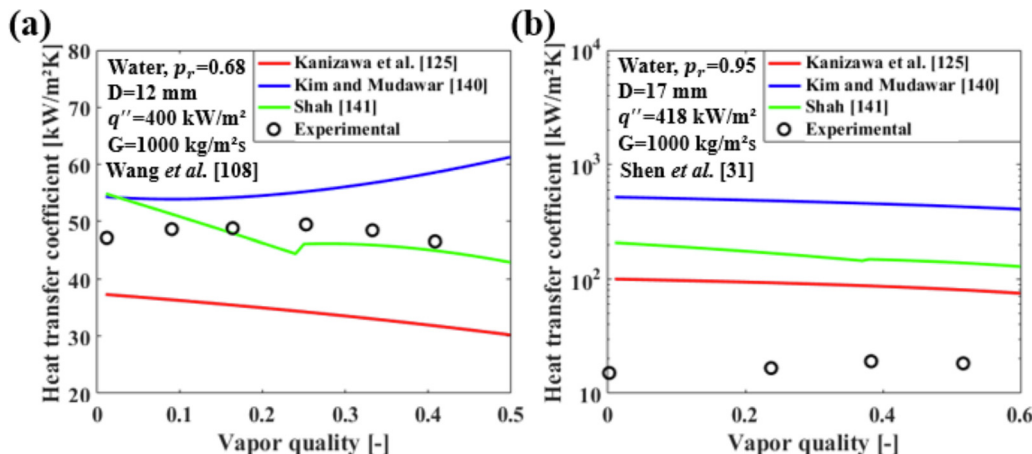


Fig. 16. (a) Comparison of the HTC experimental data from (a) Wang et al. [108] and (b) Shen et al. [31] against prediction methods.

$0.9 \leq p_r < 1$ . For this reduced pressure range none of the evaluated methods presented MAPE lower than 53.7%, even with the exclusion of the aforementioned data points.

As well as most of the evaluated pool-boiling correlations, the flow-boiling prediction methods, in general, presented higher accuracies for  $D_H < 3\text{ mm}$ . About 78% of the evaluated methods presented larger  $\lambda_{30\%}$  for diameters lower than 3 mm in comparison with  $D_H \geq 3\text{ mm}$ . The most relevant increases in  $\lambda_{30\%}$  were verified for the methods of Mikielewicz [143], Wojtan et al. [127], Saitoh et al. [124] and Keniar et al. [113]. Disregarding data from Zhang et al. [25] and Mawatari and Mori [33] at  $p_r = 0.99$ , these methods presented  $\lambda_{30\%}$ , 17.4%, 20.8%, 25.3% and 35.9% higher for diameters lower than 3 mm in comparison with  $D_H \geq 3\text{ mm}$ . It is important to remark that Wojtan et al. [127] did not consider experimental data for  $D_H < 3\text{ mm}$  in the development of their method. According to Belyaev et al. [150], at high reduced pressures, prediction methods proposed for macro-channels can present high accuracy at  $D_H < 3\text{ mm}$  because the threshold diameter for microscale transition decreases with the reduction of surface tension. According to the transition criteria proposed by Kew and Cornwell [12], Triplett et al. [13] and Tibirića and Ribatski [14], which consider surface tension, 47%, 13% and 0% of the data for  $D_H < 3\text{ mm}$  actually fall in the microchannels range, supporting the hypothesis of Belyaev et al. [150].

#### 4. Critical heat flux

The critical heat flux is associated with a deficient rewetting of the heated surface, which results in the sharp increase of wall superheating in a condition of imposed heat flux, due to the HTC reduction as a consequence of the contact of the surface with the vapor phase [151]. The CHF can be classified in two types: dryout

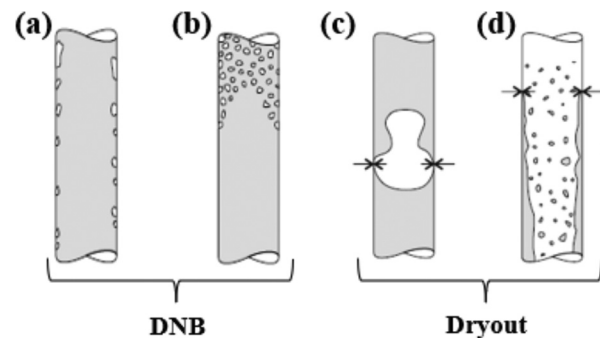


Fig. 17. Critical heat flux mechanisms during vertical flow boiling (adapted from [151]).

(DO) and departure from nucleate boiling (DNB) [9]. Dryout occurs at moderate and high vapor qualities, and is associated with the disappearance of the liquid film adjacent to the heated wall, while DNB is verified at low  $x$  or even under subcooled conditions, and is triggered when bubble nucleation prevents the liquid from contacting the heated surface [9]. According to Xie et al. [118], the sharp increase in wall temperature during DO is gentler than that in DNB condition. The difference between the flow topology during both CHF situations is verified in Fig. 17, which presents the main critical heat flux mechanisms in vertical flows described by Kanizawa and Ribatski [151]: (a) dryout under a vapor clot; (b) bubble crowding that can lead to vapor blanketing; (c) evaporation of liquid film surrounding a slug bubble; and (d) lack of liquid film on the heating surface.

**Table 6**

Experimental studies concerning critical heat flux at high reduced pressures.

Authors	Shape/ orientation/ n° of channels	Material	D <sub>H</sub>	L/D <sub>H</sub> [-]	Fluids (p <sub>r</sub> [-])	G [kg/m <sup>2</sup> s]	q'' <sub>crit</sub> [kW/m <sup>2</sup> ]	N
<i>Studies at 0.5 ≤ p<sub>r</sub> &lt; 0.8</i>								
Ozawa et al. [106]	C/H/1	SS	0.51-1	764.7-810	CO <sub>2</sub> (0.68)	300-1400	23.6-87.7	11
Cheng et al. [158]	C/VU/1	SS	2-15.8	85.7-100	R12 (0.24-0.73)	1000-6000	86.91-732.4	223
Mudawar and Bowers [159]	C/VU/1	SS 304	0.4-2.5	2.4-34.1	Water (0.01-0.78)	5000-134000	9400-276000	174
Pioro et al. [160]	C/VU/1	Inconel 600/601	4.7-6.92	65-289	R134a (0.24-0.59)	500-3000	4-400*	-
Pioro et al. [161]	C/VU,H/1	Inconel 601	6.92	65-289	R134a (0.32-0.50)	500-3000	6-412	177
Kim and Chang [162]	C/VU/1	SA 182	17.04	176.1	R134a (0.32-0.59)	285-1300	37.1-137.1	76
Kim et al. [163]	C,CR/VU/1	SA 182	17.04	117.4-176.1	R134a (0.32-0.59)	285-1300	37.1-207.4	-
Chun et al. [164]	C,A/VU/1	Inconel 600	7.75-9.9	63.8-278	R134a (0.25-0.71)	710-3500	67-491.5	89
Tan et al. [165]	C/H,HH/1	-	7	262.6	R134a (0.11-0.61)	152-1450	21.9-194.5	27
Liu et al. [166]	C/H/1	Nickel alloy GH3128	1-2	180-360	Cyclohexane (0.24-0.73)	318-1274	124.4-489.8	18
Mastrullo et al. [167]	R/H/7	Aluminum	1.33	18.8	R134a (0.16-0.58), R1234yf (0.20-0.68), R1234ze (0.14-0.50)	146-351.5	382-1006	46
Zanosko et al. [168]	C/VU/1	SS	0.95	105.3	R125 (0.44-0.7)	1800-4000	28.1-379.9	55
<i>Studies at p<sub>r</sub> ≥ 0.8</i>								
Tan et al. [9]	C/HH/1	SS 304	9.7	389.7	R134a (0.7-0.99)	250-2100	27-420	-
Belyaev et al. [150]	C/VU/1	-	0.95-1.36	105.3-147.1	RC318 (0.69-0.9), R113 (0.16-0.68)	700-4830	50.6-907	29
Vijayarangan et al. [20]	C/VU/1	SS 304	12.7	236.2	R134a (0.25-0.94)	200-2000	2.8-73.1	111
Eter et al. [111]	C/VU/1	Inconel 600	8	242.5	CO <sub>2</sub> (0.84-0.96)	494-2041	53.6-225.2	28
Cheng and Xia [169]	C,CR/VU/1	Carbon steel	11.26-11.69	138.6-143.9	Water (0.45-0.95)	400-1600	250-970	-
Sindhuja et al. [170]	C/VU/1	SS 304	12.7	236.2	R407C (0.32-0.90)	200-1600	4.8-70.7	31
Chen et al. [171]	C/VU/1	Inconel 600	8.2	292.7	Water (0.39-0.94)	1157-3776	700-3871	-
Zhang et al. [172]	C/H/1	SS	10.3	242.7	R134a (0.61-0.97)	300-1200	10-60	-
Feuerstein [173]	C/VU/1	SS	10	250	R134a (0.69-0.99)	525-4400	30.0-243.2	96

\* Normalized data for D=6.9 mm; C: Circular; CR: Circular rifled; CF: Circular finned; R: Rectangular; H: Horizontal; HH: Helical horizontal; A: Annular; VU: Vertical upward; SS: Stainless steel; N: Quantity of data points extracted.

In-tube flow boiling CHF prediction methods have been reported in the literature since the late 1940s [152]. In the beginning, these prediction methods were primarily empirical. Subsequently, in the 70s, phenomenological models were developed, however, this approach became more effective after the 1990s [20]. In 1975, Doroshchuk et al. [153] published the first look-up table for CHF prediction, an approach that was later adopted by Groeneveld et al. [154], who used an extensive database composed by 15000 experimental results for water CHF, which was updated in later publications [155,156]. In addition, several authors proposed scaling laws to adapt water look-up tables to other fluids, tube geometries and orientations. The following items present a summary of the recent literature concerning critical heat flux at  $p_r \geq 0.5$ , as well as a comparison of the gathered experimental data with 11 prediction methods and the 2006 look-up table developed by Groeneveld et al. [156].

#### 4.1. Analysis of the CHF experimental studies under high pressures

A summary of these recent experimental studies concerning CHF during flow boiling at  $p_r \geq 0.5$  is presented in Table 6. Although, in the past, high pressure critical heat flux studies were mainly focused on water flows [157], most of the recent experimental works presented in Table 6 used synthetic refrigerants as test fluids. As previously mentioned, pressurized water-cooled reactors is a subject undergoing intense study, and naturally it was the main motivation of several studies presented in Table 6 [9,158,164,171,173]. Using scaling laws, it is possible to model water flow boiling using low  $p_{crit}$  synthetic refrigerants [160], which justifies the predominance of these fluids in the recent high reduced-pressure CHF studies.

The critical heat flux database raised in the present study is composed by 1236 experimental results, with 1191 of them extracted from the studies in Table 6, and the other 45 from three

works listed in Table 3 [103,110,114]. Although these 3 studies did not evaluate the CHF, it was possible to extract from their data all the parameters required to perform the comparisons with the prediction methods. It is important to mention that data without the corresponding inlet thermodynamic state were not included in the database. Also, an energy balance verification was performed during the data survey to exclude experimental results that presented  $x_{crit} > 1$  or  $z_{CHF} > L_H$ . Only plain and straight tube data were considered in the present study, even though some studies in Table 6 evaluated different geometries. The present CHF database includes 1075 vertical and 161 horizontal flow experimental results. Most of the collected data corresponds to circular single-channels, but 46 datapoints for a rectangular multi-channels heat sink were also considered [167]. Fig. 18 summarizes the data distribution according to reduced pressure, hydraulic diameter, mass velocity and vapor quality.

The database covers eleven working fluids: water, CO<sub>2</sub>, cyclohexane and the synthetic refrigerants R113, R12, R125, R1234yf, R1234ze(E), R134a, R407C and RC318. Fig. 18(a) shows the data distribution for each group of fluids with reduced pressure. Different from the pressure drop and HTC databases, most of the CHF data at  $p_r \geq 0.5$  corresponds to synthetic refrigerants. The data distribution according to  $D_H$  is presented in Fig. 18(b), revealing that 30.6% of the data corresponds to  $D_H < 3$  mm. However, only 16.8%, 14.6% and 3.4% are classified as microchannels according to the following criteria [12,13] and [14], indicating the effect of surface tension reduction at high  $p_r$  in the macro-to-microchannel transition. A wide range of mass velocities is seen in Fig. 18(c), but it is mostly condensed in the range of  $0 < G \leq 5500$ , and 75% of the data for  $G > 5500$  kg/m<sup>2</sup>s come from a single study [159] and were mainly obtained at  $p_r < 0.5$ . Finally, Fig. 18(d) displays the distribution for critical vapor quality, indicating that both saturated and subcooled critical heat flux data were included in the database. High vapor quality DO is not commonly verified at high pressures, which is

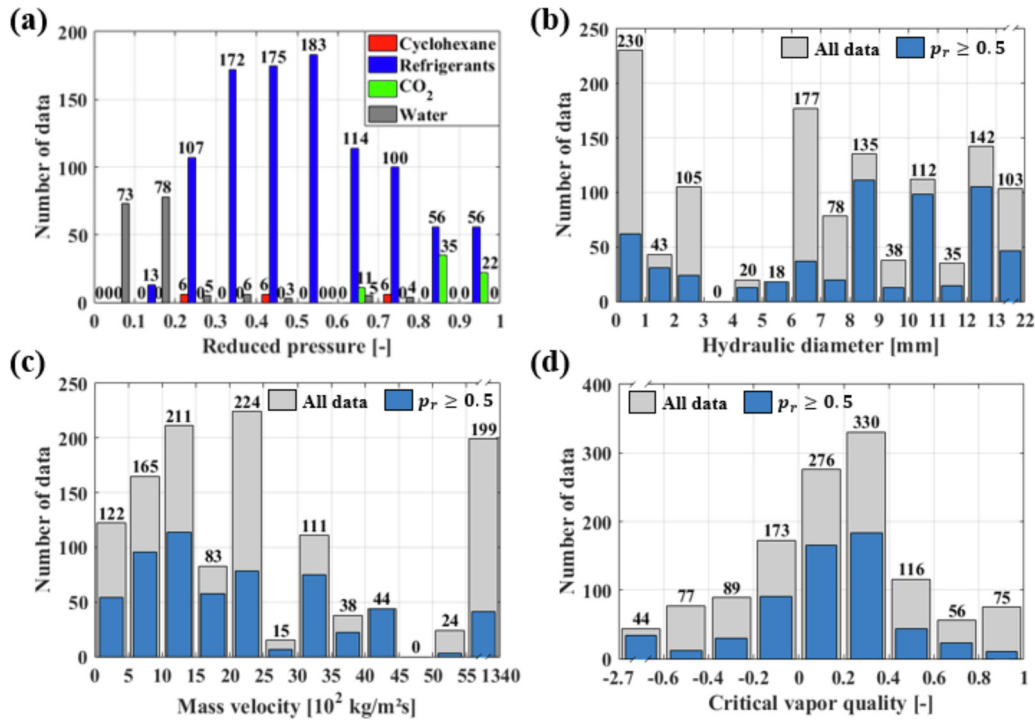


Fig. 18. Critical heat flux data distribution against (a) reduced pressure, (b) hydraulic diameter, (c) mass velocity and (d) critical vapor quality.

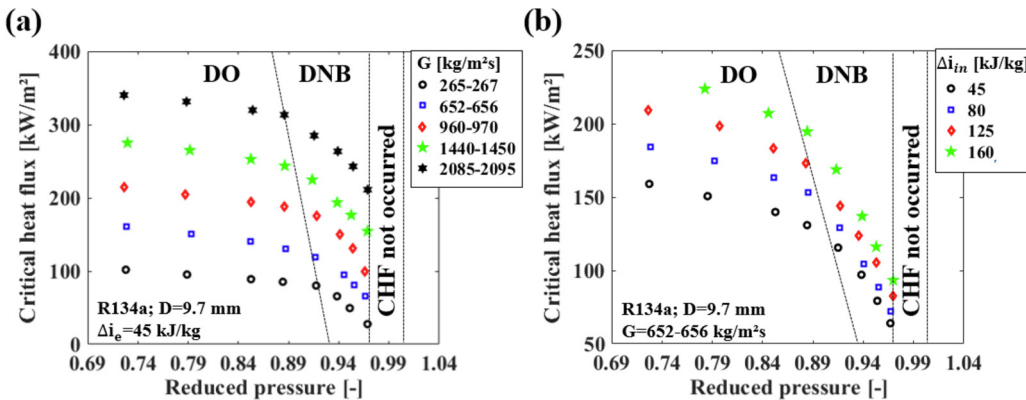


Fig. 19. Effect of the reduced pressure in the CHF reported by Tan et al. [9] for different (a) mass velocities and (b) inlet subcoolings.

confirmed by the shortage of data for  $p_r > 0.5$  in the range of  $0.8 \leq x_{crit} < 1$ . It should also be remarked that the CHF database covers inlet vapor qualities from -5.5 to 0.62.

It is a consensus that the critical heat flux increases with higher mass velocity and inlet subcooling, or lower inlet vapor quality. For a given  $q''$  and  $p_r$ , the fluid enthalpy along the channel is lower at higher  $G$  and  $\Delta T_{sub}$  (or  $\Delta i_{in}$ ), leading to the reduction of nucleation activity and smaller bubble departure diameters, which reduces their coalescence and results in higher CHFs. Furthermore, the mass velocity increase promotes rewetting of dry regions at the heated surface, avoiding both DNB and DO [174,175]. On the other hand, higher reduced pressures are usually related to decreases in CHF, due to lower surface tension and enthalpy of vaporization, which promote intensification of the nucleation activity and rate of vapor generation, causing earlier CHF. In addition, the proximity of  $\rho_l$  and  $\rho_v$  reduces buoyancy effects, inducing the coalescence of bubbles near the heated surface, such that the high vapor concentration close to the channel wall hinders surface rewetting and can eventually lead to a vapor blanket formation, resulting in DNB-type CHF [114]. These effects are all verified in Fig. 19, reproduced

from Tan et al. [9]. In contrast with the general trend, increases in CHF with reduced pressure were reported in two works [159,166]. However, the inlet temperature of the test fluid was maintained constant during their experiments, so the increases in reduced pressure were directly related to higher inlet subcooling, which can justify the higher CHF reported by these authors at higher  $p_r$ .

The experimental results presented in Fig. 19(a), as well as those reported by Feuerstein [173] indicate that the reduced pressure effect on CHF is less pronounced for dryout situations. A possible reason for this could be the reduction of the entrainment rate at higher pressures, which is associated with the approximation of the liquid and vapor phase velocities due to a lower  $\rho_l/\rho_v$ . Therefore, although the  $i_{lv}$  and  $\sigma$  reductions at high pressures account to the CHF reduction, the  $\rho_l/\rho_v$  decrease could have the opposite effect until a certain degree [176]. This is different from DNB, in which all these effects result in the decrease of CHF. It is important to mention that DNB-type critical heat flux is more likely to occur at higher pressures, mass velocities and inlet subcooling degrees [9,10,64,114,150,162], as also seen in Fig. 19, but the mechanisms that lead to the transition from DO to DNB are not fully

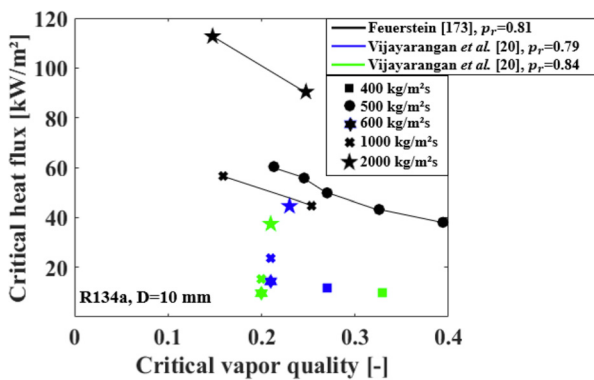


**Fig. 20.** Comparison between critical heat flux data obtained in different studies under similar experimental conditions (adapted from Feuerstein [173]).

comprehended [9]. The absence of CHF at pressures close to  $p_{crit}$  can also be verified in Fig. 19. As previously mentioned, this phenomenon is associated with the unusual behavior of thermophysical properties in the vicinity of the critical point, especially the proximity of liquid and vapor phases properties. Among the studies listed in Table 6, only Tan et al. [9] and Belyaev et al. [150] reported this phenomenon, but Mawatari and Mori [33] have also observed it. However, the absence of CHF occurs for  $p_r > 0.97$  in Fig. 19 [9], while Mawatari and Mori [33] only reported this behavior at  $p_r = 0.99$ , even though both studies used R134a.

Due to the differences in geometry and experimental conditions of the studies presented in Table 6, the comparison between datasets provided by different research groups was very difficult. The only results that could be compared are the high-pressure CHF data reported by Vijayarangan et al. [20] and Feuerstein [173], as presented by the second author and reproduced in Fig. 20. It should be remarked that Vijayarangan et al. [20] data was scaled from  $D=12.7$  mm to 10 mm through the correlation proposed by Groeneveld et al. [156]. It is verified that, at the same vapor quality and mass velocity, the CHF values from Vijayarangan et al. [20] are much lower than the experimental data reported by Feuerstein [173]. It is important to mention that, despite the proximity between the critical vapor qualities in both studies, the inlet subcoolings evaluated by Vijayarangan et al. [20],  $\Delta i_{in}=4.46-11.73$  kJ/kg, were significantly lower than those from Feuerstein [173],  $\Delta i_{in}=29.98-243.19$  kJ/kg, which may account for the high deviations between their data. The presentation of CHF data as a function of  $x_{crit}$  omits the inlet subcooling information, making it difficult to fully comprehend the results. An example of this is the CHF reduction verified in Fig. 20 for Feuerstein's data [173] when increasing  $G$  from 500 to 1000 kg/m<sup>2</sup>s. Although this result seems controversial, it must be considered that to achieve the same  $x_{crit}$ , the inlet subcooling at lower  $G$  must be higher.

#### 4.2. Comparison of critical heat flux prediction methods and experimental results

The database was compared with twelve empirical CHF prediction methods from the literature. Statistical results of the comparisons, as well as the experimental conditions for which each method was developed, are presented in Table 7. Clearly, the method of Ganesan et al. [187] was the most accurate considering both MAPE and  $\lambda_{30\%}$ , even though it was proposed for cryogenic fluids, which are not included in the present database. The methods of Katto and Ohno [178] and Hall and Mudawar [181] also presented reasonable accuracy. Though it should be remarked that 54 data points were excluded from the comparison with the method of Hall and Mudawar [181], because the calculated CHF became

negative. As seen in Table 7, this method was developed for subcooled inlet conditions ( $x_{in} < 0$ ), and for  $x_{in} > [0.9 \cdot (\frac{\rho_l}{\rho_v})^{0.724}]^{-1}$  the method returns negative values for CHF. As previously discussed, the inlet subcooling is generally related to a notable influence on the CHF, which justifies the high deviations verified in Table 7 for the prediction methods that do not consider this effect [20,182,184,185]. Nevertheless, both methods proposed by Shah [180,186] presented high deviations, even though they accounted for the effect of  $\Delta i_{in}$  and considered experimental results at high reduced pressures in their development.

The evaluation of some methods proposed exclusively for water [177,181,183] was also carried out through the application of fluid-to-fluid CHF modeling. This approach consists in calculating the CHF for an equivalent water flow, then converting it back to the real fluid [189]. First, the pressure of the equivalent water flow is determined as follows:

$$\left(\frac{\rho_l}{\rho_v}\right)_{water} = \left(\frac{\rho_l}{\rho_v}\right)_{fluid} \quad (1)$$

where the subscripts *fluid* and *water* refer to the original test fluid and the equivalent water flow, respectively. Then, the corresponding subcooling is calculated by the following relation:

$$\left(\frac{\Delta i_{in}}{i_{lv}}\right)_{water} = \left(\frac{\Delta i_{in}}{i_{lv}}\right)_{fluid}. \quad (2)$$

Two correlations were evaluated to calculate the equivalent water mass velocity. The first one was proposed by Ahmad [190], based on CHF experimental results of water, CO<sub>2</sub>, potassium, and chlorofluorocarbon (CFC) and hydrochlorofluorocarbon (HCFC) refrigerants at water-equivalent reduced pressures between 0.008 and 0.62:

$$\begin{aligned} & \left[ \left( \frac{G \cdot D}{\mu_l} \right) \cdot \left( \frac{\mu_l^2}{\sigma \cdot D \cdot \rho_l} \right)^{\frac{2}{3}} \cdot \left( \frac{\mu_v}{\mu_l} \right)^{\frac{1}{5}} \right]_{water} \\ &= \left[ \left( \frac{G \cdot D}{\mu_l} \right) \cdot \left( \frac{\mu_l^2}{\sigma \cdot D \cdot \rho_l} \right)^{\frac{2}{3}} \cdot \left( \frac{\mu_v}{\mu_l} \right)^{\frac{1}{5}} \right]_{fluid} \end{aligned} \quad (3)$$

The other mass velocity scaling law that was considered in this work is based on the Weber number and was proposed by Katto [179]:

$$\left( G \cdot \sqrt{\frac{D}{\sigma \cdot \rho_l}} \right)_{water} = \left( G \cdot \sqrt{\frac{D}{\sigma \cdot \rho_l}} \right)_{fluid} \quad (4)$$

Finally, the critical heat flux was calculated for the water flow ( $q''_{crit,water}$ ) using the prediction methods of Bowring [177], Hall and Mudawar [181] and Zhang et al. [183], and subsequently corrected to the real fluid through the similarity of boiling numbers, as follows:

$$\left( \frac{q''_{crit}}{G \cdot i_{lv}} \right)_{fluid} = \left( \frac{q''_{crit}}{G \cdot i_{lv}} \right)_{water} \quad (5)$$

The statistical results of the comparisons between the CHF database and the methods developed for water [177,181,183] using scaling laws for fluid-to-fluid CHF modeling [179,190] are presented in Table 8. No relevant error reductions were verified for two methods [181,183] associated with the CHF fluid-to-fluid modeling approach. In contrast, the method proposed by Bowring [177] presented a MAPE reduction from 56.4% to 26.5% and predicted 73% of the database within an error of 30% when combined with the scaling law of Ahmad [190], which is 35.9% higher than the previous prediction. Therefore, this method associated with the fluid-to-fluid modeling technique was the most accurate for the entire database and also for the results at reduced pressures higher than 0.5. Comparing the statistical results for [177] in

**Table 7**

Statistical analysis results of the comparison between the database and the critical heat flux methods evaluated, indicating the experimental conditions for which they were developed.

Authors	$0 < p_r < 1$		$p_r \geq 0.5$		Test conditions or application ranges
	MAPE	$\lambda_{30\%}$	MAPE	$\lambda_{30\%}$	
Vijayarangan et al. [20]	53.7	20.7	55.9	22.1	Saturated; C/S/V; R134a; $p_r$ : 0.25-0.94; $D_H$ : 12.7 mm; $L/D_H$ : 236.2; G: 200-2000 kg/m <sup>2</sup> s; 111 data points
Bowring [177]	56.4	37.1	67.5	35.8	C/S/V; Water; $p_r$ : 0.01-0.86; $D_H$ : 2-45 mm; G: 136-18600 kg/m <sup>2</sup> s
Katto and Ohno [178] <sup>1</sup>	42.3	60.8	36.2	67.4	Saturated/Subcooled; C/S/V; R12, R22, LHe, R115; $p_r$ : 0.48-0.96; $D_H$ : 1-13; $L/D_H$ : 25-333 mm; G: 10-8800 kg/m <sup>2</sup> s
Shah [180]	134.7	37.2	52.3	50.5	Saturated/Subcooled; C,R/-V; 23 Fluids: water, halocarbon refrigerants, chemicals, liquid metals, helium and cryogenics; $p_r$ : 0.001-0.96; $D_H$ : 0.32-37.8 mm; $L/D_H$ : 1.3-940; G: 3.9-29051 kg/m <sup>2</sup> s; 1443 data points
Hall and Mudawar [181] <sup>2</sup>	31.4	60.7	22.2	75.4	Subcooled; C/S/H,V; Water; $p_r$ : 0.004-0.91; $D_H$ : 0.25-15 mm; $L/D_H$ : 2-200; G: 300-30000 kg/m <sup>2</sup> s; 5544 data points
Wojtan et al. [182]	63.8	25.2	58.3	17.4	Saturated; C/S/H; R134a, R245fa; $p_r$ : 0.05-0.22; $D_H$ : 0.5-0.8; $L/D_H$ : 25-140; G: 400-1600 kg/m <sup>2</sup> s; 34 data points
Zhang et al. [183]	56.5	42.3	53.3	43.8	Saturated/Subcooled; C/S/H,V; Water; $p_r$ : 0.004-0.86; $D_H$ : 0.33-6.22 mm; $L/D_H$ : 1-975; G: 5.33-134000 kg/m <sup>2</sup> s; 2539 data points
Ong and Thome [184]	80.8	35.5	53.6	37.5	Saturated; C,R,S,M/H; R134a, R236fa, R245fa; $p_r$ : 0.04-0.22; $D_H$ : 0.32-3.04 mm; $L/D_H$ : 25-177.6; G: 90-4000 kg/m <sup>2</sup> s; 538 data points
Anwar et al. [185]	456.2	13.6	186.7	16.0	Saturated; C/S/V; R134a, R1234yf, R152a, R22, R245fa, R290, R600a; $p_r$ : 0.05-0.34; $D_H$ : 0.64-1.7 mm; $L/D_H$ : 133.1-382.8; G: 50-600 kg/m <sup>2</sup> s; 72 data points
Shah [186]	127.2	44.4	42.7	57.6	Saturated/Subcooled; C,R,S,M/H; Water, FC72, HFE7100, R12, R32, R113, R134a, R123, R236fa, R245fa; $p_r$ : 0.005-0.9; $D_H$ : 0.13-24.3 mm; $L/D_H$ : 1.97-488; G: 20-11390 kg/m <sup>2</sup> s; 878 data points
Ganesan et al. [187]	28.4	71.8	31.1	72.3	Saturated/Subcooled; C/S/H,V; LH <sub>2</sub> , LHe, LN <sub>2</sub> , LCH <sub>4</sub> ; $p_r$ : 0.1-0.93; $D_H$ : 0.5-14.1 mm; $L/D_H$ : 2.5-230.8; G: 2.2-8204 kg/m <sup>2</sup> s; 2312 data points
Song et al. [188]	67.3	45.7	71.7	63.7	Saturated/Subcooled; C/S/V; Water, R12, CO <sub>2</sub> ; $p_r$ : 0.70-0.97; $D_H$ : 1.9-24.7 mm; G: 121-10440 kg/m <sup>2</sup> s; 2652 data points

C: Circular; R: Rectangular; S: Single-channel; M: Multi-channels; H: Horizontal; V: Vertical

<sup>1</sup> Experimental conditions of the new data used by the authors to update the original method of Katto [179], which was proposed for 15 different fluids. <sup>2</sup>54 data points excluded from the comparison with the method proposed by Hall and Mudawar [181]. Statistical parameters in %.

**Table 8**

Results of the statistical analysis of the comparison between experimental data and critical heat flux prediction methods associated with scaling laws for fluid-to-fluid modeling.

Method	Scaling law	$0 < p_r < 1$		$p_r \geq 0.5$	
		MAPE	$\lambda_{30\%}$	MAPE	$\lambda_{30\%}$
Look-up table [156] <sup>1</sup>	Ahmad [190]	51.4	58.9	61.7	57.3
	Katto [179]	57.3	53.9	63.5	58.8
Bowring [177]	Ahmad [190]	26.5	73.0	19.4	83.8
	Katto [179]	27.2	72.7	18.6	85.5
Hall and Mudawar [181] <sup>2</sup>	Ahmad [190]	30.6	60.8	22.4	75.4
	Katto [179]	31.4	60.7	22.2	75.4
Zhang et al. [183]	Ahmad [190]	53.4	44.3	51.6	43.4
	Katto [179]	56.5	42.3	53.3	43.8

<sup>1</sup> 213 data points were excluded from the comparison with the look-up table because they were out of range of vapor quality and mass velocity. <sup>2</sup>54 data points were excluded from the comparison with the method proposed by Hall and Mudawar [181]. Statistical parameters in %.

Tables 7 and 8, it can be verified that the use of the fluid-to-fluid modeling technique increased the accuracy of this method specially at  $p_r \geq 0.5$ .

The fluid-to-fluid modeling technique was also adopted in the comparison between the experimental database and the look-up table developed by Groeneveld et al. [156], with statistical results also listed in Table 8. It is important to mention that 213 data points were excluded from this comparison, because their experimental conditions were out of the mass velocity or critical vapor quality ranges of the look-up table. Moreover, since the table developed by Groeneveld et al. [156] presents CHF data for a fixed tube diameter of 8 mm, prior to using Eq. (5), a diameter conversion was performed with the correlation [154]:

$$q''_{crit,water} = q''_{crit,table} \cdot \left( \frac{D}{0.008} \right)^{-0.5}, \quad (6)$$

where  $q''_{crit,table}$  is the CHF defined in the look-up table.

Fig. 21 presents the MAPE distributions according to test fluid for the 4 most accurate evaluated methods. As verified in Fig. 21(a,b), the methods proposed by Bowring [177], associated with the scaling law of Ahmad [190], and by Katto and Ohno [178] presented high mean absolute percentage errors for water CHF data. These methods are recommended for diameters greater than 2 and 1 mm, respectively. However, 93.7% of the water CHF data was obtained for  $D_H < 1$  mm, justifying the high deviations obtained by these methods for this fluid.

The method of Hall and Mudawar [181] was the most accurate in predicting water CHF data. This result was expected, since all water data points evaluated were considered in the development of this method [181]. Surprisingly, the method proposed by Ganesan et al. [187] presented a MAPE for water that was only 1.8% higher than the method of Hall and Mudawar [181], considering the whole database. In contrast, strong overestimation is verified for water data at  $p_r \geq 0.5$ , as confirmed in Fig. 21(d). The method of Ganesan et al. [187] was also highly inaccurate in predicting cyclohexane data. High deviations were also verified for the R1234yf and R1234ze(E) refrigerants, and none of the four methods was able to predict the CHF data for these fluids with MAPEs lower than 40%. These data points were extracted from a study with a microchannels-based heat sink [167], while these methods are recommended for single-channels [177,178,181,187], and some issues frequently reported for heat sinks, like non-uniform heating and fluid mal-distribution along the channels, can contribute to such deviations. Only the methods proposed by Wojtan et al. [182] and Anwar et al. [185] presented MAPEs lower than 30% for these data points, with the last one predicting 93.5% of them within the error bands of  $\pm 30\%$ . It is also important to remark that the prediction method proposed by Hall and Mudawar [181] presented MAPEs lower for  $p_r \geq 0.5$  for each test fluid evaluated, as verified in Fig. 21(c).

Fig. 22 shows the effect of the reduced pressure on the MAPEs of the 4 most accurate CHF prediction methods. High deviations

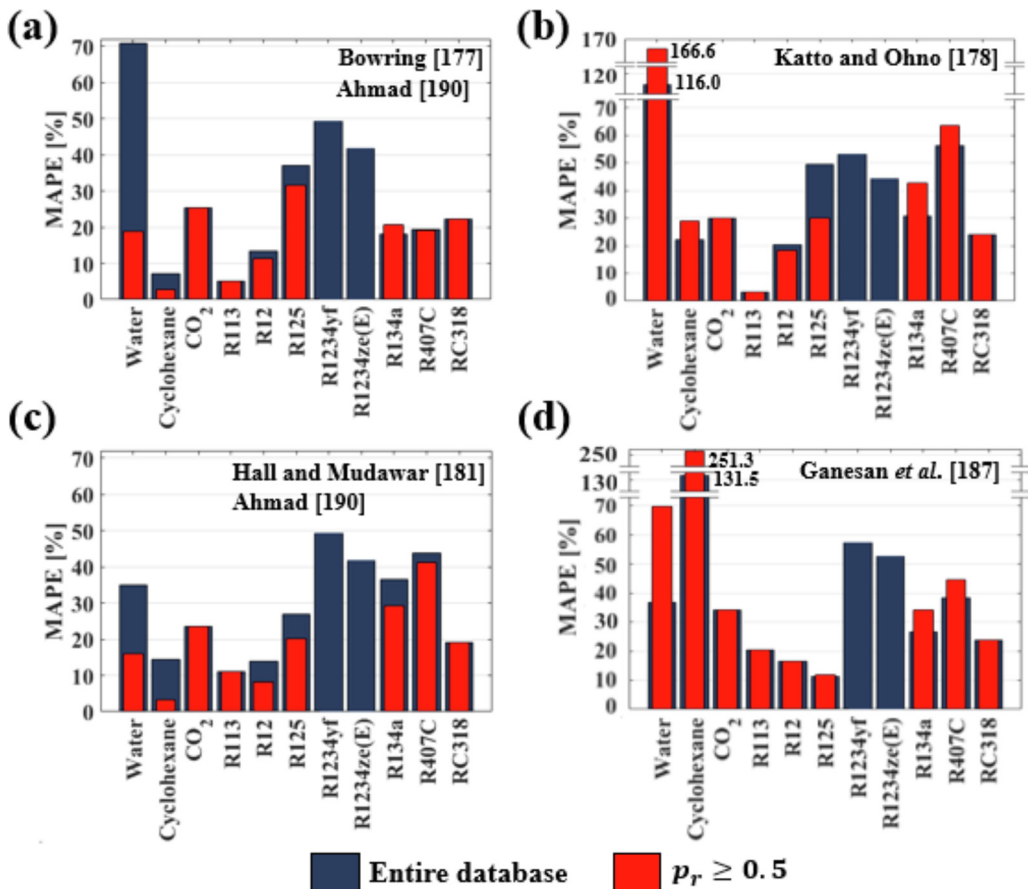


**Fig. 21.** MAPE distributions according to working fluid for the methods of (a) Bowring [177] scaled by Ahmad [190], (b) Katto and Ohno [178], (c) Hall and Mudawar [181] scaled by Ahmad [190] and (d) Ganesan et al. [187].

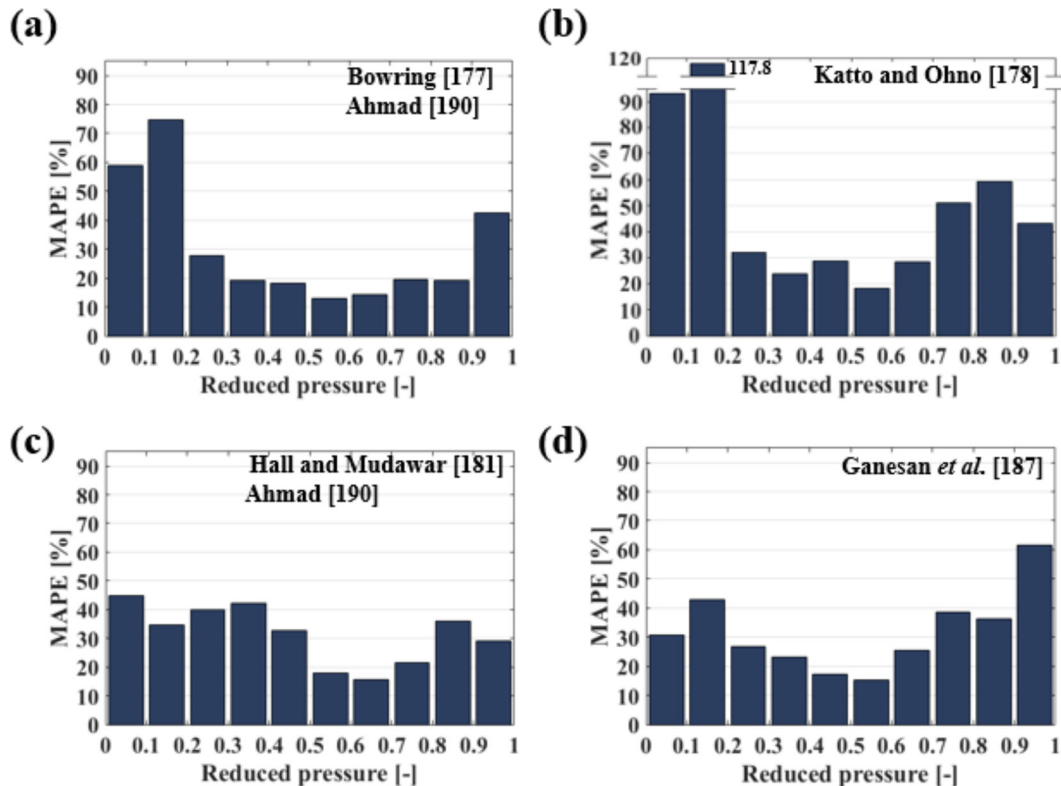


**Fig. 22.** MAPE distributions according to reduced pressure for the methods of (a) Bowring [177] scaled by Ahmad [190], (b) Katto and Ohno [178], (c) Hall and Mudawar [181] scaled by Ahmad [190] and (d) Ganesan et al. [187].

are verified at  $0 < p_r < 0.2$  for the methods proposed by Bowring [177] associated with the scaling law of Ahmad [190], and by Katto and Ohno [178]. Among the 164 experimental data in this reduced pressure range, 141 correspond to CHF water data at  $D_H < 1$  mm, and 12 to microchannels-based heat sink, justifying the high deviations verified for these methods. At intermediate reduced pressures ( $0.3 \leq p_r < 0.7$ ), both methods presented MAPEs lower than 30%. However, high deviations are also verified for the method proposed by Katto and Ohno [178] at  $0.7 \leq p_r < 1$ , while the correlation of Bowring [177] only presented significant loss of accuracy at reduced pressures higher than 0.9. The method of Hall and Muddawar [181] scaled by Ahmad [190] was the only one that presented MAPEs lower than 50% for the whole range of reduced pressure from 0 to 1 (Fig. 22(c)). Furthermore, this method was the most accurate at  $p_r \geq 0.9$ , although none of the CHF water data included in the database of the present study falls in this range. Finally, Fig. 22(d) shows that the method proposed by Ganesan et al. [187] also showed MAPEs considerably lower than those verified for the first two methods for  $0 < p_r < 0.2$ . This is associated with the surprising accuracy of this method in predicting water data. However, considering the reduced pressure range from 0.9 to 1, this last method resulted in the highest MAPE among the 4 methods presented in Fig. 22.

## 5. Conclusions

A synthesized literature review of flow boiling at high reduced pressures was presented. Based on the comprehensive discussion about the experimental studies concerning pressure drop, heat transfer coefficient and critical heat flux, the following conclusions can be drawn:

- As expected, the increase of the frictional pressure gradient with increasing mass velocity and reducing the saturation pressure was reported in all high-pressure studies from literature. In general, the increase of  $G$  and the reduction of  $p_r$  anticipated the pressure gradient peak, however, some divergent results were found;
- Different behaviors were identified for the heat transfer coefficient as a function of vapor quality: constant, decreasing, decreasing-constant, "U-shaped" and increasing. However, the constant behavior was the most commonly verified, specially at near-critical pressures, due to the strong contribution of nucleate boiling effects at high  $p_r$ , which is maintained for vapor qualities preceding the CHF;
- In general, the increase of  $q''$  and  $p_r$  increased the HTC, especially when nucleate boiling is the predominant heat transfer mechanism. The mass velocity increase raised the HTC at convective-dominant regimes, while it is irrelevant when nucleate boiling effects are predominant. However, some studies presented unexpected effects of these experimental parameters, like non-monotonic influence of  $p_r$  and  $G$  and the HTC reduction with increasing  $q''$  and  $p_r$  at near-critical pressures;
- Notable divergences were identified when comparing HTC data at high  $p_r$  from different studies under close experimental conditions, and in some cases these divergences are not limited to the HTC values, but also to their behaviors as a function of  $x$ ;
- The CHF experimental studies reported the  $q''_{crit}$  increase with increasing mass velocity and inlet subcooling, and reducing  $p_r$ . Both dryout and DNB CHF types were identified in these studies, with the second one being more likely to occur at high reduced pressures. However, some studies verified the absence of CHF at saturation pressures close to  $p_{crit}$ , due to the proximity of liquid and vapor thermophysical properties at the vicinity of the critical point.

The comparison between experimental data and prediction methods revealed that correlations based on the homogeneous model and the method proposed by Müller-Steinhagen and Heck [81] were the most accurate for frictional pressure drop prediction. The homogeneous-based correlations presented significative MAPEs reductions and  $\lambda_{30\%}$  increments for  $p_r \geq 0.5$ , and were the most accurate for  $0.9 \leq p_r < 1$ . The method of Saitoh et al. [124] presented the lowest MAPE, while the method proposed by Kanizawa et al. [125] predicted the largest parcel of the HTC database within error bands of  $\pm 30\%$ . However, the evaluated HTC prediction methods showed notable increments of the deviations with increasing  $p_r$ . A strong inaccuracy was also verified in the HTC predictions when compared with particular datasets. Comparisons with the CHF database showed that the use of the fluid-to-fluid modeling considerably increased the accuracy of the method proposed by Bowring [177]. When associated with the scaling law of Ahmad [190], this method predicted the largest parcel of CHF data within error bands of  $\pm 30\%$  and also showed the lowest MAPE. The accuracy of [177] was increased for  $p_r \geq 0.5$ , but a high MAPE is verified in  $0.9 \leq p_r < 1$ . In summary, the prediction methods are sensitive to reduced pressure variations, and none of them is suitable for all  $p_r$  ranges. Therefore, the development of new methods is still required and should occur in parallel with experimental studies at high pressures, specially at near-critical conditions.

The conducted review also indicates that the effect of the channel diameter was not sufficiently investigated at high reduced pressures, as well as the heat flux effect on the frictional pressure drop at near-critical pressures. A shortage of experimental studies concerning inclined channels was also identified. Pressure drop and heat transfer coefficient experimental data at high reduced pressures for synthetic refrigerants are still scarce, especially for low-GWP fluids. The complete replacement of HFCs and HCFCs expected for the coming years indicates that experimental studies involving low-GWP fluids will be increasingly recurrent, and this should also be expected for high reduced pressure applications.

## Declaration of Competing Interest

The authors declare that they have no known competing financial interests or personal relationships that could have appeared to influence the work reported in this paper.

## Acknowledgements

The authors gratefully acknowledge the São Paulo Research Foundation (FAPESP, Brazil) for the scholarships given to the first and second authors, under Contract Numbers 2019/22105-5 and 2015/24834-3, respectively. The authors also acknowledge the support through the Thematic Grant provided by FAPESP under Contract Number 2016/09509-01. This study was financed in part by the Coordenação de Aperfeiçoamento de Pessoal de Nível Superior – Brasil (CAPES) – Finance Code 001.

## References

- [1] G. Ribatski, L. Wojtan, J.R. Thome, An analysis of experimental data and prediction methods for two-phase frictional pressure drop and flow boiling heat transfer in micro-scale channels, *Exp. Therm. Fluid Sci.* 31 (2006) 1–19, doi:[10.1016/j.expthermflusci.2006.01.006](https://doi.org/10.1016/j.expthermflusci.2006.01.006).
- [2] T. Harirchian, S.V. Garimella, Flow regime-based modeling of heat transfer and pressure drop in microchannel flow boiling, *Int. J. Heat Mass Transf.* 55 (2012) (2012) 1246–1260, doi:[10.1016/j.ijheatmasstransfer.2011.09.024](https://doi.org/10.1016/j.ijheatmasstransfer.2011.09.024).
- [3] X. Fang, Y. Yuan, A. Xu, L. Tian, Q. Wu, Review of correlations for subcooled flow boiling heat transfer and assessment of their applicability to water, *Fusion Eng. Des.* 122 (2017) 52–63, doi:[10.1016/j.fusengdes.2017.09.008](https://doi.org/10.1016/j.fusengdes.2017.09.008).
- [4] X. Fang, F. Zhuang, C. Chen, Q. Wu, Y. Chen, Y. Chen, Y. He, Saturated flow boiling heat transfer: review and assessment of prediction methods, *Heat Mass Transf.* 55 (2019) 197–222, doi:[10.1007/s00231-018-2432-1](https://doi.org/10.1007/s00231-018-2432-1).

- [5] J. Weisman, The current status of theoretically based approaches to the prediction of the critical heat flux in flow boiling, *Nucl. Technol.* (99) (1992) 1–21, doi:[10.13182/NT92-A34699](https://doi.org/10.13182/NT92-A34699).
- [6] G.P. Celata, Modeling of critical heat flux in subcooled flow boiling, *Heat Transf. Res.* 29 (1998), doi:[10.1615/HeatTransRes.v29.i4-5.140](https://doi.org/10.1615/HeatTransRes.v29.i4-5.140).
- [7] S.G. Kandlikar, Critical heat flux in subcooled flow boiling—an assessment of current understanding and future directions for research, *Multiph. Sci. Technol.* 13 (2001), doi:[10.1615/MultSciTechn.v13.i3-4.40](https://doi.org/10.1615/MultSciTechn.v13.i3-4.40).
- [8] M. Bruder, G. Bloch, T. Sattelmayer, Critical heat flux in flow boiling—review of the current understanding and experimental approaches, *Heat Transf. Eng.* 38 (3) (2017) 347–360, doi:[10.1080/01457632.2016.1189274](https://doi.org/10.1080/01457632.2016.1189274).
- [9] L. Tan, C. Chen, X. Dong, Z. Gong, M. Wang, Experimental study on CHF of R134a flow boiling in a horizontal helically-coiled tube near the critical pressure, *Exp. Therm. Fluid Sci.* 82 (2017) 472–481, doi:[10.1016/j.expthermflusci.2016.12.005](https://doi.org/10.1016/j.expthermflusci.2016.12.005).
- [10] X. Lei, W. Zhang, J. Zhang, N. Dinh, H. Li, Experimental investigations on the boiling heat transfer of horizontal flow in the near-critical region, *Int. J. Heat Mass Transf.* 125 (2018) 618–628, doi:[10.1016/j.ijheatmasstransfer.2018.04.043](https://doi.org/10.1016/j.ijheatmasstransfer.2018.04.043).
- [11] I.H. Bell, J. Wronski, S. Quoilin, V. Lemort, Pure and pseudo-pure fluid thermophysical property evaluation and the open-source thermophysical property library CoolProp, *Ind. Eng. Chem. Res.* 53 (2014) 2498–2508, doi:[10.1021/ie4033999](https://doi.org/10.1021/ie4033999).
- [12] P.A. Kew, K. Cornwell, Correlations for the prediction of boiling heat transfer in small-diameter channels, *Appl. Therm. Eng.* 17 (1997) 705–715.
- [13] K.A. Triplett, S.M. Ghiaasiaan, S.I. Abdel-Khalik, D.L. Sadowski, Gas-liquid two-phase flow in microchannels Part I: Two-phase flow patterns, *Int. J. Multiphase Flow* 25 (1999) 377–394, doi:[10.1016/S0301-9322\(98\)00054-8](https://doi.org/10.1016/S0301-9322(98)00054-8).
- [14] C.B. Tibirica, G. Ribatski, Flow boiling phenomenological differences between micro-and macroscale channels, *Heat Transf. Eng.* 36 (2015) 937–942, doi:[10.1080/01457632.2015.972276](https://doi.org/10.1080/01457632.2015.972276).
- [15] J. Pettersen, Flow vaporization of CO<sub>2</sub> in microchannel tubes, *Exp. Therm. Fluid Sci.* 28 (2004) 111–121, doi:[10.1016/S0894-1777\(03\)00029-3](https://doi.org/10.1016/S0894-1777(03)00029-3).
- [16] T. Aimi, N. Nakamura, H. Umekawa, M. Ozawa, M. Shoji, Flow pattern and boiling heat transfer of CO<sub>2</sub> at high pressure in horizontal mini-channels, in: International Heat Transfer Conference, 49361, 2010, pp. 307–316, doi:[10.1115/IHTC14-22560](https://doi.org/10.1115/IHTC14-22560).
- [17] R. Mastrullo, A.W. Mauro, J.R. Thome, G.P. Vanoli, CO<sub>2</sub> and R410A: two-phase flow visualizations and flow boiling measurements at medium (0.50) reduced pressure, *Appl. Therm. Eng.* 49 (2012) 2–8, doi:[10.1016/j.applthermaleng.2011.10.021](https://doi.org/10.1016/j.applthermaleng.2011.10.021).
- [18] R. Charnay, J. Bonjour, R. Revellin, Experimental investigation of R-245fa flow boiling in minichannels at high saturation temperatures: Flow patterns and flow pattern maps, *Int. J. Heat Fluid Flow* 46 (2014) 1–16, doi:[10.1016/j.ijheatfluidflow.2013.12.002](https://doi.org/10.1016/j.ijheatfluidflow.2013.12.002).
- [19] V.V. Yagov, Generic features and puzzles of nucleate boiling, *Int. J. Heat Mass Transf.* 52 (2009) 5241–5249, doi:[10.1016/j.ijheatmasstransfer.2009.03.071](https://doi.org/10.1016/j.ijheatmasstransfer.2009.03.071).
- [20] B.R. Vijayarangan, S. Jayanti, A.R. Balakrishnan, Studies on critical heat flux in flow boiling at near critical pressures, *Int. J. Heat Mass Transf.* 49 (2006) 259–268, doi:[10.1016/j.ijheatmasstransfer.2005.06.029](https://doi.org/10.1016/j.ijheatmasstransfer.2005.06.029).
- [21] R. Charnay, R. Revellin, J. Bonjour, Discussion on the validity of prediction tools for two-phase flow pressure drops from experimental data obtained at high saturation temperatures, *Int. J. Refrig.* 54 (2015) 98–125 a, doi:[10.1016/j.ijrefrig.2015.02.014](https://doi.org/10.1016/j.ijrefrig.2015.02.014).
- [22] M.A. Qyoun, A. Khan, S. Ali, M.S. Khurram, N. Mao, A. Naquash, A.A. Noon, T. He, M. Lee, Assessment of working fluids, thermal resources and cooling utilities for Organic Rankine Cycles: State-of-the-art comparison, challenges, commercial status, and future prospects, *Energy Convers. Manage.* 252 (2022) 115055, doi:[10.1016/j.enconman.2021.115055](https://doi.org/10.1016/j.enconman.2021.115055).
- [23] M.M. Marinheiro, G.M. Coraça, L. Cabezas-Gómez, G. Ribatski, Detailed transient assessment of a small-scale concentrated solar power plant based on the organic Rankine cycle, *Appl. Therm. Eng.* 204 (2022) 117959, doi:[10.1016/j.applthermaleng.2021.117959](https://doi.org/10.1016/j.applthermaleng.2021.117959).
- [24] R. Charnay, R. Revellin, J. Bonjour, Flow boiling heat transfer in minichannels at high saturation temperatures: Part I—experimental investigation and analysis of the heat transfer mechanisms, *Int. J. Heat Mass Transf.* 87 (2015) 636–652 b, doi:[10.1016/j.ijheatmasstransfer.2015.03.081](https://doi.org/10.1016/j.ijheatmasstransfer.2015.03.081).
- [25] Y. Zhang, R. Tian, X. Dai, D. Wang, Y. Ma, H. Li, L. Shi, Experimental study of R134a flow boiling in a horizontal tube for evaporator design under typical Organic Rankine Cycle pressures, *Int. J. Heat Fluid Flow* 71 (2018) 210–219 a, doi:[10.1016/j.ijheatfluidflow.2018.04.008](https://doi.org/10.1016/j.ijheatfluidflow.2018.04.008).
- [26] D. Hellenschmidt, P. Petagna, Effects of saturation temperature on the boiling properties of carbon dioxide in small diameter pipes at low vapour quality: Heat transfer coefficient, *Int. J. Heat Mass Transf.* 172 (2021) 121094, doi:[10.1016/j.ijheatmasstransfer.2021.121094](https://doi.org/10.1016/j.ijheatmasstransfer.2021.121094).
- [27] R. Mastrullo, A.W. Mauro, A. Rosato, G.P. Vanoli, Carbon dioxide heat transfer coefficients and pressure drops during flow boiling: Assessment of predictive methods, *Int. J. Refrig.* 33 (2010) 1068–1085, doi:[10.1016/j.ijrefrig.2010.04.005](https://doi.org/10.1016/j.ijrefrig.2010.04.005).
- [28] L. Cheng, J.R. Thome, Cooling of microprocessors using flow boiling of CO<sub>2</sub> in a micro-evaporator: Preliminary analysis and performance comparison, *Appl. Therm. Eng.* 29 (2009) 2426–2432, doi:[10.1016/j.applthermaleng.2008.12.019](https://doi.org/10.1016/j.applthermaleng.2008.12.019).
- [29] D. Hellenschmidt, P. Petagna, Effects of saturation temperature on the boiling properties of carbon dioxide in small diameter pipes at low vapour quality: Pressure drop, *Int. J. Heat Mass Transf.* 163 (2020) 120209, doi:[10.1016/j.ijheatmasstransfer.2020.120209](https://doi.org/10.1016/j.ijheatmasstransfer.2020.120209).
- [30] S.Y. Chun, H.J. Chung, S.K. Moon, S.K. Yang, M.K. Chung, T. Schoesae, M. Arimoto, Effect of pressure on critical heat flux in uniformly heated vertical annulus under low flow conditions, *Nucl. Eng. Des.* 203 (2001) 159–174, doi:[10.1016/S0029-5493\(00\)00307-1](https://doi.org/10.1016/S0029-5493(00)00307-1).
- [31] Z. Shen, D. Yang, G. Chen, F. Xiao, Experimental investigation on heat transfer characteristics of smooth tube with downward flow, *Int. J. Heat Mass Transf.* 68 (2014) 669–676, doi:[10.1016/j.ijheatmasstransfer.2013.09.045](https://doi.org/10.1016/j.ijheatmasstransfer.2013.09.045).
- [32] Z. Shen, D. Yang, H. Xie, X. Nie, W. Liu, S. Wang, Flow and heat transfer characteristics of high-pressure water flowing in a vertical upward smooth tube at low mass flux conditions, *Appl. Therm. Eng.* 102 (2016) 391–401 a, doi:[10.1016/j.applthermaleng.2016.03.150](https://doi.org/10.1016/j.applthermaleng.2016.03.150).
- [33] T. Mawatari, H. Mori, An experimental study on characteristics of post-CHF heat transfer in the high subcritical pressure region near to the critical pressure, *J. Therm. Sci. Technol.* 11 (2016) 1–14, doi:[10.1299/jst.2016jst0006](https://doi.org/10.1299/jst.2016jst0006).
- [34] S.S. Bertsch, E.A. Groll, S.V. Garimella, Review and comparative analysis of studies on saturated flow boiling in small channels, *Nanoscale Microscale Thermophys. Eng.* 12 (2008) 187–227, doi:[10.1080/15567260802317357](https://doi.org/10.1080/15567260802317357).
- [35] S.G. Kandlikar, History, advances, and challenges in liquid flow and flow boiling heat transfer in microchannels: a critical review, *J. Heat Transf.* 134 (2012), doi:[10.1115/1.4005126](https://doi.org/10.1115/1.4005126).
- [36] M.M. Mahmoud, T.G. Karayannidis, Heat transfer correlation for flow boiling in small to micro tubes, *Int. J. Heat Mass Transf.* 66 (2013) 553–574, doi:[10.1016/j.ijheatmasstransfer.2013.07.042](https://doi.org/10.1016/j.ijheatmasstransfer.2013.07.042).
- [37] G. Ribatski, A critical overview on the recent literature concerning flow boiling and two-phase flows inside micro-scale channels, *Exp. Heat Transf.* 26 (2013) 198–246, doi:[10.1080/08916152.2012.737189](https://doi.org/10.1080/08916152.2012.737189).
- [38] S.M. Kim, I. Mudawar, Review of databases and predictive methods for heat transfer in condensing and boiling mini/micro-channel flows, *Int. J. Heat Mass Transf.* 77 (2014) 627–652, doi:[10.1016/j.ijheatmasstransfer.2014.05.036](https://doi.org/10.1016/j.ijheatmasstransfer.2014.05.036).
- [39] X. Fang, F. Zhuang, C. Chen, Q. Wu, Y. Chen, Y. He, Saturated flow boiling heat transfer: review and assessment of prediction methods, *Heat Mass Transf.* 55 (2019) 197–222, doi:[10.1007/s00231-018-2432-1](https://doi.org/10.1007/s00231-018-2432-1).
- [40] M. Mitchell, B. Muftahidinov, T. Winchen, Z. Jedrzejewski-Szmejk, Engauge Digitizer Software, 2019 Webpage: <http://markummitchell.github.io/engauge-digitizer>. Accessed June 12, 2021.
- [41] S. Klein, F. Alvarado, Engineering Equation Solver, F-Chart Software, Box (2002).
- [42] B.R. Vijayarangan, S. Jayanti, A.R. Balakrishnan, Pressure drop studies on two-phase flow in a uniformly heated vertical tube at pressures up to the critical point, *Int. J. Heat Mass Transf.* 50 (2007) 1879–1891, doi:[10.1016/j.ijheatmasstransfer.2006.10.018](https://doi.org/10.1016/j.ijheatmasstransfer.2006.10.018).
- [43] M. Zhang, R.L. Webb, Correlation of two-phase friction for refrigerants in small-diameter tubes, *Exp. Therm Fluid Sci.* 25 (2001) 131–139, doi:[10.1016/S0894-1777\(01\)00066-8](https://doi.org/10.1016/S0894-1777(01)00066-8).
- [44] D.C. Adams, P.S. Hrnjak, T.A. Newell, Pressure Drop and Void Fraction in Microchannels Using Carbon Dioxide, Ammonia, and R245fa as Refrigerants, Air Conditioning and Refrigeration Center, College of Engineering, University of Illinois at Urbana-Champaign, 2003.
- [45] S. Jeong, E. Cho, H.K. Kim, Evaporative heat transfer and pressure drop of CO<sub>2</sub> in a microchannel tube, in: ASME 3rd International Conference on Microchannels and Minichannels, 2005, pp. 103–108, doi:[10.1115/ICMM2005-75180](https://doi.org/10.1115/ICMM2005-75180).
- [46] P. Vassallo, K. Keller, Two-phase frictional pressure drop multipliers for SUVA R-134a flowing in a rectangular duct, *Int. J. Multiphase Flow* 32 (2006) 466–482, doi:[10.1016/j.ijmultiphaseflow.2006.01.004](https://doi.org/10.1016/j.ijmultiphaseflow.2006.01.004).
- [47] M. Ducoulbier, S. Colasson, J. Bonjour, P. Haberschill, Carbon dioxide flow boiling in a single microchannel—Part I: Pressure drops, *Exp. Therm Fluid Sci.* 35 (2011) 581–596 a, doi:[10.1016/j.expthermflusci.2010.12.010](https://doi.org/10.1016/j.expthermflusci.2010.12.010).
- [48] D.H. Kim, S. Jeong, Effect of micro-grooves on the two-phase pressure drop of CO<sub>2</sub> in a mini-channel tube, *Int. J. Refrig.* 36 (2013) 2040–2047, doi:[10.1016/j.ijrefrig.2013.05.019](https://doi.org/10.1016/j.ijrefrig.2013.05.019).
- [49] S. Grauso, R. Mastrullo, A.W. Mauro, G.P. Vanoli, Two-phase adiabatic frictional pressure gradients for R410A and CO<sub>2</sub> in a macro channel: Experiments and a simplified predictive method for annular flow from low to medium reduced pressures, *Exp. Therm Fluid Sci.* 52 (2014) 79–87, doi:[10.1016/j.expthermflusci.2013.08.024](https://doi.org/10.1016/j.expthermflusci.2013.08.024).
- [50] G. Lillo, R. Mastrullo, A.W. Mauro, F. Pelella, L. Viscito, Experimental thermal and hydraulic characterization of R448A and comparison with R404A during flow boiling, *Appl. Therm. Eng.* 161 (2019) 114146, doi:[10.1016/j.applthermaleng.2019.114146](https://doi.org/10.1016/j.applthermaleng.2019.114146).
- [51] J. Wang, H. Li, B. Guo, S. Yu, Y. Zhang, T. Chen, Experimental investigation on the frictional pressure drop of high pressure steam-water two-phase flows in an optimized internally-ribbed tube, in: Proceedings of the International Conference on Power Engineering (ICOPE), The Japan Society of Mechanical Engineers, 2009, pp. 1–341, doi:[10.1299/jsmcopicope.2009.1\\_1-341\\_1](https://doi.org/10.1299/jsmcopicope.2009.1_1-341_1).
- [52] W. Liu, H. Tamai, K. Takase, Pressure drop and void fraction in steam-water two-phase flow at high pressure, *J. Heat Transf.* 135 (2013), doi:[10.1115/1.4023678](https://doi.org/10.1115/1.4023678).
- [53] M. Hammer, H. Deng, L. Liu, M. Langsholt, S.T. Munkejord, Upward and downward two-phase flow of CO<sub>2</sub> in a pipe: Comparison between experimental data and model predictions, *Int. J. Multiphase Flow* 138 (2021) 103590, doi:[10.1016/j.ijmultiphaseflow.2021.103590](https://doi.org/10.1016/j.ijmultiphaseflow.2021.103590).
- [54] S.G. Kandlikar, Fundamental issues related to flow boiling in minichannels and microchannels, *Exp. Therm Fluid Sci.* 26 (2002) 389–407, doi:[10.1016/S0894-1777\(02\)00150-4](https://doi.org/10.1016/S0894-1777(02)00150-4).

- [55] T.A. Moreira, R.W. Morse, K.M. Dressler, G. Ribatski, A. Berson, Liquid-film thickness and disturbance-wave characterization in a vertical, upward, two-phase annular flow of saturated R245fa inside a rectangular channel, *Int. J. Multiphase Flow* 132 (2020) 103412, doi:10.1016/j.ijmultiphaseflow.2020.103412.
- [56] J. Moreno-Quibén, J.R. Thome, Flow pattern based two-phase frictional pressure drop model for horizontal tubes. Part I: Diabatic and adiabatic experimental study, *Int. J. Heat Fluid Flow* 28 (2007) 1049–1059, doi:10.1016/j.ijheatfluidflow.2007.01.003.
- [57] Da Silva, J. D. Estudo Teórico-Experimental da Perda de Pressão Durante a Ebulação Convectiva de Refrigerantes Halogenados no Interior de Microcanais Circulares, São Carlos School of Engineering, University of São Paulo (Masters dissertation, São Carlos, 2012).
- [58] C.B. Tibiricá, G. Ribatski, Flow boiling in micro-scale channels—Synthesized literature review, *Int. J. Refrig.* 36 (2013) 301–324, doi:10.1016/j.ijrefrig.2012.11.019.
- [59] S. Grauso, R. Mastrullo, A.W. Mauro, G.P. Vanoli, CO<sub>2</sub> and propane blends: experiments and assessment of predictive methods for flow boiling in horizontal tubes, *Int. J. Refrig.* 34 (2011) 1028–1039, doi:10.1016/j.ijrefrig.2011.03.001.
- [60] R. Mastrullo, A.W. Mauro, L. Viscito, Flow boiling of R452A: Heat transfer data, dry-out characteristics and a correlation, *Exp. Therm. Fluid Sci.* 105 (2019) 247–260, doi:10.1016/j.experimentflusci.2019.04.006.
- [61] D. Yang, J. Pan, C.Q. Zhou, X. Zhu, Q. Bi, T. Chen, Experimental investigation on heat transfer and frictional characteristics of vertical upward rifled tube in supercritical CFB boiler, *Exp. Therm. Fluid Sci.* 35 (2011) 291–300, doi:10.1016/j.experimentflusci.2010.09.011.
- [62] J. Zhang, A. Desideri, M.R. Kærn, T.S. Ommen, J. Wronski, F. Haglind, Flow boiling heat transfer and pressure drop characteristics of R134a, R1234yf and R1234ze in a plate heat exchanger for organic Rankine cycle units, *Int. J. Heat Mass Transf.* 108 (2017) 1787–1801, doi:10.1016/j.ijheatmasstransfer.2017.01.026.
- [63] H.K. Oh, C.H. Son, Flow boiling heat transfer and pressure drop characteristics of CO<sub>2</sub> in horizontal tube of 4.57-mm inner diameter, *Appl. Therm. Eng.* 31 (2011) 163–172, doi:10.1016/j.applthermaleng.2010.08.026.
- [64] A.V. Belyaev, A.N. Varava, A.V. Dedov, A.T. Komov, An experimental study of flow boiling in minichannels at high reduced pressure, *Int. J. Heat Mass Transf.* 110 (2017) 360–373, doi:10.1016/j.ijheatmasstransfer.2017.03.045.
- [65] A. Desideri, J. Zhang, M.R. Kærn, T.S. Ommen, J. Wronski, V. Lemort, F. Haglind, An experimental analysis of flow boiling and pressure drop in a brazed plate heat exchanger for organic Rankine cycle power systems, *Int. J. Heat Mass Transf.* 113 (2017) 6–21, doi:10.1016/j.ijheatmasstransfer.2017.05.063.
- [66] D. Steiner, *Heat transfer to boiling saturated liquids*, VDI-Wärmeatlas, VDI Heat Atlas, 1993.
- [67] S.Z. Rouhani, E Axelsson, Calculation of void volume fraction in subcooled and quality boiling regions, *Int. J. Heat Mass Transf.* 13 (1970) 383–393.
- [68] H. Blasius, Das aehnlichkeitgesetz bei reibungsvorgängen in flüssigkeiten, in: Mitteilungen über Forschungsarbeiten auf dem Gebiete des Ingenieurwesens, Springer, Berlin, Heidelberg, 1913, pp. 1–41, doi:10.1007/978-3-662-02239-9\_1.
- [69] W. McAdams, W. Woods, R. Bryan, Vaporization inside horizontal tubes II: Benzene-oil mixtures, *Trans. ASME* 64 (1942) 193–200.
- [70] A. Cicchitti, C. Lombardi, M. Silvestri, G. Soldaini, R. Zavattarelli, Two-phase cooling experiments—pressure drop, heat transfer and burnout measurements, *Energia Nucleare* 7 (1960) 407–425.
- [71] A.E. Dukler, M. Wicks III, R.G. Cleveland, Frictional pressure drop in two-phase flow: B. An approach through similarity analysis, *AIChE J.* 10 (1964) 44–51, doi:10.1002/aic.690100118.
- [72] D.R.H. Beattie, P.B. Whalley, A simple two-phase frictional pressure drop calculation method, *Int. J. Multiphase Flow* 8 (1982) 83–87, doi:10.1016/0301-9322(82)90009-X.
- [73] S. Lin, C.C.K. Kwok, R.Y. Li, Z.H. Chen, Z.Y. Chen, Local frictional pressure drop during vaporization of R-12 through capillary tubes, *Int. J. Multiphase Flow* 17 (1991) 95–102, doi:10.1016/0301-9322(91)90072-B.
- [74] M.M. Awad, Y.S. Muzychka, Effective property models for homogeneous two-phase flows, *Exp. Therm. Fluid Sci.* 33 (2008) 106–113, doi:10.1016/j.experimentflusci.2008.07.006.
- [75] R.W. Lockhart, R.C. Martinelli, Proposed correlation of data for isothermal two-phase, two component flow in pipes, *Chem. Eng. Prog.* 45 (1949) 39–48.
- [76] D. Chisholm, Pressure gradients due to friction during the flow of evaporating two-phase mixtures in smooth tubes and channels, *Int. J. Heat Mass Transf.* 16 (1973) 347–358, doi:10.1016/0017-9310(73)90063-X.
- [77] L. Friedel, Improved friction pressure drop correlation for horizontal and vertical two-phase pipe flow, in: Proc. of European Two-Phase Flow Group Meet, Ispra, Italy, 1979.
- [78] K. Mishima, T. Hibiki, Some characteristics of air-water two-phase flow in small diameter vertical tubes, *Int. J. Multiphase Flow* 22 (1996) 703–712, doi:10.1016/0301-9322(96)00010-9.
- [79] T. Yamamoto, Y. Ueda, I. Ishihara, M. Ozawa, H. Umekawa, R. Matsumoto, Flow boiling heat transfer of carbon dioxide at high pressure in horizontal mini-channels, 6th International Conference on Multiphase Flow, 2007.
- [80] S.M. Kim, I. Mudawar, Universal approach to predicting two-phase frictional pressure drop for mini/micro-channel saturated flow boiling, *Int. J. Heat Mass Transf.* 58 (2013) 718–734 a, doi:10.1016/j.ijheatmasstransfer.2012.11.045.
- [81] H. Müller-Steinhagen, K. Heck, A simple friction pressure drop correlation for two-phase flow in pipes, *Chem. Eng. Process.* 20 (1986) 297–308, doi:10.1016/0255-2701(86)80008-3.
- [82] Y. Xu, X. Fang, A new correlation of two-phase frictional pressure drop for evaporating flow in pipes, *Int. J. Refrig.* 35 (2012) 2039–2050, doi:10.1016/j.ijrefrig.2012.06.011.
- [83] D.F. Sempétegui-Tapia, G. Ribatski, Two-phase frictional pressure drop in horizontal micro-scale channels: experimental data analysis and prediction method development, *Int. J. Refrig.* 79 (2017) 143–163, doi:10.1016/j.ijrefrig.2017.03.024.
- [84] C.B. Tibiricá, D.M. Rocha, I.L.S. Sueth Jr, G. Bochio, G.K.K. Shimizu, M.C. Barbosa, S. dos Santos Ferreira, A complete set of simple and optimized correlations for microchannel flow boiling and two-phase flow applications, *Appl. Therm. Eng.* 126 (2017) 774–795, doi:10.1016/j.applthermaleng.2017.07.161.
- [85] R.K. Shah, A.L. London, Laminar flow forced convection in ducts. Advances in Heat Transfer Supplement 1, Academic Press, New York, 1978, doi:10.1016/B978-0-12-020051-1.50012-7.
- [86] R. Yun, Y. Kim, M.S. Kim, Y. Choi, Boiling heat transfer and dryout phenomenon of CO<sub>2</sub> in a horizontal smooth tube, *Int. J. Heat Mass Transf.* 46 (2003) 2353–2361, doi:10.1016/S0017-9310(02)00540-9.
- [87] S.H. Yoon, E.S. Cho, Y.W. Hwang, M.S. Kim, K. Min, Y. Kim, Characteristics of evaporative heat transfer and pressure drop of carbon dioxide and correlation development, *Int. J. Refrig.* 27 (2004) 111–119, doi:10.1016/j.ijrefrig.2003.08.006.
- [88] R. Yun, Y. Kim, M.S. Kim, Convective boiling heat transfer characteristics of CO<sub>2</sub> in microchannels, *Int. J. Heat Mass Transf.* 48 (2005) 235–242 a, doi:10.1016/j.ijheatmasstransfer.2004.08.019.
- [89] J.M. Cho, M.S. Kim, Experimental studies on the evaporative heat transfer and pressure drop of CO<sub>2</sub> in smooth and micro-fin tubes of the diameters of 5 and 9.52 mm, *Int. J. Refrig.* 30 (2007) 986–994, doi:10.1016/j.ijrefrig.2007.01.007.
- [90] K.I. Choi, A.S. Pamitran, C.Y. Oh, J.T. Oh, Boiling heat transfer of R-22, R-134a, and CO<sub>2</sub> in horizontal smooth minichannels, *Int. J. Refrig.* 30 (2007) 1336–1346 a, doi:10.1016/j.ijrefrig.2007.04.007.
- [91] K.I. Choi, A.S. Pamitran, J.T. Oh, Two-phase flow heat transfer of CO<sub>2</sub> vaporization in smooth horizontal minichannels, *Int. J. Refrig.* 30 (2007) 767–777 b, doi:10.1016/j.ijrefrig.2006.12.006.
- [92] E. Hihara, C. Dang, Boiling heat transfer of carbon dioxide in horizontal tubes, in: Heat Transfer Summer Conference, 42762, Vancouver, Canada, 2007, pp. 843–849.
- [93] Y.J. Kim, J.M. Cho, M.S. Kim, Experimental study on the evaporative heat transfer and pressure drop of CO<sub>2</sub> flowing upward in vertical smooth and micro-fin tubes with the diameter of 5 mm, *Int. J. Refrig.* 31 (2008) 771–779, doi:10.1016/j.ijrefrig.2007.12.001.
- [94] H.K. Oh, H.G. Ku, G.S. Roh, C.H. Son, S.J. Park, Flow boiling heat transfer characteristics of carbon dioxide in a horizontal tube, *Appl. Therm. Eng.* 28 (2008) 1022–1030, doi:10.1016/j.applthermaleng.2007.06.032.
- [95] J.M. Cho, Y.J. Kim, M.S. Kim, Experimental studies on the evaporative heat transfer and pressure drop of CO<sub>2</sub> and CO<sub>2</sub>/propane mixtures flowing upward in smooth and micro-fin tubes with outer diameter of 5 mm for an inclination angle of 45, *Int. J. Refrig.* 33 (2010) 922–931, doi:10.1016/j.ijrefrig.2010.02.002.
- [96] K.I. Choi, M. Rifaldi, A.S. Pamitran, J.T. Oh, Characteristics of two-phase flow boiling heat transfer and pressure drop of NH<sub>3</sub>, C<sub>3</sub>H<sub>8</sub> and CO<sub>2</sub> in horizontal circular small tubes, in: International Heat Transfer Conference, 49361, 2010, pp. 407–413, doi:10.1115/IHTC14-22660.
- [97] D. Del Col, Flow boiling of halogenated refrigerants at high saturation temperature in a horizontal smooth tube, *Exp. Therm. Fluid Sci.* 34 (2010) 234–245, doi:10.1016/j.experimentflusci.2009.10.035.
- [98] A.S. Pamitran, K.I. Choi, J.T. Oh, Evaporation heat transfer coefficient in single circular small tubes for flow natural refrigerants of C<sub>3</sub>H<sub>8</sub>, NH<sub>3</sub>, and CO<sub>2</sub>, *Int. J. Multiphase Flow* 37 (2011) 794–801, doi:10.1016/j.ijmultiphaseflow.2011.02.005.
- [99] C. Dang, N. Haraguchi, T. Yamada, M. Li, E. Hihara, Effect of lubricating oil on flow boiling heat transfer of carbon dioxide, *Int. J. Refrig.* 36 (2013) 136–144, doi:10.1016/j.ijrefrig.2012.09.020.
- [100] S. Grauso, R. Mastrullo, A.W. Mauro, G.P. Vanoli, Flow boiling of R410A and CO<sub>2</sub> from low to medium reduced pressures in macro channels: Experiments and assessment of prediction methods, *Int. J. Heat Mass Transf.* 56 (2013) 107–118, doi:10.1016/j.ijheatmasstransfer.2012.09.015.
- [101] L. Jiang, J. Liu, L. Zhang, X. Xu, A research on the dryout characteristics of CO<sub>2</sub>'S flow boiling heat transfer process in mini-channels, *Int. J. Refrig.* 83 (2017) 131–142, doi:10.1016/j.ijrefrig.2017.07.017.
- [102] M. Billiet, B. Ameel, R. Charbay, R. Revellin, M. De Peape, Flow regime based heat transfer correlation for R245fa in a 3 mm tube, *Int. J. Heat Mass Transf.* 117 (2018) 1304–1311, doi:10.1016/j.ijheatmasstransfer.2017.10.062.
- [103] L. Köckert, A.F. Badea, X. Cheng, D. Yu, D. Klingel, Studies on post-dryout heat transfer in R-134a vertical flow, *Int. J. Adv. Nucl. Reactor Des. Technol.* 3 (2021) 44–53, doi:10.1016/j.jandt.2021.05.001.
- [104] J.L. Gasche, Carbon dioxide evaporation in a single microchannel, *J. Braz. Soc. Mech. Sci. Eng.* 28 (2006) 69–83, doi:10.1590/S1678-58782006000100008.
- [105] X. Zhu, Q. Bi, D. Yang, T. Chen, An investigation on heat transfer characteristics of different pressure steam-water in vertical upward tube, *Nucl. Eng. Des.* 239 (2009) 381–388, doi:10.1016/j.nucengdes.2008.10.026.
- [106] M. Ozawa, T. Ami, H. Umekawa, R. Matsumoto, T. Hara, Forced flow boiling of carbon dioxide in horizontal mini-channel, *Int. J. Therm. Sci.* 50 (2011) 296–308, doi:10.1016/j.ijthermalsci.2010.04.017.

- [107] W. Gang, Q. Bi, H. Wang, Z. Yang, X. Zhu, Z. Hu, Forced convection heat transfer using high temperature and pressure water in an upward-inclined tube, *J. Heat Transf.* 134 (2012), doi:[10.1115/1.4004901](https://doi.org/10.1115/1.4004901).
- [108] H. Wang, Q. Bi, Z. Yang, W. Gang, R. Hu, Experimental investigation on heat transfer characteristics of high pressures water in a vertical upward annular channel, *Exp. Therm Fluid Sci.* 45 (2013) 169–179, doi:[10.1016/j.expthermflusci.2012.11.001](https://doi.org/10.1016/j.expthermflusci.2012.11.001).
- [109] S. Wang, D. Yang, B. Xie, L. Wang, Y. Wang, Experimental investigation on heat transfer characteristics of water in inclined downward tube of a supercritical pressure CFB boiler, *J. Therm. Sci.* 24 (2015) 478–487, doi:[10.1007/s11630-015-0811-1](https://doi.org/10.1007/s11630-015-0811-1).
- [110] H. Zahlan, D. Groeneveld, S. Tavoularis, Measurements of convective heat transfer to vertical upward flows of CO<sub>2</sub> in circular tubes at near-critical and supercritical pressures, *Nucl. Eng. Des.* 289 (2015) 92–107, doi:[10.1016/j.nucengdes.2015.04.013](https://doi.org/10.1016/j.nucengdes.2015.04.013).
- [111] A. Eter, D. Groeneveld, S. Tavoularis, Convective heat transfer at high subcritical pressures in tubes with and without flow obstacles, *Nucl. Eng. Des.* 318 (2017) 1–23, doi:[10.1016/j.nucengdes.2017.04.013](https://doi.org/10.1016/j.nucengdes.2017.04.013).
- [112] Q. Guo, M. Li, X. Tian, Experimental study on flow boiling heat transfer characteristics of R134a, R245fa and R134a/R245fa mixture at high saturation temperatures, *Int. J. Therm. Sci.* 150 (2020) 106195, doi:[10.1016/j.ijthermalsci.2019.106195](https://doi.org/10.1016/j.ijthermalsci.2019.106195).
- [113] K. Keniar, F. Mazzelli, S. Garimella, Experimental investigation of carbon dioxide flow boiling in a single microchannel, *Int. J. Heat Mass Transf.* 159 (2020) 120100, doi:[10.1016/j.ijheatmasstransfer.2020.120100](https://doi.org/10.1016/j.ijheatmasstransfer.2020.120100).
- [114] X. Lei, R. Peng, Z. Guo, H. Li, K. Ali, X. Zhou, Experimental comparison of the heat transfer of carbon dioxide under subcritical and supercritical pressures, *Int. J. Heat Mass Transf.* 152 (2020) 119562, doi:[10.1016/j.ijheatmasstransfer.2020.119562](https://doi.org/10.1016/j.ijheatmasstransfer.2020.119562).
- [115] M. Jiménez-Arreola, C. Wieland, A. Romagnoli, Direct vs indirect evaporation in Organic Rankine Cycle (ORC) systems: A comparison of the dynamic behavior for waste heat recovery of engine exhaust, *Appl. Energy* 242 (2019) 439–452, doi:[10.1016/j.apenergy.2019.03.011](https://doi.org/10.1016/j.apenergy.2019.03.011).
- [116] Z. Shen, D. Yang, K. Mao, J. Long, S. Wang, Heat transfer characteristics of water flowing in a vertical upward rifled tube with low mass flux, *Exp. Therm Fluid Sci.* 70 (2016) 341–353 b, doi:[10.1016/j.expthermflusci.2015.09.021](https://doi.org/10.1016/j.expthermflusci.2015.09.021).
- [117] A. Taklifi, M.A. Akhavan-Behabadi, P. Hanafizadeh, A. Aliaabadi, Effect of heat and mass flux on heat transfer characteristics of water forced convection inside vertical and inclined rifled tubes, *Appl. Therm. Eng.* 117 (2017) 169–177 b, doi:[10.1016/j.applthermaleng.2017.02.015](https://doi.org/10.1016/j.applthermaleng.2017.02.015).
- [118] H. Xie, D. Yang, Y. Zhao, H. Jiang, M. Qu, Experimental investigation on critical heat flux for water flowing in a vertical uniformly heated rifled tube under near-critical pressures, *J. Therm. Sci.* 27 (2018) 527–540, doi:[10.1007/s11630-018-1030-3](https://doi.org/10.1007/s11630-018-1030-3).
- [119] H. Wang, W. Wang, Q. Bi, Experimental investigation on boiling heat transfer of high pressure water in a SCWR sub-channel, *Int. J. Heat Mass Transf.* 105 (2017) 799–810, doi:[10.1016/j.ijheatmasstransfer.2016.09.088](https://doi.org/10.1016/j.ijheatmasstransfer.2016.09.088).
- [120] S. Chen, Y. Xiao, H. Gu, Experimental study on boiling heat transfer in a three-rod bundle at near-critical pressure, *Ann. Nucl. Energy* 131 (2019) 196–209, doi:[10.1016/j.anucene.2019.03.038](https://doi.org/10.1016/j.anucene.2019.03.038).
- [121] S.G. Kandlikar, Development of a flow boiling map for subcooled and saturated flow boiling of different fluids inside circular tubes, *J. Heat Transf.* 113 (1991) 190–200, doi:[10.1115/1.2910524](https://doi.org/10.1115/1.2910524).
- [122] S. Sandler, B. Zajaczkowski, Z. Krolicki, Review on flow boiling of refrigerants R236fa and R245fa in mini and micro channels, *Int. J. Heat Mass Transf.* 126 (2018) 591–617, doi:[10.1016/j.ijheatmasstransfer.2018.05.048](https://doi.org/10.1016/j.ijheatmasstransfer.2018.05.048).
- [123] Z. Liu, R.H.S. Winterton, A general correlation for saturated and subcooled flow boiling in tubes and annuli, based on a nucleate pool boiling equation, *Int. J. Heat Mass Transf.* 34 (1991) 2759–2766, doi:[10.1016/0017-9310\(91\)90234-6](https://doi.org/10.1016/0017-9310(91)90234-6).
- [124] S. Saitoh, H. Daiguij, E. Hihara, Correlation for boiling heat transfer of R-134a in horizontal tubes including effect of tube diameter, *Int. J. Heat Mass Transf.* 50 (2007) 5215–5225, doi:[10.1016/j.ijheatmasstransfer.2007.06.019](https://doi.org/10.1016/j.ijheatmasstransfer.2007.06.019).
- [125] F.T. Kanizawa, C.B. Tibiricá, G. Ribatski, Heat transfer during convective boiling inside microchannels, *Int. J. Heat Mass Transf.* 93 (2016) 566–583, doi:[10.1016/j.ijheatmasstransfer.2015.09.083](https://doi.org/10.1016/j.ijheatmasstransfer.2015.09.083).
- [126] K. Stephan, M. Abdelsalam, Heat-transfer correlations for natural convection boiling, *Int. J. Heat Mass Transf.* 23 (1980) 73–87, doi:[10.1016/0017-9310\(80\)90140-4](https://doi.org/10.1016/0017-9310(80)90140-4).
- [127] L. Wojtan, T. Ursenbacher, J.R. Thome, Investigation of flow boiling in horizontal tubes: Part II—Development of a new heat transfer model for stratified-wavy, dryout and mist flow regimes, *Int. J. Heat Mass Transf.* 48 (2005) 2970–2985, doi:[10.1016/j.ijheatmasstransfer.2004.12.013](https://doi.org/10.1016/j.ijheatmasstransfer.2004.12.013).
- [128] L. Cheng, G. Ribatski, J.R. Thome, New prediction methods for CO<sub>2</sub> evaporation inside tubes: Part II—An updated general flow boiling heat transfer model based on flow patterns, *Int. J. Heat Mass Transf.* 51 (2008) 125–135, doi:[10.1016/j.ijheatmasstransfer.2007.04.001](https://doi.org/10.1016/j.ijheatmasstransfer.2007.04.001).
- [129] G.M. Lazarrek, S.H. Black, Evaporative heat transfer, pressure drop and critical heat flux in a small vertical tube with R-113, *Int. J. Heat Mass Transf.* 25 (1982) 945–960, doi:[10.1016/0017-9310\(82\)90070-9](https://doi.org/10.1016/0017-9310(82)90070-9).
- [130] T.N. Tran, M.W. Wambsganss, D.M. France, Small circular-and rectangular-channel boiling with two refrigerants, *Int. J. Multiphase Flow* 22 (1996) 485–498, doi:[10.1016/0301-9322\(96\)00002-X](https://doi.org/10.1016/0301-9322(96)00002-X).
- [131] L. Sun, K. Mishima, An evaluation of prediction methods for saturated flow boiling heat transfer in mini-channels, *Int. J. Heat Mass Transf.* 52 (2009) 5323–5329, doi:[10.1016/j.ijheatmasstransfer.2009.06.041](https://doi.org/10.1016/j.ijheatmasstransfer.2009.06.041).
- [132] M.M. Shah, Chart correlation for saturated boiling heat transfer: equations and further study, *ASHRAE Transact.* 88 (1982).
- [133] K.E. Gungor, R.H.S. Winterton, Simplified general correlation for saturated flow boiling and comparison of correlation with data, *Chem. Eng. Res. Des.* 65 (1987) 148–156.
- [134] D.S. Jung, M. McLinden, R. Radermacher, Didion, D. A study of flow boiling heat transfer with refrigerant mixtures, *Int. J. Heat Mass Transf.* 32 (1989) 1751–1764, doi:[10.1016/0017-9310\(89\)90057-4](https://doi.org/10.1016/0017-9310(89)90057-4).
- [135] S.G. Kandlikar, P. Balasubramanian, An extension of the flow boiling correlation to transition, laminar, and deep laminar flows in minichannels and microchannels, *Heat Transf. Eng.* 25 (2004) 86–93, doi:[10.1080/01457630490280425](https://doi.org/10.1080/01457630490280425).
- [136] S.G. Kandlikar, A general correlation for saturated two-phase flow boiling heat transfer inside horizontal and vertical tubes, *J. Heat Transf.* 112 (1990) 219–228, doi:[10.1115/1.2910348](https://doi.org/10.1115/1.2910348).
- [137] M. Ozawa, T. Ami, I. Ishihara, H. Umekawa, R. Matsumoto, Y. Tanaka, T. Yamamoto, Y. Ueda, Flow pattern and boiling heat transfer of CO<sub>2</sub> in horizontal small-bore tubes, *Int. J. Multiphase Flow* 35 (2009) 699–709, doi:[10.1016/j.ijmultiphaseflow.2009.04.003](https://doi.org/10.1016/j.ijmultiphaseflow.2009.04.003).
- [138] M. Duocoulobier, S. Colasson, J. Bonjour, P. Haberschill, Carbon dioxide flow boiling in a single microchannel—Part II: Heat transfer, *Exp. Therm Fluid Sci.* 35 (2011) 597–611 b, doi:[10.1016/j.expthermflusci.2010.11.014](https://doi.org/10.1016/j.expthermflusci.2010.11.014).
- [139] V.V. Yagov, M.V. Minko, Heat transfer in two-phase flow at high reduced pressures, *Therm. Eng.* 58 (2011) 283–294, doi:[10.1134/S0040601511040136](https://doi.org/10.1134/S0040601511040136).
- [140] S.M. Kim, I. Mudawar, Universal approach to predicting saturated flow boiling heat transfer in mini/micro-channels—Part II: Two-phase heat transfer coefficient, *Int. J. Heat Mass Transf.* 64 (2013) 1239–1256 b, doi:[10.1016/j.ijheatmasstransfer.2013.04.014](https://doi.org/10.1016/j.ijheatmasstransfer.2013.04.014).
- [141] M.M. Shah, Unified correlation for heat transfer during boiling in plain mini/micro and conventional channels, *Int. J. Refrig.* 74 (2017) 606–626, doi:[10.1016/j.ijrefrig.2016.11.023](https://doi.org/10.1016/j.ijrefrig.2016.11.023).
- [142] J. Mikielewicz, Semi-empirical method of determining the heat-transfer coefficient for subcooled, saturated boiling in a channel, *Int. J. Heat Mass Transf.* 17 (1974) 1129–1134, doi:[10.1016/0017-9310\(74\)90114-8](https://doi.org/10.1016/0017-9310(74)90114-8).
- [143] D. Mikielewicz, J. Mikielewicz, J. Tesmar, Improved semi-empirical method for determination of heat transfer coefficient in flow boiling in conventional and small diameter tubes, *Int. J. Heat Mass Transf.* 50 (2007) 3949–3956, doi:[10.1016/j.ijheatmasstransfer.2007.01.024](https://doi.org/10.1016/j.ijheatmasstransfer.2007.01.024).
- [144] M.G. Cooper, Heat flow rates in saturated nucleate pool boiling—a wide-ranging examination using reduced properties, *Adv. Heat Transf.* 16 (1984) 157–239, doi:[10.1016/S0065-2717\(08\)70205-3](https://doi.org/10.1016/S0065-2717(08)70205-3).
- [145] R. Yun, Y. Kim, M.S. Kim, Flow boiling heat transfer of carbon dioxide in horizontal mini tubes, *Int. J. Heat Fluid Flow* 26 (2005) 801–809 b, doi:[10.1016/j.ijheatfluidflow.2005.01.004](https://doi.org/10.1016/j.ijheatfluidflow.2005.01.004).
- [146] L. Cheng, G. Ribatski, L. Wojtan, J.R. Thome, New flow boiling heat transfer model and flow pattern map for carbon dioxide evaporating inside horizontal tubes, *Int. J. Heat Mass Transf.* 49 (2006) 4082–4094, doi:[10.1016/j.ijheatmasstransfer.2006.04.003](https://doi.org/10.1016/j.ijheatmasstransfer.2006.04.003).
- [147] C. He, C. Liu, H. Gao, H. Xie, Y. Li, S. Wu, J. Xu, The optimal evaporation temperature and working fluids for subcritical organic Rankine cycle, *Energy* 38 (2012) 136–143, doi:[10.1016/j.energy.2011.12.022](https://doi.org/10.1016/j.energy.2011.12.022).
- [148] W. Su, L. Zhao, S. Deng, Simultaneous working fluids design and cycle optimization for Organic Rankine cycle using group contribution model, *Appl. Energy* 202 (2017) 618–627, doi:[10.1016/j.apenergy.2017.03.133](https://doi.org/10.1016/j.apenergy.2017.03.133).
- [149] A.F. Babatunde, O.O. Sunday, A review of working fluids for Organic Rankine Cycle (ORC) applications, in: *IOP Conference Series: Materials Science and Engineering*, 012019, 2018, p. 413.
- [150] A.V. Belyaev, A.N. Varava, A.V. Dedov, A.T. Komov, Critical heat flux at flow boiling of refrigerants in minichannels at high reduced pressure, *Int. J. Heat Mass Transf.* 122 (2018) 732–739, doi:[10.1016/j.ijheatmasstransfer.2018.02.027](https://doi.org/10.1016/j.ijheatmasstransfer.2018.02.027).
- [151] F.T. Kanizawa, G. Ribatski, *Flow Boiling and Condensation in Microscale Channels*, Springer Nature, 2021 doi:[10.1007/2F978-3-030-68704-5](https://doi.org/10.1007/2F978-3-030-68704-5).
- [152] D.C. Groeneveld, A. Ireland, J. Kaizer, A. Vasic, An overview of measurements, data compilations and prediction methods for the critical heat flux in water-cooled tubes, *Nucl. Eng. Des.* 331 (2018) 211–221, doi:[10.1016/j.nucengdes.2018.02.031](https://doi.org/10.1016/j.nucengdes.2018.02.031).
- [153] V.E. Boroshchuk, L.L. Levitan, F.P. Lantzman, *Investigation into burnout in uniformly heated tubes*, ASME paper 75-WA-HT-22, 1975.
- [154] D.C. Groeneveld, S.C. Cheng, T. Doan, 1986 AECL-UO critical heat flux lookup table, *Heat Transf. Eng.* 7 (1986) 46–62, doi:[10.1080/01457638608939644](https://doi.org/10.1080/01457638608939644).
- [155] D.C. Groeneveld, L.K.H. Leung, P.L. Kirillov, V.P. Bobkov, I.P. Smogalev, V.N. Vinogradov, X.C. Huang, E. Royer, The 1995 look-up table for critical heat flux in tubes, *Nucl. Eng. Des.* 163 (1996) 1–23, doi:[10.1016/0029-5493\(95\)01154-4](https://doi.org/10.1016/0029-5493(95)01154-4).
- [156] D.C. Groeneveld, J.Q. Shan, A.Z. Vasić, L.K.H. Leung, A. Durmazay, J. Yang, S.C. Cheng, A. Tanase, The 2006 CHF look-up table, *Nucl. Eng. Des.* 237 (2007) 1909–1922, doi:[10.1016/j.nucengdes.2007.02.014](https://doi.org/10.1016/j.nucengdes.2007.02.014).
- [157] W. Liu, J. Shan, S. Peng, G. Jiang, Y. Liu, The study of critical heat flux in up-flow boiling vertical round tube under high pressure, *Science and Technology of Nuclear Installations*, 2019, doi:[10.1155/2019/3695685](https://doi.org/10.1155/2019/3695685).
- [158] X. Cheng, F.J. Erbacher, U. Müller, F.G. Pang, Critical heat flux in uniformly heated vertical tubes, *Int. J. Heat Mass Transf.* 40 (1997) 2929–2939, doi:[10.1016/S0017-9310\(96\)00344-4](https://doi.org/10.1016/S0017-9310(96)00344-4).

- [159] I. Mudawar, M.B. Bowers, Ultra-high critical heat flux (CHF) for subcooled water flow boiling—I: CHF data and parametric effects for small diameter tubes, *Int. J. Heat Mass Transf.* 42 (1999) 1405–1428, doi:[10.1016/S0017-9310\(98\)00241-5](https://doi.org/10.1016/S0017-9310(98)00241-5).
- [160] I.L. Pioro, D.C. Groeneveld, S.C. Cheng, S. Doerffer, A.Ž. Vasić, Y.V. Antoshko, Comparison of CHF measurements in R-134a cooled tubes and the water CHF look-up table, *Int. J. Heat Mass Transf.* 44 (2001) 73–88, doi:[10.1016/S0017-9310\(00\)00093-4](https://doi.org/10.1016/S0017-9310(00)00093-4).
- [161] I.L. Pioro, D.C. Groeneveld, L.K.H. Leung, S.S. Doerffer, S.C. Cheng, Y.V. Antoshko, Y. Guo, A. Vasić, Comparison of CHF measurements in horizontal and vertical tubes cooled with R-134a, *Int. J. Heat Mass Transf.* 45 (2002) 4435–4450, doi:[10.1016/S0017-9310\(02\)00149-7](https://doi.org/10.1016/S0017-9310(02)00149-7).
- [162] C.H. Kim, S.H. Chang, CHF characteristics of R-134a flowing upward in uniformly heated vertical tube, *Int. J. Heat Mass Transf.* 48 (2005) 2242–2249, doi:[10.1016/j.ijheatmasstransfer.2004.12.025](https://doi.org/10.1016/j.ijheatmasstransfer.2004.12.025).
- [163] C.H. Kim, I.C. Bang, S.H. Chang, Critical heat flux performance for flow boiling of R-134a in vertical uniformly heated smooth tube and rifled tubes, *Int. J. Heat Mass Transf.* 48 (2005) 2868–2877, doi:[10.1016/j.ijheatmasstransfer.2005.01.039](https://doi.org/10.1016/j.ijheatmasstransfer.2005.01.039).
- [164] S-Y. Chun, S-D. Hong, Y-S. Cho, W-P. Baek, Comparison of the CHF data for water and refrigerant HFC-134a by using the fluid-to-fluid modeling methods, *Int. J. Heat Mass Transf.* 50 (2007) 4446–4456, doi:[10.1016/j.ijheatmasstransfer.2005.06.039](https://doi.org/10.1016/j.ijheatmasstransfer.2005.06.039).
- [165] L.Z. Tan, J.T. Han, C.N. Chen, P.C. Dou, Comparison of critical heat flux for R-134a flow boiling in a horizontal straight tube and a helically-coiled tube, *Adv. Mater. Res.* 588 (2012) 1813–1816, doi:[10.4028/www.scientific.net/AMR.588-589.1813](https://doi.org/10.4028/www.scientific.net/AMR.588-589.1813).
- [166] Z. Liu, Q. Bi, Z. Yang, Y. Guo, J. Yan, Critical heat flux of cyclohexane in uniformly heated minichannels with high inlet subcooling, *Exp. Therm Fluid Sci.* 63 (2015) 106–114, doi:[10.1016/j.expthermflusci.2015.01.012](https://doi.org/10.1016/j.expthermflusci.2015.01.012).
- [167] R. Mastrullo, A.W. Mauro, J.R. Thome, G.P. Vanoli, L. Viscito, Critical heat flux: Performance of R1234yf, R1234ze and R134a in an aluminum multi-minichannel heat sink at high saturation temperatures, *Int. J. Therm. Sci.* 106 (2016) 1–17, doi:[10.1016/j.ijthermalsci.2016.03.011](https://doi.org/10.1016/j.ijthermalsci.2016.03.011).
- [168] A.I. Zanosko, A.V. Dedov, A.V. Belyaev, Experimental study of critical heat flux at flow boiling of R125 in small diameter channel, *J. Phys.* 1370 (2019) 012005.
- [169] L. Cheng, G. Xia, Experimental study of CHF in a vertical spirally internally ribbed tube under the condition of high pressures, *Int. J. Therm. Sci.* 41 (2002) 396–400, doi:[10.1016/S1290-0729\(02\)01330-3](https://doi.org/10.1016/S1290-0729(02)01330-3).
- [170] R. Sindhuja, A.R. Balakrishnan, S.S. Murthy, Critical heat flux of R-407C in upflow boiling in a vertical pipe, *Appl. Therm. Eng.* 28 (2008) 1058–1065, doi:[10.1016/j.applthermaleng.2007.06.030](https://doi.org/10.1016/j.applthermaleng.2007.06.030).
- [171] Y. Chen, M. Zhao, K. Bi, B. Yang, D. Zhang, K. Du, Critical heat flux of flowing water in tube for pressure up to near critical point—experiment and prediction, *J. Nucl. Eng. Radiat. Sci.* 4 (2018), doi:[10.1115/1.4038215](https://doi.org/10.1115/1.4038215).
- [172] Y. Zhang, R. Tian, X. Dai, Y. Ma, H. Li, L. Shi, Experimental study on sharp increase of wall temperature in vapor generator for organic rankine cycle, in: 7th International Conference on Informatics, Environment, Energy and Applications, 2018, pp. 189–194, doi:[10.1145/3208854.3208884](https://doi.org/10.1145/3208854.3208884).
- [173] F. Feuerstein, Investigation of Heat Transfer Near the Critical Point of R134a, Karlsruhe Institut für Technologie (KIT), 2019 phd Thesis.
- [174] A. Kaya, M.R. Özdemir, A. Koşar, High mass flux flow boiling and critical heat flux in microscale, *Int. J. Therm. Sci.* 65 (2013) 70–78, doi:[10.1016/j.ijthermalsci.2012.10.021](https://doi.org/10.1016/j.ijthermalsci.2012.10.021).
- [175] R.W. Morse, T.A. Moreira, J. Chan, K.M. Dressler, G. Ribatski, E.T. Hurlbut, G.F. McCarrol, G.F. Nellis, Berson, A. Critical heat flux and the dryout of liquid film in vertical two-phase annular flow, *Int. J. Heat Mass Transf.* 177 (2021) 121487, doi:[10.1016/j.ijheatmasstransfer.2021.121487](https://doi.org/10.1016/j.ijheatmasstransfer.2021.121487).
- [176] S. Basu, S. Ndao, G.J. Michna, Y. Peles, M.K. Jensen, Flow boiling of R134a in circular microtubes-Part II: Study of critical heat flux condition, *J. Heat Transf.* 133 (2011), doi:[10.1115/1.4003160](https://doi.org/10.1115/1.4003160).
- [177] R.W. Bowring, A simple but accurate round tube uniform heat flux, dry-out correlation over the pressure range 0.7–12 MN/m<sup>2</sup> (100–2500 psia, *AEEW Reports* 759 (1972).
- [178] Y. Katto, H. Ohno, An improved version of the generalized correlation of critical heat flux for the forced convective boiling in uniformly heated vertical tubes, *Int. J. Heat Mass Transf.* 27 (1984) 1641–1648, doi:[10.1016/0017-9310\(84\)90276-X](https://doi.org/10.1016/0017-9310(84)90276-X).
- [179] Y. Katto, A generalized correlation of critical heat flux for the forced convection boiling in vertical uniformly heated round tubes, *Int. J. Heat Mass Transf.* 21 (1978) 1527–1542, doi:[10.1016/0017-9310\(78\)90009-1](https://doi.org/10.1016/0017-9310(78)90009-1).
- [180] M.M. Shah, Improved general correlation for critical heat flux during upflow in uniformly heated vertical tubes, *Int. J. Heat Fluid Flow* 8 (1987) 326–335, doi:[10.1016/0142-727X\(87\)90069-5](https://doi.org/10.1016/0142-727X(87)90069-5).
- [181] D.D. Hall, I. Mudawar, Critical heat flux (CHF) for water flow in tubes-II: Subcooled CHF correlations, *Int. J. Heat Mass Transf.* 43 (2000) 2605–2640, doi:[10.1016/S0017-9310\(99\)00192-1](https://doi.org/10.1016/S0017-9310(99)00192-1).
- [182] L. Wojtan, R. Revellin, J.R. Thome, Investigation of saturated critical heat flux in a single, uniformly heated microchannel, *Exp. Therm Fluid Sci.* 30 (2006) 765–774, doi:[10.1016/j.expthermflusci.2006.03.006](https://doi.org/10.1016/j.expthermflusci.2006.03.006).
- [183] W. Zhang, T. Hibiki, K. Mishima, Y. Mi, Correlation of critical heat flux for flow boiling of water in mini-channels, *Int. J. Heat Mass Transf.* 49 (2006) 1058–1072, doi:[10.1016/j.ijheatmasstransfer.2005.09.004](https://doi.org/10.1016/j.ijheatmasstransfer.2005.09.004).
- [184] C.L. Ong, J.R. Thome, Macro-to-microchannel transition in two-phase flow: Part 2—Flow boiling heat transfer and critical heat flux, *Exp. Therm Fluid Sci.* 35 (2011) 873–886, doi:[10.1016/j.expthermflusci.2010.12.003](https://doi.org/10.1016/j.expthermflusci.2010.12.003).
- [185] Z. Anwar, B.E. Palm, R. Khodabandeh, Dryout characteristics of natural and synthetic refrigerants in single vertical mini-channels, *Exp. Therm Fluid Sci.* 68 (2015) 257–267, doi:[10.1016/j.expthermflusci.2015.04.016](https://doi.org/10.1016/j.expthermflusci.2015.04.016).
- [186] M.M. Shah, A general correlation for critical heat flux in horizontal channels, *Int. J. Refrig.* 59 (2015) 37–52, doi:[10.1016/j.ijrefrig.2015.06.027](https://doi.org/10.1016/j.ijrefrig.2015.06.027).
- [187] V. Ganeshan, R. Patel, J. Hartwig, I. Mudawar, Universal Critical Heat Flux (CHF) correlations for cryogenic flow boiling in uniformly heated tubes, *Int. J. Heat Mass Transf.* 120678 (2021), doi:[10.1016/j.ijheatmasstransfer.2020.120678](https://doi.org/10.1016/j.ijheatmasstransfer.2020.120678).
- [188] M. Song, X. Liu, X. Cheng, Prediction of critical heat flux (CHF) for the high-pressure region in uniformly heated vertical round tubes, *Ann. Nucl. Energy* 158 (2021) 108303, doi:[10.1016/j.anucene.2021.108303](https://doi.org/10.1016/j.anucene.2021.108303).
- [189] R.M. Tain, S.C. Cheng, D.C. Groeneveld, Critical heat flux measurements in a round tube for CFCs and CFC alternatives, *Int. J. Heat Mass Transf.* 36 (1993) 3039–2049, doi:[10.1016/S0017-9310\(05\)80135-8](https://doi.org/10.1016/S0017-9310(05)80135-8).
- [190] S.Y. Ahmad, Fluid to fluid modeling of critical heat flux: a compensated distortion model, *Int. J. Heat Mass Transf.* 16 (1973) 641–662, doi:[10.1016/0017-9310\(73\)90229-9](https://doi.org/10.1016/0017-9310(73)90229-9).